# WIRELESS NETWORKS, FROM COLLECTIVE BEHAVIOR TO THE PHYSICS OF PROPAGATION

Thesis by

Massimo Franceschetti

In Partial Fulfillment of the Requirements

for the Degree of

Doctor of Philosophy

California Institute of Technology

Pasadena, California

2003

(Defended October 2, 2002)

# Contents

# List of Figures

# Acknowledgements

I am grateful to the Caltech professors of my candidacy and defense committees, for listening to what I had to say, and for sharing their comments: Yaser Abu Mostafa, Jehoshua Bruck, Babak Hassibi, Robert McEliece, Leonard Schulman, and Richard Wilson.

I am grateful to Ronald Meester, for writing the book on percolation theory that sparked my interest in the topic, for listening to my ideas to generalize the theory, for inviting me to the Netherlands to prove theorems with him, and for ending up being a mentor and a friend.

I am grateful to Leonard Schulman, for being my second advisor at Caltech, and for believing the idea that the theory of random walks can be used to model wave propagation.

I am grateful to Lorna Booth, for arguing with me, for disproving many of my conjectures, and for bringing me to Amsterdam's cafes to do math.

I am grateful to Matthew Cook, who was very influential to my way of looking at research problems, and who listened to (and sometimes broke) many of my proofs.

I am grateful to many other scientists in the wider community, especially to Venkat Anantharam, David Culler, P. R. Kumar, David Tse, for stimulating discussions. Geoffrey Grimmett, Greg Lawler, Matthew Harris, Miodrag Potkonjak, and Sergei Zuyev answered to my e-mails and helped me to dig into some literature. Rob van den Berg, Michel Dekking, Richard Gill, Harry Kesten, Joan Segers, and Bálint Tóth read what became Chapter 2 of this thesis, providing useful comments.

I am also grateful to my parents for their support. My dad, especially for his lecture on propagation and random walks at Caltech, and the inspirational discussions that followed; and to my mom, for complaining that I was going to the beach and surfing too much and working too little, and for complaining that I was working too much and surfing too little.

Finally, I am grateful to my advisor, Jehoshua Bruck. He was always there when I wanted to talk to him, always ready to share his objective opinion and to offer guidelines; but he also gave me the freedom and independence to explore whatever interested me. His typical remark in these years has been: "I am a noise generator, I tell you a lot of things, but at the end you will do whatever you like." I will try to continue following this advice.

My work was supported by a graduate fellowship in my first year at the Institute, and by a research assistantship for the following years, funded by the Caltech Lee Center for Advanced Networking. The experimental data reported in Chapter 4 are courtesy of Ericsson Telecomunicazioni SpA, Rome, Italy.

# Abstract

This thesis addresses some of the key challenges in the emerging wireless scenario. It focuses on the problems of connectivity, coverage, and wave propagation, following a mathematically rigorous approach. The questions addressed are very basic and extremely easy to state. Their solution, however, can be difficult and leads to the development of a new kind of percolation theory, to a new theorem in geometry, and to a new model of wave propagation in urban environments. The problems are connected together to provide guidelines in the design of wireless networks.

# Chapter 1 Introduction

## 1.1 The wireless scenario

Any technology that allows exchange of information between two points in absence of any physical connection between them can be defined as wireless communication. Nowadays the most striking example of wireless communication is provided by the cellular telephone system. In this case, the service area is divided into cells that are served by fixed stations, usually connected to a wired network. Customers in the service area connect to the fixed stations, switching from one to the other when crossing a cell boundary. These cellular systems rely on a mature technology, which is however appropriate only to the particular service they exploit: voice transmission. This technology is likely to be inadequate to handle the challenges of the very near future, namely, wide-band wireless transmission and increasing number of customers.

Wide-band transmission allows to merge different types of information: voice, video, data, to be transmitted along the same channel. One key problem is to design wireless networks in a way that makes possible to deliver large amounts of data to many customers in an efficient and cost-effective way. The new emerging scenario will be characterized by smaller cells providing ad hoc coverage to clusters of homes and buildings, rather than the current rigidly planned cellular division and uniform coverage of the entire service area. This leads to a better exploitation of the spatial resource, and, consequently, to the possibility of handling larger amounts of data and servicing larger numbers of customers. Small cells also represent a cost-effective solution to the so-called "last mile" problem, where new service areas must be connected to a high capacity fiberoptic backbone.

Allowing different types of information, wide-band transmission brings new applications into the wireless domain. Portable devices can be used to browse the Web, to watch movies, to play interactive games in real time, and to securely transfer and

manage private data stored remotely. Inside buildings, distributed laptop computers can be networked and multi-hop wireless connections can be established. Similar reconfigurable situations can be envisaged in wireless networks of sensors monitoring the environment, or in emergency situations. These new applications bring new challenges to the network designer, from hardware (development of portable devices, sensors, and home terminals) to software (protocol design, modulation and coding techniques, architecture), with the communication channel in between. This must be fully characterized by the electromagnetic viewpoint. Electromagnetic signal spatial decay, time and space dispersion, interference, are all items that must be clarified in a way that the link design may rely on a solid background, evolving from the today semi-empirical approach, mainly based on experimental measurements, to a scientific one.

## 1.2 Contribution

The contribution of this thesis is to address some of the basic challenges in the emerging wireless scenario. At the same time, it leads to advances in pure mathematics (probability and geometry), computation theory (algorithms), and physics (propagation), opening new directions of research in all of these areas.

We focus on the key problems of connectivity, coverage, and wave propagation in wireless networks. Despite the simplicity of the questions we ask, their solution can be difficult and requires the invention of new methods. Our questions not only demonstrate mathematical ingenuity, but, being inspired by real problems, they provide a wide picture of wireless networks, from the analysis of their collective behavior, to the optimization of their design, to the physical modeling of their transmission mechanism.

The organization of the thesis is as follows. We introduce all the problems in this chapter, using simple examples that may seem, at first sight, totally unrelated to wireless networks, but that make a little story and are fun to play with. At the end of the chapter, we connect all the problems together and show how their combined

solution can be used in the design of wireless networks. Each problem is then re-examined as the topic of a separate chapter. The last chapter discusses extensions and future directions of research.

The first problem we consider is motivated by the question of long-distance multi-hop connectivity, and leads to the development of a new kind of percolation theory; this is derived in a mathematically rigorous way in Chapter 2. The second problem we consider is motivated by the question of efficient network coverage, and leads to a basic theorem in geometry that can be applied at the early design stage of a wireless network; this is presented in Chapter 3. The third problem is to give a reliable model of the electromagnetic signal decay in cluttered environments. This leads to a new model of the physics of propagation of a wireless signal, related to the classical theory of radiative transfer, that is applied to predict the propagation loss of an urban wireless channel in Chapter 4.

There are several publications associated with this thesis. The work on percolation theory and connectivity of wireless networks, written in collaboration with Lorna Booth, Jehoshua Bruck, and Ronald Meester (2002 a,b), has been presented at the 2002 IEEE International Symposium of Information Theory, and will appear in the journal *Annals of Applied Probability*. The work on coverage and the associated geometric theorem, written in collaboration with Jehoshua Bruck and Matthew Cook (2002), is currently under review for publication. The work on wave propagation, written in collaboration with Jehoshua Bruck and Leonard Schulman (2002 a,b,c), has been presented at the 2002 IEEE International Symposium on Antennas and Propagation, and is under review for journal publication.

## 1.3 Problem 1. The lazy gardener

Mario is a gardener who waters the flowers in a beautiful large square garden. The flowers have grown at random locations inside the garden. To minimize his work, Mario decides to divide the flowers into groups and, using his watering pot, to water each group individually, each time leaving a circular wet mark on the ground where

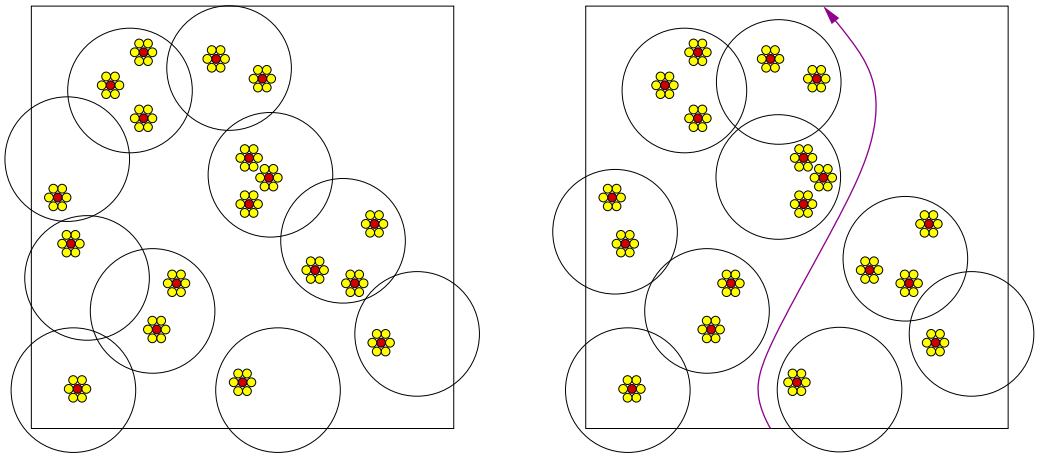

Figure 1.1: **The lazy gardener.** *Flowers are randomly distributed in the garden, and discs represent wet marks on the ground. The line indicates a possible dry crossing of the garden. If Mario decides to water the flowers as depicted on the right-hand side, the wet area won't span the entire garden and he will be able to go back, without getting his feet wet.*

the group is located. He starts his watering procedure at one side of the garden, working his way toward the opposite side. Once he has finished, will he be able to traverse the garden back to the side where he started, without getting his feet wet? Note that, for certain locations of the flowers, this may depend on Mario's watering strategy, see Fig. 1.1.

The problem above is similar to a simpler one described by Grimmett (1999) to introduce continuum percolation: lilies inhabit a beautiful large square pond. They have grown at random locations. Can a snail arriving at the pond traverse it without falling into the water? A picture of the snail's route appears in Fig. 1.2. Problems like these may be rephrased in terms of the following fundamental question of stochastic geometry: ascertain the minimal density of points in the plane which guarantees, for a given covering strategy, the existence of an infinite cluster of discs covering all the points. This question has been studied in the context of continuum percolation, where, as in the snail's lily pond example, each point of a two-dimensional Poisson point process is the center of a disc of given (or random) radius $r$, but the generalization to different covering strategies was not, until now.

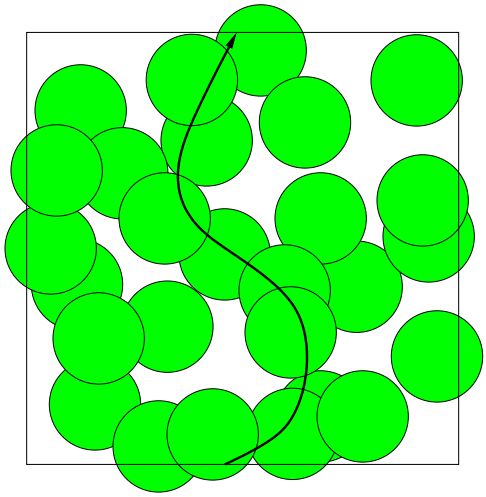

Figure 1.2: **The snail's lily pond.** *Discs represent randomly distributed lilies inside the pond. The line indicates a possible dry crossing of the pond.*

### 1.3.1 Background

Continuum percolation theory was originally introduced by Gilbert (1961), who was motivated by networks of wireless broadcasting stations. In his formulation, points of a two-dimensional Poisson point process represent wireless transmitting stations of range $2r$ and he asks if the system can provide some long-distance, multi-hop communication. He shows the existence of a critical value $\lambda_c$ for the density of the transmitters, such that, for $\lambda > \lambda_c$, an unbounded connected component of transmitters forms, with probability one, and long-distance multi-hop communication is possible. A simulation of Gilbert's model is depicted in Fig. 1.3, where discs of unitary radius are randomly distributed in a large square area. On the left-hand side of the figure the density of the discs is $\lambda = 0.3$, the system is below criticality, and only isolated clusters can be found. On the right-hand side of the figure, the density of the discs is $\lambda = 0.4$, the system has reached its percolation threshold, and the largest cluster spans the entire simulation plane.

Gilbert's model has attracted the attention, in the past forty years, of mathematicians and physicists. Mathematicians have been attracted by the charm and the beauty of the apparent simplicity of its open problems. Physicists recognized the applicability of the model to different phenomena, like impurity conduction in lightly

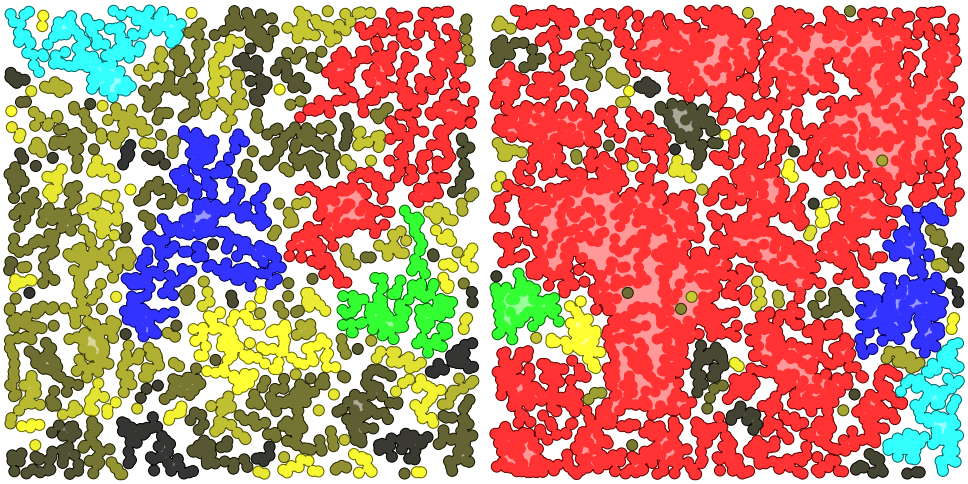

Figure 1.3: **Gilbert's model.** *In this simulation discs of radius $r = 1$ are centered at each random point. Components are identified by the same color. On the left-hand side of the figure, the density of the process is $\lambda = 0.3$; on the right-hand side $\lambda = 0.4$. Extensive Monte Carlo simulations show that an unbounded component of discs forms at the critical value $\lambda_c \approx 0.36$, see Quintanilla, Torquato, and Ziff (2000) .*

doped semiconductors, ferromagnetism in a dilute system of magnetic atoms in a non magnetic host crystal, and cross-linking of polymers.

Before Gilbert's work, other models that exhibit phase transitions had also been studied. Percolation theory, in its original discrete formulation, considered square lattices where each pair of adjacent cells can be connected, independently, with probability $p$. The first mathematically rigorous paper on the topic is due to Broadbent and Hammersley (1957), who coined the term "percolation" and proved the existence of a critical probability $p_c$, such that, for $p > p_c$, the largest connected cluster is infinite. Historically, first ideas go back to Flory (1941) and Stockmayer (1943), who studied (in a less formal framework) gel formation in polymers and introduced what is known today as percolation on the Bethe lattice, or Cayley tree. Additional studies of phase transitions connected to percolation, performed by Kadanoff (1966), sparked the work for which Ken Wilson (1971 a,b) was awarded the Nobel prize in physics in 1982. These studies are related to the calculation of the critical exponents, which are observed experimentally and describe how physical quantities vary close to the critical point. Whereas the critical percolation probability $p_c$ depends on the type of lattice, critical exponents are believed to depend only on the space dimension and

to be independent from the local details of the structure of the model, i.e., they are the same for different lattices, and even for continuum and discrete percolation. The intuition behind Wilson's work is that the same "fixed point" interaction is reached at criticality in all of these systems. Recent rigorous results on critical exponents can be found in the work of Smirnov and Werner (2001) and in the references therein.

Phase transitions were also studied in the context of graph theory by Erdös and Rényi (1959, 1960, 1961 a, b), who considered a set of $n$ vertices, each pair having the same probability, regardless of their separation, of being connected by an edge, and looked at the resulting connectivity of the graph for $n \to \infty$.

Even if many results in the applied literature have yet to be mathematically verified, the field of phase transitions is now well developed and excellent mathematics reference texts for the theory of percolation are Grimmett (1999) and Kesten (1980); for continuum percolation is Meester and Roy (1996); and for random graphs is Bolobás (1985). Another book, popular among physicists, is Binney, Dowrick, Fisher, and Newman (1992).

Recently there has been a renewed interest in the application of these models to modern wired and wireless networks. See, for example, the works of Fabrikant, Koutsoupias, and Papadimitriou (2002); Gupta and Kumar (1998, 2000); Newman (2002); Xue and Kumar (2002). In these works the stochastic models proposed for wireless networks consider "flat' networks, in which, as in Gilbert's formulation, all nodes cooperate to route each other's data packets. Our theory provides an extension to "clustered" networks, in which a subset of the nodes provide coverage to clusters of clients and route data packets from source to destination. See Fig. 1.4 for a visual example.

### 1.3.2 New model

In our clustered model clients are randomly distributed on the plane. They communicate by connecting to wireless base stations that forward their messages to destination in a multi-hop fashion. All the clients use the same transmission power, therefore any

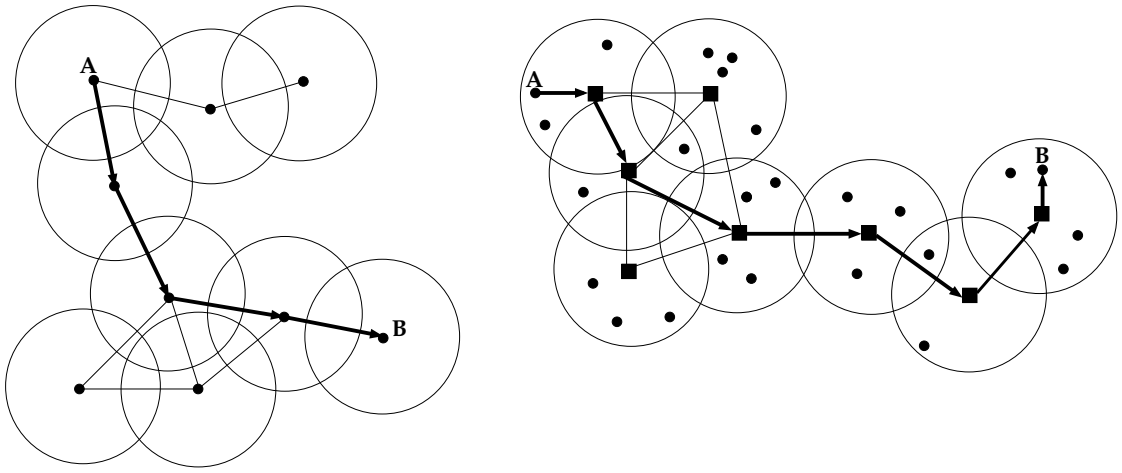


Figure 1.4: **Flat vs. clustered wireless networks.** *In a flat, ad hoc network (left-hand side of the figure), all nodes are considered equal, and can route data packets to destination. In a clustered, wireless backbone network (right-hand side of the figure), a subset of the nodes acts as wireless base stations, providing coverage to clusters of clients, and routing data packets through the network.*

client that is within a given distance $r$ to a base station can connect to it, and we say that the client is covered by the base station. The network is completely wireless, hence, base stations can connect to other base stations only up to a limited distance $R$. A covering algorithm decides where to place the base stations, according to the distribution of the clients, in such a way that each client is covered by at least one station, and each station covers at least one client. In this scenario, we are interested in determining the conditions on the covering algorithm, and on the transmission power of the nodes (i.e., on the radii $r$ and $R$), for which an unbounded connected component of base stations almost surely (a.s.) forms, when the density $\lambda$ of the clients exceeds a given threshold, and thus the network can provide some long-distance multi-hop communication.

This model applies to commercial cellular networks that provide services to clients, and in which all links are wireless. It also applies to sensor networks, in which a large number of small sensors is deployed to monitor the activity of a random distribution of particles. In this case $R$ would be the radius of communication of the sensors and $r$ would represent their sensing range. One could also think of a dynamic scenario in which the clients or the particles move, and the covering stations, deployed on a fixed

grid, are each turned on or off at any given time, to minimize power consumption.

In the study of the model our aim is twofold. On one side, we answer some very natural questions that arise from a purely mathematical point of view. On the other side, we note that some of our results can be used as guidelines in the design of real networks. One key result, from an engineering point of view, is that the network can provide some long-distance multi-hop communication, regardless of the algorithm used to place the covering stations, if the density of the clients is high enough and their communication range is less than half the communication range of the base stations. As the ratio between the two communication ranges becomes greater than half, a malicious covering algorithm that never provides long-distance multi-hop communication in the network exists even if we constrain the base stations to be placed at the vertices of a fixed grid—which is the typical scenario in the case of commercial networks. This means that in the latter case one should be careful in the design of the covering algorithm to avoid the possibility of having a perpetually disconnected network.

### 1.3.3 Main results

We group all results into three categories: (non) existence of an unbounded connected component for different classes of covering algorithms, scaling results, and results regarding the optimality of certain algorithms. We show that, for any covering algorithm, there is no unbounded connected component for a density of points $\lambda$ sufficiently small (depending on the algorithm). On the other hand, there are covering algorithms that never form an unbounded connected component, whatever the value of $\lambda$. Furthermore, we divide covering algorithms into families that do form an unbounded connected component, for large $\lambda$, and families that do not. We then show how this percolation property is affected by the scaling of the radii $r$ and $R$. Finally, we show (constructively) that a certain class of practical algorithms can achieve a density of covering discs arbitrarily close to the minimal one, and we also construct an optimal algorithm in terms of this minimal density.

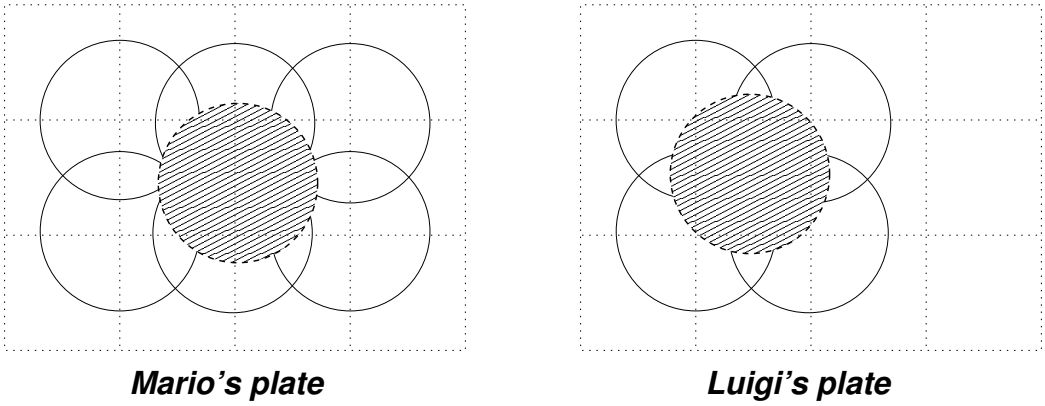


Figure 1.5: **The dinner game.** *Mario's plate requires six discs placed at the vertices of the grid to be fully covered, while Luigi's plate requires only four. In this case, Mario beats Luigi 5 to 7.*

Before looking at all this, we introduce the two remaining problems that are the subject of this thesis.

## 1.4 Problem 2. The dinner game

Let's return to Mario and his beautiful garden. Once he finishes watering the flowers, Mario returns home where he eats dinner with his brother Luigi. After dinner they decide to use the grid design of their table cloth and their empty plates to play the following game. Each of them places a plate on the table and then tries to completely cover the plate placed by his opponent by new plates of the same size, but centered only at grid points. The objective of the game is to end up using less plates than the opposite player. What is the optimal strategy that guarantees Mario's at least a tie with Luigi? A winning combination for Mario is depicted in Fig. 1.5. His plate (represented as a shaded disc) requires six plates placed at the vertices of the grid to be fully covered, while Luigi's plate requires only four plates placed on the grid.

A more general version of this problem can be phrased in terms of the following fundamental question of combinatorial geometry: how many discs of given radius $r$, centered at the vertices of an infinite square grid of given spacing $L$, are required, in the worst case, to completely cover an arbitrary disc of radius $r$ placed on the plane,

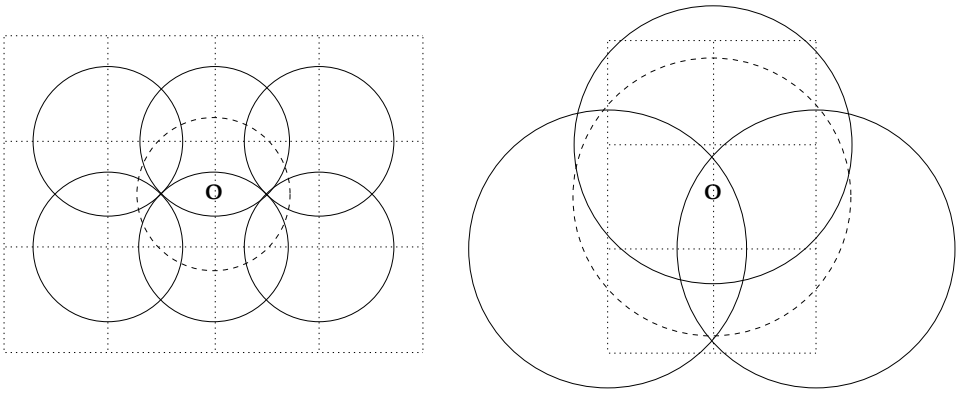


Figure 1.6: **Geometric disc covering.** *On the left-hand side of the figure, the dashed line disc requires six discs centered at lattice vertices to be fully covered. On the right-hand side of the figure, it requires only three discs.*

and how is this worst case achieved?

The answer to this question depends on the ratio of the radius $r$ to the grid spacing $L$, as illustrated in Fig. 1.6. On the left-hand side of the figure, six solid line discs, centered at grid vertices, are required to cover a dashed line disc placed half way between two adjacent grid vertices. If the ratio of $r$ to the grid spacing $L$ is increased (right-hand side of the figure), then fewer discs centered at grid vertices are required to cover the same dashed line disc. We present a geometric theorem that shows that the number of discs of radius $r$ centered at the vertices of a square grid of spacing $L$ that are necessary and sufficient to completely cover an arbitrary disc of radius $r$ placed on the plane is an integer $\mathcal{N} \in \{3, 4, 5, 6\}$, whose value depends on the ratio $r/L$. The necessary condition of the theorem is proved constructively, by showing a disc placement that requires the maximum number of $\mathcal{N}$ grid discs to be covered, thus providing the optimal strategy to play the dinner game.

### 1.4.1 Application to wireless networks and main result

How can we apply the solution to the geometric disc covering outlined above to the design of radio cellular networks? Let us consider a scenario in which a telecommunication company plans the deployment of a new network in a city. One key problem is to decide where to position base stations, according to a distribution of demand

points, to achieve optimum quality of service, with minimum costs. At the early design stage, interference effects are neglected, simplistic propagation models are assumed, and the problem is to suggest initial design strategies. We assume that, by paying a local tax, the company can install base stations at the city traffic lights. In this way, all base stations are placed at some vertices of a square grid, corresponding to the street intersections, in a way that each demand point is within a given distance from a base station. Following this design the company estimates a cost of deployment of, say, 500 euros (€) per base station. Alternatively, the company can place the stations optimally, without constraining them to be at the street intersections. This means identifying a minimum cardinality set of locations of the base stations that cover all the demand points. This strategy can potentially lead to a smaller number of installations, but its estimated cost of deployment is, for instance, 1700 € per base station, due to higher manufacturing and installation costs, and because the company may need to pay, or to give a discount, to the owner of the building, or land, where it intends to place a base station. Hence, the company faces the following dilemma: is it better to choose the grid design that may lead to a larger number of less expensive base stations, or is it better to choose locations optimally, potentially using less, but more expensive base stations?

The solution to the puzzle above depends on the ratio of the communication range $r$ of a base station to the city block length $L$. Consider the limiting case in which all demand points lie inside a circle of radius $r$, thus requiring a single non-grid base station of cost $C_{ng}$. Alternatively, we can serve all the points with a number $\mathcal{N}$ of grid base station that depends on the ratio $r/L$, and that is provided by our theorem. The corresponding cost is in this case $\mathcal{N} \cdot C_g$, where $C_g$ is the cost of one grid base station. By applying our geometric result, we are therefore in a position to solve the puzzle. Accordingly, we will show that the following holds for any distribution of the demand points:

- For $C_{ng} > 6C_g$, the network grid design is cost-effective if $r/L \geq \sqrt{2}/2$.
- For $C_{ng} > 5C_g$, the network grid design is cost-effective if $r/L \geq \sqrt{10}/4$.

- For $C_{ng} > 4C_g$, the network grid design is cost-effective if $r/L \geq 1$.
- For $C_{ng} > 3C_g$, the network grid design is cost-effective if $r/L \geq 5\sqrt{2}/4$.

In all remaining cases, a non-grid network design can be cost-effective for some distribution of demand points. By referring to the cost values given in the example, we have $1700/500 = 3.4 > 3$, hence the company should always choose a grid design if the ratio of the communication range of the base stations to the city block length is greater or equal to $\frac{5\sqrt{2}}{4}$.

### 1.4.2 Model assumptions

The described scenario relies on several assumptions. We assume a city formed by regularly spaced blocks; to use existing traffic light poles as potential transmitting locations; and to identify demand nodes that represent the expected network traffic. A square grid city model better applies to some U.S. urban and suburban areas than to older, and more irregular, European cities (despite we have used euros in our example!). The idea of using existing traffic light poles to place base stations in a city has been exploited by several telecommunication companies in the recent years, both in the U.S. and Europe, to build microcellular networks with higher capacities than traditional cellular systems, see Greenstein et al. (1992). Finally, the concept of demand nodes was introduced by Tutschku and Tran-Gia (1998), and the International Telecommunication Union (1999) has recently proposed its standardization. According to their definition, a demand node represents the center of an area with a certain traffic demand and each node stands for the same portion of traffic load. Hence, different traffic patterns correspond to different node distributions: highly populated business districts typically lead to dense distributions of demand nodes, while suburban and rural areas lead to sparser distributions. More details on the identification of demand nodes can be found in the survey of Tran-Gia, Leibnitz, and Tutschku (2000).

We also point out how one could argue that constraining (as we also did in the percolation model described in the previous section) each demand point to be within a

given distance from a base station, corresponds to assuming base station transmitters to have rotational symmetric range, that is not an accurate physical representation of what is often in practice an anisotropic and time-varying communication range, due to shadowing and fading effects. However, we argue that a circle that bounds the maximal range can be used as a first-order approximation at the early design stage of the network, as hexagonal cell shapes are universally adopted to approximate circular radiation patterns in the design and analysis of cellular systems, see Rappaport (1996); and as circular radiation patterns are assumed in the calculation of the throughput capacity of ad hoc wireless networks, see Grossglauser and Tse (2001), Gupta and Kumar (2000), and Kulkarni and Viswanath (2001).

There is no doubt that our model can be improved, relaxing some, or all previous assumptions. This, however, does not lead to a simple analytical evaluation, as we provide, of the range of parameters that suggest a grid or non-grid design. Our contribution consists in suggesting initial design strategies, determining if there is an early indication of convenience of a grid design that can be later validated by more accurate numerical solvers.

Before turning to mathematical details, we can still play a little more with another problem: let's look at what Mario is up to.

## 1.5 Problem 3. The sleepy drunk

Thanks to a theorem he read in a Caltech PhD thesis, Mario beats Luigi at their dinner game and Luigi must then buy him a large flask of wine. Mario drinks the entire flask and starts wandering around town in a state of supreme intoxication. He walks in a funny way: initially he proceeds in a straight line, but suddenly he turns through any angle whatever and walks in a straight line for another while, and so on. Every time he turns he feels dizzy and risks tripping over and falling asleep. How far does he get, before finally falling asleep? A picture of Mario's drunken walk appears in Fig 1.7.

The problem above is related to wave propagation in cluttered environments.

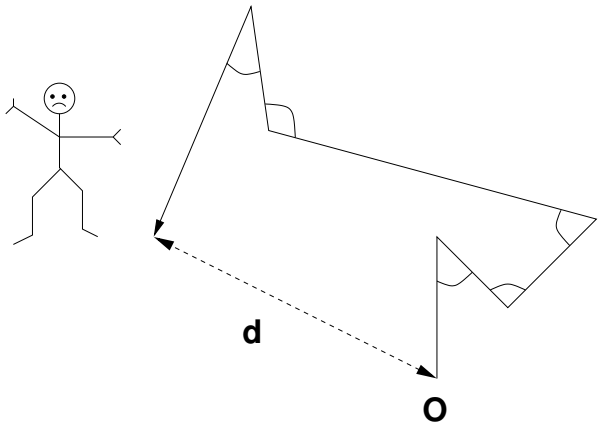


Figure 1.7: **Mario's drunken walk.** *After getting drunk, Mario starts wandering around and reaches a distance d away from his origin point, before finally falling asleep.*

The physics of propagation in rich scattering environments, such as urban areas, are still largely unknown. We know that the propagation mechanism must obey Maxwell equations, but we do not know how to analytically solve these equations in complex environments, where different objects can reflect electromagnetic waves in many directions and partially absorb them. In this case, simplified models of propagation that can be analytically or numerically solved are of interest. Mario's drunken walk constitutes an example of one such model of propagation in urban microcellular systems.

### 1.5.1 Background

Radio microcells used for wireless personal communication have become more and more popular in the last few years, and today many telecommunication companies use them to provide coverage to densely populated areas. Internet providers also started using them to provide high-speed wireless internet access. These microcells are regions of few hundred meters in diameter, served by radio base stations. They are one or two orders of magnitude smaller than traditional radio cells used for personal communication. The reduction in size requires the use of low antennas (typically below 10 m), transmission at low power (typically below 10 W), and has the advantage of increasing the overall capacity of the system. Another effect of using low transmit-

ting antennas is that the propagation mechanism is dominated by the large amount of scattering and diffraction due to the many objects encountered by the radiated signal, and exact analytical solutions, obtained by solving Maxwell equations in the given environment, cannot be sought for. Hence, prediction of propagation loss, essential in the network planning stage, is typically done using empirical formulas that fit experimental data.

In almost all work done in both line-of-sight (LOS) and non-line-of-sight (NLOS) conditions, the propagation loss is empirically modeled using an inverse power law in the distance to the transmitter. This inverse power law model goes back to the empirical formula given by Hata (1980), following previous work of Okumura et al. (1968), based on extensive experimental measurements made in the nineteen-sixties in Japan. When adapting the Okumura-Hata formula to smaller cells, there is experimental evidence of a power law exponent that increases as a function of the distance between the transmitter and the receiver. To accommodate to this variation, telecommunication companies started using path loss models characterized by a breakpoint distance at which the exponent of the inverse power law is changed. The existence of such a breakpoint can be theoretically justified, in LOS conditions, using a simplified two-ray propagation model consisting of the direct and ground reflected ray, see Fig. 1.8. This model predicts the existence of a breakpoint distance $r_b$ at which the characteristic of power loss with distance $r$ from the transmitter is changed from the mode $r^{-2}$ (for $r < r_b$) to the mode $r^{-4}$ (for $r > r_b$), and has been used by Xia et al. (1993) to predict LOS power attenuation in microcellular systems. The model can also be refined considering the two additional rays reflected by the buildings along the street, but this extension does not change the predicted transition to the $r^{-4}$ mode, see Bertoni et al. (1994). Hence, this simple ray model cannot explain the experimentally observed power loss modes of $r^{-q}$, with $q$ in the range 4 to 10 beyond the breakpoint, that have been reported, for example, in Blaunstein et al. (1995,1996,1998), Feurstein et al. (1994), and Green (1989). Recently, a possible explanation of this phenomenon has been proposed by Blaunstain et al. (1998), introducing a lossy waveguide model to describe wave propagation along straight streets

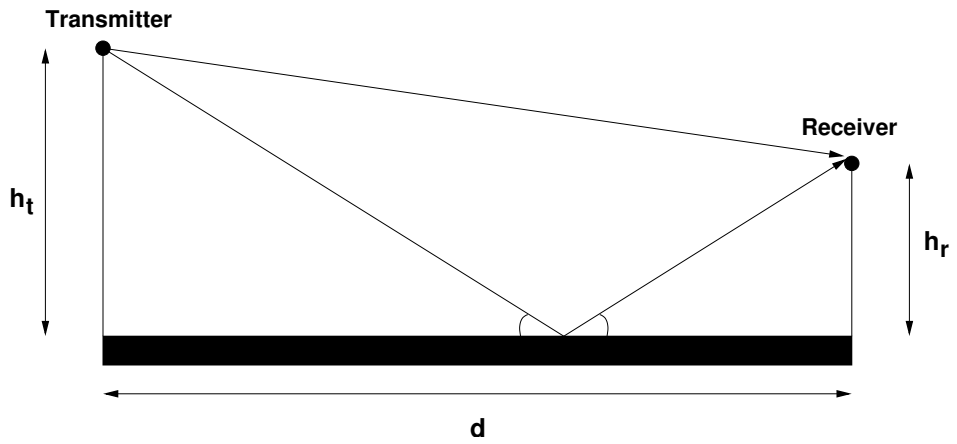


Figure 1.8: **Two-ray ground reflection model.** *This model considers the direct signal path and a ground reflected signal path between transmitter and receiver. At large distances it predicts a received power that falls off with distance raised at the fourth power.*

with randomly distributed walls of buildings and gaps between them. This model predicts a smooth transition from an $r^{-2}$ mode to an exponential attenuation mode that can explain the empirical high-order power law of $r^{-q}$, $q > 4$, obtained in most experiments.

In NLOS conditions, empirical path loss formulas of the type $r^{-q}$ have also been used, and, by using low transmitting antennas, values of $q$ considerably larger than 4 after a breakpoint have been used to fit experimental data, see for example the work of Erceg et al. (1999). In this case the propagation mechanism must be based on multiple scattering and diffraction effects that allow coverage of NLOS locations. For example, in urban areas, lamp posts, street signs, trees and vegetation, pedestrians, cars, irregularly sited and textured building walls (common in older European constructions) can scatter energy in many directions, allowing reception of signal in shaded areas. These effects are difficult to predict, and additional efforts have been made to develop approximate models that can justify the experimental findings. Maciel et al. (1993), and Xia and Bertoni (1992) proposed a model based on multiple forward diffraction over a row of parallel, equispaced buildings of the same height. Their model, however, can only predict values of the path loss exponent $q$ less than 4.5. Recently, Franceschetti G. et al. (1999) proposed an analytic model based on random walks, rather than wave interference effects. They model a city as a random

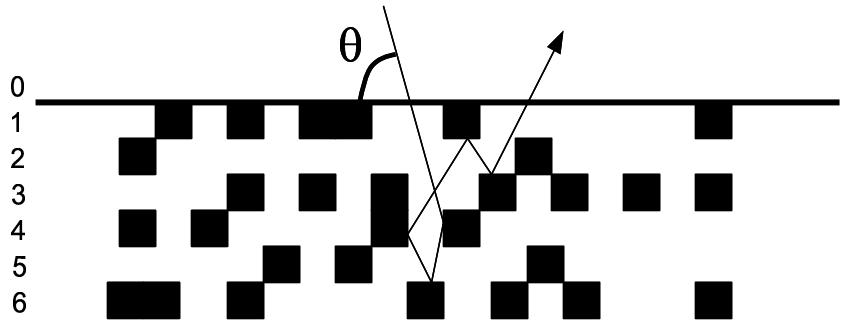


Figure 1.9: **Ray penetration in a random environment.** *In this model, a city is represented as a discrete site percolating lattice, where the site occupation probability $p_c$ represents the density of the buildings that are assumed to be perfect reflectors. A plane wave impinging the lattice penetrates a number of levels that is a function of $p_c$ and of the impinging angle $\theta$.*

medium of lossless scatterers and consider a random walk formulation of the problem of optical ray penetration inside the medium, see Figure 1.9. The idea is to have a plane wave entering an urban area at a certain incident angle. Their main result is an approximate analytical formula for the penetration depth as a function of the density of the scatterers and of the wave's incident angle. Their study, however, not considering signal attenuation inside the medium, nor considering locating the transmitter inside the medium, does not lead to a path loss formula that can be experimentally validated.

Our work extends the model of Franceschetti G. et al. (1999) considering an isotropic source placed inside the environment and including in the model signal attenuation and losses due to absorption. It turns out that by solving Mario's sleepy drunk problem we can also solve the proposed propagation model and obtain a path loss formula that can be experimentally validated. The obtained path loss formula rather accurately (in comparison to other models and to the experimental data) describes the smooth transition of power attenuation from the free space mode $r^{-2}$ to an exponential attenuation, and is, in the medium range, close to the empirical formulas that use high-order power laws, after a breakpoint, to fit experimental data. Our analytical solution is validated by showing agreement with experimental data collected by Ericsson SpA in the city of Rome, Italy.

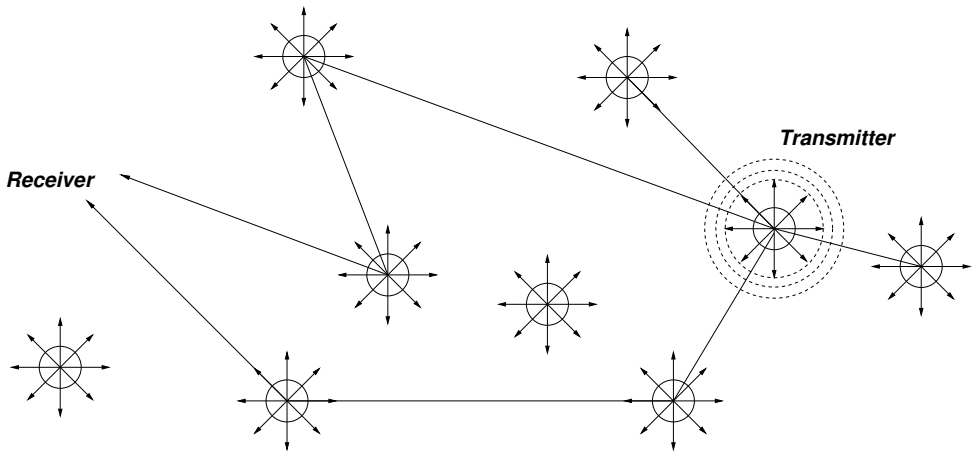


Figure 1.10: **Propagation model.** *Each photon radiating from an isotropic source propagates in the environment following a piecewise continuous trajectory, modeled as a random walk. Each time the photon hits an obstacle, it turns in a random direction, or it is absorbed by the obstacle.*

### 1.5.2 New model and main results

We refer to the canonical scenario depicted in Fig. 1.10. A monochromatic isotropic wave radiated by a transmitter reaches the intended receiver undergoing multiple scattering from different obstacles placed in the environment. The scattering mechanism is lossy: at each reflection the wave undergoes a prescribed attenuation. This physical picture is modeled in probabilistic terms as Mario's drunken walk. The wave is composed of emitted photons that move following a piecewise linear random walk inside the medium. We assume that each time a photon hits an obstacle, it has a probability $\gamma$ of being absorbed, and a probability $(1-\gamma)$ of being scattered in a random direction. We are interested in computing both the power density and the power flux at distance $r$ from the transmitter. The former equals the number of photons entering an infinitesimal sphere of radius $\Delta r$ placed at distance $r$, normalized to the sphere surface; the latter is defined as the number of photons leaving a sphere centered at the transmitter and of radius $r$, normalized to the sphere surface. Both quantities are related to the probability density function (*p.d.f.*) of a photon to be absorbed at a distance $r$ from the source, which also corresponds to the p.d.f. of Mario falling asleep and stopping his walk at a distance $r$ from the origin. We derive exact (in 1-D and 2-D) and approximate (in 2-D and 3-D) analytical formulas for this power

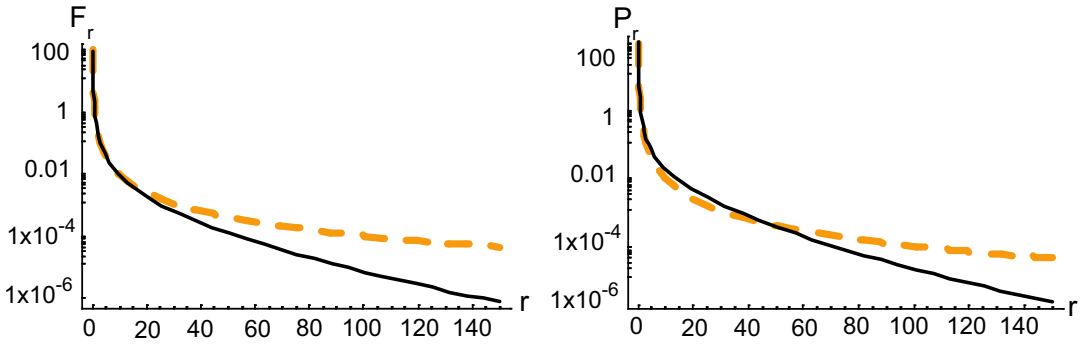


Figure 1.11: **Results of the model compared to free space propagation.** *The dashed line curves represent the free space $1/r^2$ attenuation law, the continuous line curves represent the predicted power flux $F_r$ (left-hand side of the figure) and power density $P_r$ (right-hand side of the figure) of our 3-D probabilistic model. We note that the flux model presents a smooth transition from the $1/r^2$ law to an exponential attenuation; the power density model, although very similar, predicts slightly higher power near the source. The breakpoint at which the model starts diverging from the $1/r^2$ law is determined by the values of $\eta$ and $\gamma$. In the figure these values are determined from the experiments presented in Chapter 4 of the thesis.*

density and power flux, as functions of the absorption coefficient $\gamma$ and of the average step length $1/\eta$ of the random walk (which is essentially a measure of the density of obstacles in the environment). Results for the 3-D case are plotted and compared with free space propagation in Fig. 1.11. We observe how our model predicts a transition to an exponential propagation loss as the distance between transmitter and receiver increases, and the absorption of the obstacles starts being a dominant factor.

An advantage of the proposed model is that it does not necessarily rely on experimental data to tune the parameters $\gamma$ and $\eta$ using regression analysis (as is common with empirical formulas): in principle, these parameters can be chosen by estimating directly the amount of clutter in the environment and the absorption coefficient of the scatterers, which can be less expensive than performing experiments. Indeed, when we compare our model with experimental data, we find values of the parameters that correspond to having on average one obstacle every ten meters, with an absorption coefficient of $12\% \sim 17\%$, which is reasonable for the urban area considered.

### 1.5.3 Model assumptions

We understand that our probabilistic modeling is an oversimplified version of the real propagation problem. Our random walk formulation essentially assumes the obstacles to be small, thus re-radiating as point sources: a stream of photons hitting an obstacle spreads uniformly because each photon is scattered in a random direction (or it is absorbed). Popular numerical solvers, based on ray tracing techniques, assume, on the contrary, that the obstacles are large and planar, thus re-radiating according to the laws of geometrical optics. However, there is numerical and experimental evidence, see Tarng and Ju (1999), that these solvers underestimate the real attenuation, when used to predict the path loss in microcells. Tarng and Ju (1999) show that better matching with experimental data is obtained by decomposing the large obstacles into smaller, more uniformly scattering patches.

Finally, we point out the existence of extensive literature on wave propagation in random media. An excellent, comprehensive reference book on the subject is the one by Ishimaru (1978). This literature is usually not accounted for in more recent cellular communication works. This is essentially due to the popular aforementioned assumption that obstacles in cellular systems are mainly large and planar, thus re-radiating according to the laws of geometrical optics. On the other hand, wave propagation in random media typically assumes obstacles to be small and to re-radiate almost as point sources (applications are, for instance, in radiation in foggy atmospheres). Given our small obstacles approximation, it is interesting to see how our model relates to the classical theory of propagation in random environments. In Chapter 4, we highlight the similarities between our analytical results and corresponding numerical solutions derived from electromagnetics as described in Ishimaru (1978) and we show how our model allows an interpretation of the results of the transport theory of propagation in the light of the recurrence properties of random walks. We believe that it is quite intriguing to find such relationships between models that are based on so very different premises.

## 1.6 Putting it all together

What is all this theory good for? How do all these puzzles that we solve fit together? Why is this a thesis in engineering? We claim that the theories developed in this thesis are useful to give guidelines in the design of wireless networks. The work on wave propagation can give us an idea of the maximum radius of communication of a wireless transmitter in an urban area. This information can be used in conjunction with our geometric disc covering theorem, to determine, at the very early design stage, conditions for which a grid network design is cost-effective, for any expected traffic demand. Information on the maximum radius of communication, and on the network design strategy, can then be used to analyze the connectivity of the network. For example, if a designer finds out that the communication range of the clients is larger than half the communication range of the base stations, then our results on percolation show that he must be careful in the way he decides to position the base stations to provide coverage to the clients, because a perhaps economically appealing grid-based covering strategy may lead to a perpetual disconnected network.

We have already pointed out how all of our results hold within the assumptions of a model. One cannot hope to have a closed-form mathematical solution for every real engineering problem, including all the details of a real scenario. In practice numerical solvers can be used to validate, and sometimes complete, or even correct the theory; and theories can always be improved by the invention of new, more powerful methods that allow solving more complicated models. The spirit of our work is close to the one of the applied mathematician that is called to give design guidelines to the practical engineer and that is forced, by the limited powers of his formal methods, to act within the limits of a model. At the same time, however, our mathematical spirit sometimes drifts away from the application to explore concepts (like the optimal algorithms, or the shift invariant algorithms described in the next chapter) that are interesting from a pure mathematical point of view. We hope that the reader will forgive us this weakness, dictated by the pure curiosity to discover some truth.

# Chapter 2 A new model of percolation

In this chapter, we present our new model of percolation. Boolean models, in which each point of a two-dimensional Poisson point process is the center of a disc of given (or random) radius $r$, have been extensively studied. We consider the generalization in which a deterministic algorithm (given the points of the point process) places the discs on the plane, in such a way that each disc covers at least a point of the point process and that each point is covered by at least one disc.

We look at the percolation properties of this generalized model, focusing on the (non) existence of an unbounded connected component of discs, for different classes of covering algorithms. We also explore the notion of optimal covering algorithms.

## 2.1 Summary of results

We group the results that we present in this chapter in the following four categories: non-existence results, existence results for different classes of covering algorithms, scaling results, and results concerning the optimality of certain algorithms. In the following, we let $X$ be a two-dimensional Poisson point process of density $\lambda$. The points of $X$ represent the clients that are covered by base stations.

**Non-existence results.** Our first results regard the non-existence of an unbounded component of overlapping covering discs. We show (Theorem 2.1) that for any algorithm covering all the points of $X$ by discs of radius $r$, there exists a $\lambda_0 > 0$ such that for all $0 < \lambda \leq \lambda_0$, $P_\lambda$(there is an infinite component) $= 0$. Then we show that the symmetric result, i.e., the almost sure (a.s.) existence of an unbounded connected component for large values of $\lambda$, is not generally true, but depends on the type of covering algorithm. It is known that a covering that places a disc centered at each point of $X$ forms a.s. an unbounded connected component for large values of $\lambda$ (Gilbert 1961). In order to show that this result does not generalize to all coverings, we spec-

ify a covering algorithm that does not form an unbounded connected component for any value of $\lambda$.

**Existence results.** We proceed by identifying different families of covering algorithms that form an unbounded connected component a.s. for large values of $\lambda$. One of such coverings, that is practical for our applications, is a *grid covering*. We show (Theorem 2.4) that for any algorithm covering all the points of $X$ by discs of radius $r$ centered at the vertices of a grid, there exists a $\lambda_1 < \infty$, such that for all $\lambda > \lambda_1$, $P_\lambda(\text{there is an infinite connected component}) = 1$.

Another family of coverings that we consider are the *flat coverings*. A flat covering has the property that the restriction to any box of size $n \times n$ contains at most $k(n)$ discs, for any value of $\lambda$. We show in Theorem 2.3 that, for flat coverings, there exists a $\lambda_1 < \infty$, such that for all $\lambda > \lambda_1$, $P_\lambda(\text{there is an infinite connected component}) = 1$.

A third class of algorithms that we examine are the *shift invariant coverings*. These algorithms are defined by the requirement that the covering commutes with shifts of the points. We ask whether a shift invariant algorithm necessarily forms a.s. an unbounded connected component for large values of $\lambda$, and we answer this question negatively, by constructing a shift invariant algorithm that does not exhibit this property.

**Scaling results.** We then introduce a further extension of our model. We note that when we consider overlapping discs as connected components, then we implicitly assume, in our model of a wireless network, that the maximum radius of communication between two base stations is twice as large as the maximum radius of communication between clients and base stations. This observation leads to the natural question of what would happen if the ratio between the two radii is different from two.

In the standard Poisson Boolean model, that places a disc centered at each point of a Poisson point process $X$, considering a different radius for connectivity corresponds to a simple scaling operation, hence it does not change the basic properties of the model. In our extended model, however, this leads to more interesting results. Call $r$ the radius of the discs used to cover the points of $X$ and $R$ the maximum distance

sufficient to connect disc centers. We show (Theorem 2.9) that

- If $R/r \leq 1$, then, for any grid $G$, there is a covering algorithm that places discs only at the vertices of $G$, and a.s. does not form an unbounded connected component, for any value of $\lambda$.
- If $1 < R/r < 2$, then, for some given dense grid $G$, there is a covering algorithm that places discs only at the vertices of $G$, and a.s. does not form an unbounded connected component, for any value of $\lambda$.
- If $R/r = 2$, then, for any grid $G$, any covering algorithm that places discs only at the vertices of $G$ forms a.s. an unbounded connected component for large values of $\lambda$.
- If $R/r > 2$, then any algorithm forms a.s. an unbounded connected component for large values of $\lambda$, even if it is not grid-based.

Note that the latter case is useful in practice, because it states that if base stations can communicate at a distance larger than twice the maximum communication distance to the clients, an unbounded connected component forms a.s. for large values of the density of the clients, regardless of the covering algorithm used to build the cellular network.

**Optimality Results.** Finally, we show (constructively, in Theorem 2.12) the existence of algorithms that are optimal in achieving a minimal density of covering discs. We also show that a certain class of practical algorithms can achieve densities arbitrarily close to the optimal.

## 2.2 Notation and definitions

To formally present the results discussed above, we need to introduce some notation and make some definitions. Let $\mathbb{R}^2$ be the Euclidean plane, let $\mathcal{B}^2$ be the $\sigma$-algebra of Borel sets in $\mathbb{R}^2$ and let $\ell(\cdot)$ be Lebesgue measure in $\mathbb{R}^2$. Let $N$ be the collection of

all counting measures on $(\mathbb{R}^2, \mathcal{B}^2)$, which assign finite measure to bounded Borel sets and for which the measure of a point is at most 1. In this way, $N$ can be identified with the set of all configurations of points in $\mathbb{R}^2$, without limit points. Let $\mathcal{N}$ be the $\sigma$-algebra of $N$ generated by sets of the form $\{\nu \in N : \nu(A) = k\}$, for all integers $k$ and bounded Borel sets $A$. A (planar) point process $X$ is defined as a measurable mapping from a probability space $(\Omega, \mathcal{F}, P)$ into $(N, \mathcal{N})$. For $A \in \mathcal{B}^2$, we denote by $X(A)$ the random number of points inside $A$. In this paper, $X$ will always be a Poisson process with density $\lambda > 0$. We sometimes abuse notation and write $x \in \nu$, for $x \in \mathbb{R}^2$ and $\nu \in N$, to express that $x$ is one of the points of $\nu$.

We define a shift operation $T_t : \mathbb{R}^2 \to \mathbb{R}^2$ as a translation in $\mathbb{R}^2$ over the vector $t \in \mathbb{R}^2$, such that $T_t(x) = t + x$ for all $x \in \mathbb{R}^2$. The shift $T_t$ induces in a natural way a shift transformation on $N$, which we also denote by $T_t$. Let, for all $x \in \mathbb{R}^2$ and $r \geq 0$, $D(x, r)$ be the disc of radius $r$ centered at $x$: $D(x, r) = \{y \in \mathbb{R}^2 : |y - x| \leq r\}$. A circle of radius $r$ centered at $x$ is the set $\{y \in \mathbb{R}^2 : |y - x| = r\}$. The boundary of a set $A$ will be denoted by $\partial A$.

We call two discs $D_i, D_j$ *adjacent* if $D_i \bigcap D_j \neq \emptyset$. We write $D_i \leftrightarrow D_j$ if there exists a sequence $D_{i_1}, D_{i_2}, \ldots, D_{i_k}$ of discs such that $D_{i_1} = D_i$, $D_{i_k} = D_j$, and $D_{i_l}$ is adjacent to $D_{i_{l+1}}$ for $1 \leq l < k$. A *(connected) component* or *cluster* is a set $\{D_i : i \in J\}$ of discs which is maximal with the property that $D_i \leftrightarrow D_j$ for all $i, j \in J$. We identify a component with the set of centers of the discs in it.

We next formally define a covering algorithm: A *covering algorithm* $\mathcal{A}$ with discs of radius $r$, is a measurable mapping $\mathcal{A} : N \to N$ with the following properties:

1. for all $x \in \mathcal{A}(\nu)$ there exists $y \in \nu$ such that $y \in D(x, r)$,

2. for all $y \in \nu$ there exists $x \in \mathcal{A}(\nu)$ such that $y \in D(x, r)$.

We define the *occupied region* $C$ of $\mathcal{A}(\nu)$ as the union $\bigcup_{x \in \mathcal{A}(\nu)} D(x, r)$.

In this paper, we examine different classes of covering algorithms, which we define as follows:

*Grid Algorithms.* Let $G \subset \mathbb{R}^2$ be the set of all vertices of a two-dimensional lattice. A grid algorithm $\mathcal{A}$ constrains the covering discs to be centered at the vertices of $G$.

That is, $x \in \mathcal{A}(\nu)$ implies $x \in G$. Naturally we require $G$ to be such that every point can be covered by a disc centered at some vertex of $G$.

*Flat Algorithms.* A flat algorithm $\mathcal{A}$ has the property that its restriction to any box of size $n \times n$ contains at most $k(n)$ discs, for some $k(n) < \infty$. Note that $k(n) < \infty$ for some $n$, immediately implies that $k(m) < \infty$, for any $m$, as we can cover an $m \times m$ square by a finite number of $n \times n$ squares.

*Finite Horizon Algorithms.* Let $B_n(x)$ be the box of size $n \times n$ centered at $x$, and let, for all $\nu \in N$, $\nu|_{B_n(x)}$ denote the restriction of $\nu$ to $B_n(x)$. In other words, $\nu|_{B_n(x)}$ can be identified with the set of points $\{\nu \cap B_n(x)\}$. We say that a covering algorithm $\mathcal{A}$ has finite horizon if there exists a constant $h \geq 0$ (the *horizon*), so that whenever $\nu|_{B_{n+2h}(x)} = \nu'|_{B_{n+2h}(x)}$, we have $\mathcal{A}(\nu)|_{B_n(x)} = \mathcal{A}(\nu')|_{B_n(x)}$, for all $n$ and $x$. In words, this means that changing $\nu$ outside $B_{n+2h}(x)$ does not change the covering inside $B_n(x)$.

*Shift Invariant Algorithms.* A shift invariant algorithm $\mathcal{A}$ is defined by the property that $T_t(\mathcal{A}(\nu)) = \mathcal{A}(T_t(\nu))$, for all $t$.

*$n$-Square Algorithms.* An $n$-square algorithm is obtained as follows. Partition the plane into boxes of size $n \times n$. For each such box $B_n$, the covering of the points inside $B_n$ should use the minimal number of discs possible.

Suppose now that we want to cover the points of $X$ by the covering algorithm $\mathcal{A}$, that is, we consider the measurable map $\mathcal{A} \circ X : \Omega \to N$. This Boolean model is denoted by $(X, \mathcal{A}) = (X, \lambda, r, \mathcal{A})$, where $\lambda$ is the density of $X$, and $r$ the radius of the covering discs. The law of this process is denoted by $P_{\lambda,r}$. The standard Poisson Boolean model that places a disc of radius $r$, centered at each point of $X$ is obtained when we take $\mathcal{A}$ to be the identity, and is denoted by $(X, \lambda, r)$. In this model there exists $\lambda_c(r)$ such that for $\lambda \leq \lambda_c(r)$ we have no infinite cluster a.s., while for $\lambda > \lambda_c(r)$ there is an infinite cluster with probability 1. We often denote $\lambda_c(1)$ by $\lambda_c$ and scaling implies that $\lambda_c(r) = \lambda_c(1)/r^2$ (see Meester and Roy (1996) for more details).

Next, we define the *density* of $(X, \mathcal{A})$. Let $N_{(X,\mathcal{A})}(n)$ be the (random) number of discs centered inside the box $B_n(0)$. The density of $(X, \mathcal{A})$ is given by $\lim_{n\to\infty} N_{(X,\mathcal{A})}(n)/n^2$, whenever this limit exists a.s. and is an a.s. constant.

Finally, we introduce one more piece of terminology. If $(X, \mathcal{A})$ contains an unbounded component of discs with positive probability, we say that $(X, \mathcal{A})$ *percolates*.

## 2.3 Percolation

In this long section we think of $r$ as being fixed, while $\lambda$ varies. Accordingly, we sometimes write $P_\lambda = P_{\lambda,r}$. We also use $P$ to mean $P_{1,1}$. The expectation under $P$ we denote by $E$.

Our first result deals with the lack of percolation for small values of $\lambda$.

**Theorem 2.1** *For any covering algorithm $\mathcal{A}$, there exists a $\lambda_0(r) > 0$ such that for all $0 < \lambda \leq \lambda_0$, $(X, \lambda, r, \mathcal{A})$ does not percolate.*

**Proof of Theorem 2.1.** Assume that, with positive probability, there is an unbounded connected component of covering discs for $(X, \lambda, r, \mathcal{A})$. Then with positive probability, there is an unbounded connected component in the Poisson Boolean model $(X, \lambda, 2r)$. That is because two intersecting covering discs in $(X, \lambda, r, \mathcal{A})$ cover points that are at a distance of at most $4r$ to each other; and the Poisson Boolean model $(X, \lambda, 2r)$ places discs of radius $2r$ at each of the covered points. We then choose $\lambda_0 = \lambda_c/(2r)^2$, so that $(X, \lambda, 2r)$ does not form an unbounded connected component a.s. for $\lambda \leq \lambda_0$. □

A symmetric result to Theorem 2.1, i.e., percolation for large values of $\lambda$, depends on the type of covering algorithm used:

**Proposition 2.2** *There exists a covering algorithm $\mathcal{A}$, such that for all $\lambda$, $(X, \lambda, r, \mathcal{A})$ does not percolate.*

**Proof of Proposition 2.2.** The proof is constructive. Draw circles of radii $\{3kr, k \in \mathbb{N}\}$ around the origin, and notice that a.s. no Poisson point falls on any of these circles. Then cover the Poisson points, with discs of radius $r$, without intersecting these circles. Notice that the circles divide the plane into finite annuli and, since

each cluster of discs resides in at most one of these finite annuli, each cluster must be bounded, whatever the value of $\lambda$. □

We next look at families of algorithms that do percolate for large values of $\lambda$, starting with flat algorithms. Recall that each such algorithm, $\mathcal{A}$, has the property that the restriction of $\mathcal{A}$ to any box of size $n \times n$ contains at most $k = k(n)$ discs, for any value of $\lambda$. Note that this really is a weak requirement, since we can *completely* cover the box using at most $\alpha\lceil(n/r)\rceil^2$ discs, for some $\alpha \leq 1$. Any 'sensible' algorithm should therefore be flat.

**Theorem 2.3** *Let $\mathcal{A}$ be a flat covering algorithm. Then there exists $\lambda_1 < \infty$, so that $(X, \lambda, r, \mathcal{A})$ percolates for all $\lambda > \lambda_1$.*

At first sight, the statement of the theorem is counterintuitive, since we claim that we force percolation by *restricting* the number of discs. The point is that by restricting the number of discs (independently of $\lambda$), the requirement of covering all points with this restricted number of discs makes percolation unavoidable.
Two consequences of Theorem 2.3 and its proof that are important in practice, are the following theorems.

**Theorem 2.4** *For any grid covering algorithm $\mathcal{A}$, there exists a $\lambda_1 < \infty$, such that $(X, \lambda, r, \mathcal{A})$ percolates for all $\lambda > \lambda_1$.*

This theorem can be proved by application of Theorem 2.3, as all grid algorithms are flat. The proof below however is more elegant and offers more insight into the structure of grid algorithms.

**Proof of Theorem 2.4.** The proof relies on a construction that maps the covering discs to a discrete site-percolation model. We illustrate the idea by considering a square lattice and a distance between two neighboring lattice vertices of one. Call a covering disc centered at a lattice vertex a grid disc. Clearly, the radius of a disc must be $r \geq \frac{\sqrt{2}}{2}$, in order to be able to cover all possible points on the plane by using only grid discs. For any $r \geq \frac{\sqrt{2}}{2}$, the number of grid discs that intersect a lattice square $ABCD$ is finite and they partition the square into some number $k_r$ of small regions

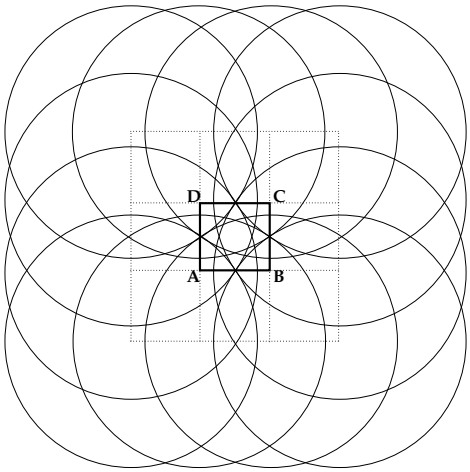


Figure 2.1: **Mapping to the site percolation model.** *The grid discs partition the square ABCD into a finite number of small areas.*

$A_i$ (see Figure 2.1). If at least one point of the Poisson point process falls into each region $A_i$, then the entire square $ABCD$ must be covered by grid discs. Now view each lattice square as a site of a site percolation model. Call the site occupied if there is at least one point of the Poisson process situated inside each region $A_i$, for $i = 1 \ldots k_r$. Note that the occupancy of a site is independent of the occupancy of other sites and the probability of a site being occupied is given by $p = \prod_{i=1}^{k_r}(1 - e^{-\lambda \ell(A_i)})$. Moreover, if two adjacent sites are both occupied, then the corresponding covering discs form a connected component. Thus, if there is an unbounded component of occupied adjacent sites, then there is an unbounded connected component of covering discs. Next, we choose $\lambda$ large enough so that $p > p_c$, where $p_c$ is the critical probability for site percolation on a square lattice. The a.s. existence of an unbounded connected component of covering discs immediately follows. □

**Theorem 2.5** *For any $n > 0$ there exists a $\lambda_n < \infty$, such that for any $n$-square algorithm $\mathcal{A}_n$, $(X, \lambda, r, \mathcal{A}_n)$ percolates for all $\lambda > \lambda_n$.*

Since an $n$-square algorithm is flat, it follows from Theorem 2.3 that for each $n$-square algorithm, we can find such a $\lambda_n$. The fact that this $\lambda_n$ depends only on $n$ and not on the particular $n$-square algorithm we choose, follows from the proof of this theorem, by noting that $\lambda_1$ in the statement of the theorem only depends on $k(n)$.

Another version of Theorem 2.3 requires an upper bound on the density of discs, the shift invariance of the algorithm under a pair of linearly independent shifts and the algorithm to be finite horizon.

**Theorem 2.6** *Let $\mathcal{A}$ be a finite horizon covering algorithm such that a constant $\delta < \infty$ exists such that*

$$\limsup_{n\to\infty} \frac{\textit{number of discs in } B_n}{n^2} < \delta, \ \textit{a.s.} \ ,$$

*and which is stationary under a pair of linearly independent shifts. Then there exists $\lambda_1 < \infty$, so that $(X, \lambda, r, \mathcal{A})$ percolates for all $\lambda > \lambda_1$.*

Johan Segers (personal communication) has pointed out that although finite horizon algorithms of bounded density which are stationary under any *pair* of linearly independent vectors must percolate, for a sufficiently high density of points, there exist finite horizon covering algorithms of bounded density which are stationary under shifts of *one* vector, and do not percolate for any $\lambda$.

Before we prove Theorems 2.3 and 2.6, we first state and prove a preliminary geometric lemma.

**Lemma 2.7** *Consider a collection of discs of radius $r$, with the property that at most $k(n) < \infty$ discs intersect any box of size $n \times n$. Then there exists an $\epsilon = \epsilon(n, r) > 0$ with the following property: if there are, either, at least two clusters that intersect the boundaries of both $B_{n+r}(x)$ and $B_{n+2r}(x)$, or a cluster wholly contained in $B_{n+2r}(x)$, then there is a circle of radius $\epsilon$, contained in $B_{n+3r}(x)$, which is not intersected by any disc.*

**Proof of Lemma 2.7.** We write $B_n = B_n(x)$. All discs that intersect $B_{n+3r}$ must be centered inside $B_{n+5r}$. Therefore, at most $k = k(n + 5r)$ discs intersect $B_{n+3r}$. Let $C$ be a component that intersects the boundaries of both $B_{n+r}$ and $B_{n+2r}$. The number of discs in $C$ that intersect $B_{n+2r}$ is denoted by $l$. Note that $l \leq k$.

Consider a section $AB$ of the perimeter of $C$, from the boundary of $B_{n+r}$ to the boundary of $B_{n+2r}$, which does not intersect either of these boundaries except at its

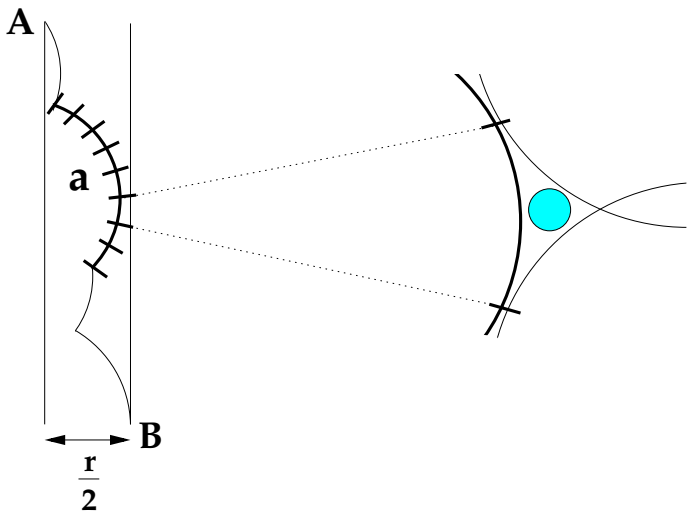


Figure 2.2: **Subdividing the arc.** An edge $AB$ of a component $C$ connecting the two boundaries of $B_{n+r}$ and $B_{n+2r}$, has length at least $r/2$. This edge contains an arc $a$ of length at least $r/2l$. Arc $a$ is divided up into $k$ sections, and by one of these we can place a small disc of radius $\epsilon$ that is not contained in any cluster.

ends (see Figure 2.2). This section has length at least $r/2$, and consists of parts of the boundaries of at most $l$ discs, each of which appears only once. This latter fact follows from the observation that, since the distance between the boundaries of the two boxes is only $r/2$, any disc that contributes to an arc in $AB$, must overlap the boundary of at least one box. Moreover, note that were $AB$ to contain two disjoint arcs from the same disc, then any disc overlapping that disc in order to make these arcs disjoint, must overlap the boundary of the box not overlapped by the first disc. Therefore these arcs would be in disjoint sections of $\partial C \cap B_{n+2r}/(B_{n+r} \cup \partial B_{n+2r})$. See Figure 2.3. It follows that at least one arc in $AB$ is of length at least $r/2l$. Call this arc $a$.

Note that there are at most $k-1$ discs intersecting $B_{n+3r}$, if we do not count the one that has $a$ as a part of its boundary, and none of them intersect $a$, except at its end points. If we divide $a$ into $k$ arcs of equal size, then each of these discs will be nearest to one of these smaller arcs – assign this arc to this disc. One of the smaller arcs (of size at least $r/2kl$ ) will, however, have no disc is assigned to it. This means that the space left by discs tangent to the ends of this smaller arc cannot be

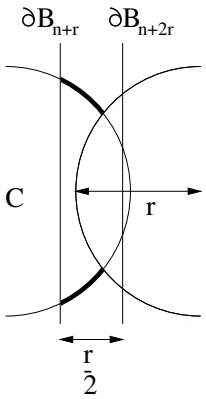


Figure 2.3: **No discs can have two disjoint components in $AB$.** Two disjoint arcs from the perimeter of one disc, in a component $C$ connecting the two boundaries of $B_{n+r}$ and $B_{n+2r}$, must be in disjoint parts of $\partial C \cap B_{n+2r}/(B_{n+r} \cap \partial B_{n+2r})$.

covered, and we can choose $\epsilon$ so small that a disc of radius $\epsilon$ fits into this space (see Figure 2.2). The value of $\epsilon$ that we have to choose only depends upon $r$ and $n$.

The same argument applies to a component wholly contained in $B_{n+2r}$, by considering its perimeter rather than its boundary between $B_{n+r}$ and $B_{n+2r}$. □

**Proof of Theorem 2.3.** Let $t, u \in \mathbb{Z}$, and denote the box of size $n \times n$ centered at $(tn, un)$ by $B_n(tn, un)$, as before. Let $\epsilon$ be chosen as in Lemma 2.7. We say that the vertex $(t, u)$ is a *neighbor* of $(t', u')$ if the boxes $B_n(tn, un)$ and $B_n(t'n, u'n)$ share an edge or corner. We call a vertex $(t, u)$ *good* if all discs of radius $\epsilon$ contained in $B_{n+3r}(tn, un)$ contain at least one point of the Poisson process. Denote the event that $(t, u)$ is good by $G(t, u)$. It is clear that when $\lambda \to \infty$, the probability of $G(t, u)$ converges to 1. It is also clear that $G(t, u)$ and $G(t', u')$ are independent whenever $\max\{|t - t'|, |u - u'|\} \geq \lceil \frac{3r}{n} \rceil$, for $n$ larger than $2r$. Hence, the configuration of good sites is formed through a discrete, finite-range dependent percolation process, and it follows then from Durrett and Griffeath (1983) that for $\lambda$ high enough, the good vertices percolate, i.e., contain an infinite component of good squares with probability one. What does this mean for our covering? Consider a good square $B_n$. By Lemma 2.7 any component cannot be wholly contained in $B_{n+2r}$, therefore, a component that covers points inside $B_{n+2r}$, must also intersect the boundary of $B_{n+2r}$. Also by Lemma 2.7, there can be only one component that intersects the boundaries

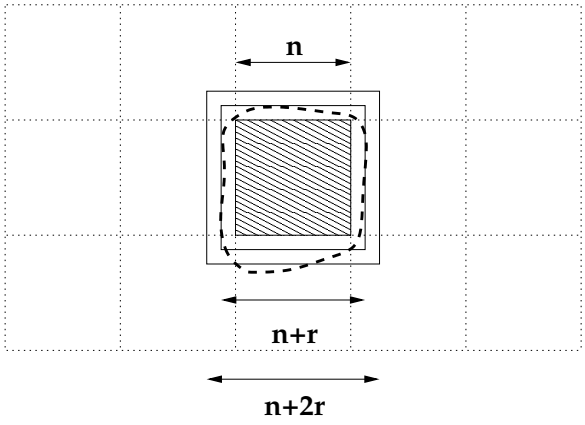


Figure 2.4: **A good square.** There is only one component of discs (represented by the dashed line) that intersects both $B_{n+2r}$ and $B_{n+r}$. This component must reach to within $2\epsilon$ of all edges of $B_{n+r}$, and will therefore intersect a component of an adjacent good square.

of both $B_{n+2r}$ and $B_{n+r}$. For $n$ larger than $2\epsilon$ such component exists and must reach to within $2\epsilon$ of *all* edges of $B_{n+r}$, as, by the definition of a good square, there is no disc of radius $\epsilon$ inside $B_{n+r}$ without any points of the Poisson process inside it (see Figure 2.4). Thus, the components associated with adjacent good squares must overlap, and we must have an infinite component of discs with probability one. □

We thank Johan Segers for the remark that this proof does not depend upon the algorithm being finite horizon.

**Proof of Theorem 2.6.** The proof in this case is a little more complicated, but uses the same idea as that of Theorem 2.3. Without loss of generality assume that the algorithm be stationary under the shifts $T_{(m,0)}$ and $T_{(0,m)}$, for some $m$. Let $h$ be the horizon of the algorithm, and assume $m > \max(1, h + 5r)$, again without loss of generality. Choose $\gamma > 0$ sufficiently small so that $1 - \gamma$ is strictly above the critical point for site percolation on the lattice $\{(tm, tu) : t, u \in \mathbb{Z}\}$ with edges between neighboring sites. Take $n$, a multiple of $m$, so large that the probability that $B_{n+5r}$ is intersected by more than $(\delta + 1)(n + 5r)^2$ discs is less than $\gamma$, uniformly in $\lambda$. We then use $(\delta + 1)(n + 5r)^2$ as our $k$ in the lemma, and find an $\epsilon$ such that, if we have at most $(\delta + 1)(n + 5r)^2$ discs intersecting $B_{n+5r}$ in the way described in the lemma, then we must have a circle of radius $\epsilon$ empty of Poisson points.

In the proof of the theorem we then call $B_n$ good if $B_{n+3r}$ has both no disc of radius $\epsilon$ empty of Poisson points in it and $B_{n+5r}$ contains at most $(\delta+1)(n+5r)^2$ points. Other boxes are called good analogously. If $\lambda$ is high enough, these boxes percolate, and we again have an infinite component of discs. □

We have seen that both finite-horizon, shift-invariant algorithms under a bounded density condition and flat algorithms necessarily percolate for high enough $\lambda$. It is natural to ask whether this always holds for shift invariant algorithms. It turns out that for these algorithms, in general large values of the density $\lambda$ of the points do not guarantee the a.s. existence of an unbounded connected component. This is shown by describing a shift invariant covering algorithm that does not form an unbounded connected component for all $\lambda$:

**Theorem 2.8** *There exists a shift invariant covering algorithm $\mathcal{A}$ of all the points of $X$ by discs of radius $r$, such that for all $\lambda$, $(X, \lambda, r, \mathcal{A})$ does not percolate.*

The proof of Theorem 2.8 is constructive and rather technical, so we will sketch the algorithm here, and postpone the proof to the end of the chapter. The covering we describe can be seen as a shift-invariant variant of that in Theorem 2.2 and will also have a density of discs centers equal to the density of points.

**Sketch of proof of Theorem 2.8.** Without loss of generality, consider using covering discs of radius $r = 1$. As the covering should be a deterministic function of the points, we must first calculate $\lambda$ in the realization of the point configuration. We do this by setting

$$\lambda = \lim_{n\to\infty} \frac{\text{number of points in } B_n(0)}{n^2}$$

if this limit exists and is constant, which happens with probability 1, and otherwise we take $\lambda = 1$.

Our construction places circles of radii $r = 18^m$, with $m \in \mathbb{N}$, where we see certain configurations of points in the plane. The resulting structure is composed of clusters of circles that are finite, but enclose every bounded region of the plane. We then find

some curves near the boundaries of these clusters and cover all the points with discs of radius 1, without touching these curves.

Let us define a *potential-point* to be a Poisson point with at least one other point in the half-disc of radius $\frac{1}{2}$ to the right of it, and no points in the disc of radius 1 centered at it, except in the aforementioned half-disc. We then call a potential point an *m-point*, for integer $m$, if it has its nearest neighboring point between $b_m$ and $b_{m+1}$ away, where $b_1 = \frac{1}{2}, b_2, b_3 \ldots$ is a decreasing sequence of positive numbers, such that the density of $m$-points is exactly $\epsilon 18^{-2m}$, for some small number $\epsilon > 0$. How small $\epsilon$ will be required to depend upon $\lambda$. Around each $m$-point we place an m-circle of radius $18^m$.

A theorem of Meester and Roy (1994) allows us to show that every bounded region of the plane is a.s. wholly enclosed in some m-circle. Lots more work, based upon an idea of Meester and Roy (1996) for fractal continuum percolation, shows us that each cluster of overlapping m-circles is finite, and moreover the maximal connected component of points strictly within distance 9 of any m-circle is also finite.

We construct *smooth* curves based upon the finite m-circle clusters. Consider some maximal set of m-circles such that, if we take the locus of all points in the plane at a distance of at most 4 from the circles, then this region forms a connected set, and run a disc of radius 2 around the outside of this set (see Figure 2.5). The disc traces out a kind of finite sausage shape around the clusters.

We take the inside edge of this sausage as our curve, and note that a covering disc (of radius 1) can get arbitrarily close to any point of the curve without touching it. We construct these smooth curves for each set of sufficiently close clusters, noting that they surround every bounded area in the plane, are always finite, and never come within distance $8 < 9$ of each other.

We finally cover our Poisson points as follows:

If a point is at a distance more than 2 from every smooth curve, then we center a covering disc at the point.

If a point is within distance 2 of a smooth curve, then we place a disc so that its perimeter covers the point, and so that the center of the disc is at the maximum

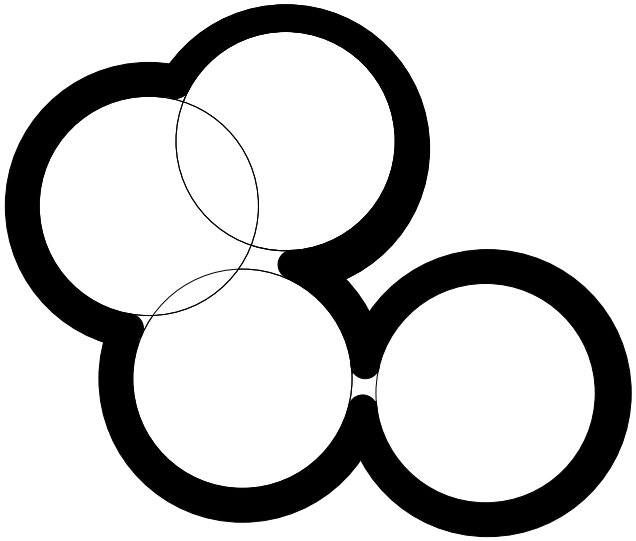

Figure 2.5: **Sausages.** By sliding a disc of radius 2 along the boundary of some cluster, we trace a kind of sausage shape.

distance away from the smooth curve. If there are a number of such possible positions, we choose the leftmost.

It immediately follows that, for any given value of $\lambda$, a.s. there is no percolation.

For more details on the proof, the reader can refer to the last section of this chapter.

## 2.4 Scaling

In this section we consider an extension that is useful to model the transmission power in wireless communication networks. We look at the percolation properties of our model, for different values of the connectivity range of the base stations and of the clients.

Let $r$ be the clients' connectivity range and let $R$ be the base stations' connectivity range. It follows that discs of radius $r$ are used to cover the points of $X$ and two disc centers are considered connected, if their distance is less than, or equal to $R$ (see Figure 2.6). We are interested in the a.s. existence of an unbounded connected component of disc centers, for large values of the density $\lambda$ of the Poisson point

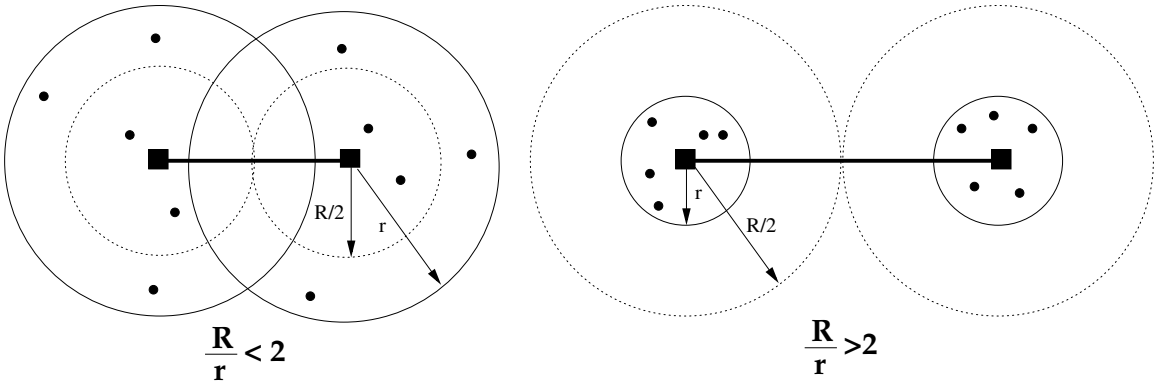


Figure 2.6: **Scaling.** Points are covered by solid line discs of radius $r$. Discs centers are considered connected if their distance is at most $R$.

process. Our result is the following.

**Theorem 2.9 (The Scaling Theorem)** *Let $G \subset \mathbb{R}^2$ be the set of all vertices of a square lattice in which the distance between two neighboring lattice vertices is $\delta$. Call two disc centers connected if their distance is at most $R$. We have:*

***Case 1***. *If $\frac{R}{r} \leq 1$ then, for any $\delta > 0$, there exists a grid covering algorithm $\mathcal{A}$ that places discs only at the vertices of $G$, such that, for all $\lambda$, $(X, \lambda, r, \mathcal{A})$ does not percolate.*

***Case 2***. *If $1 < \frac{R}{r} < 2$ then, there exists a $\delta > 0$, depending on $\frac{R}{r}$, such that there exists a grid covering algorithm $\mathcal{A}$ that places discs only at the vertices of $G$ and, for all $\lambda$, $(X, \lambda, r, \mathcal{A})$ does not percolate.*

***Case 3***. *If $\frac{R}{r} = 2$ then, for any $\delta > 0$, for any grid covering algorithm $\mathcal{A}$, there exists a $\lambda_1 < \infty$, such that, for all $\lambda > \lambda_1$, $(X, \lambda, r, \mathcal{A})$ percolates.*

***Case 4***. *If $\frac{R}{r} > 2$ then, for any covering algorithm $\mathcal{A}$, there exists a $\lambda_1 < \infty$, such that, for all $\lambda > \lambda_1$, $(X, \lambda, r, \mathcal{A})$ percolates.*

Note that Case 4 of the theorem states that in a wireless network in which base stations can communicate at a distance larger than twice the maximum communication distance to the clients, an unbounded connected component forms a.s. for large values of the density of the clients, regardless of the covering algorithm used to build the cellular network.

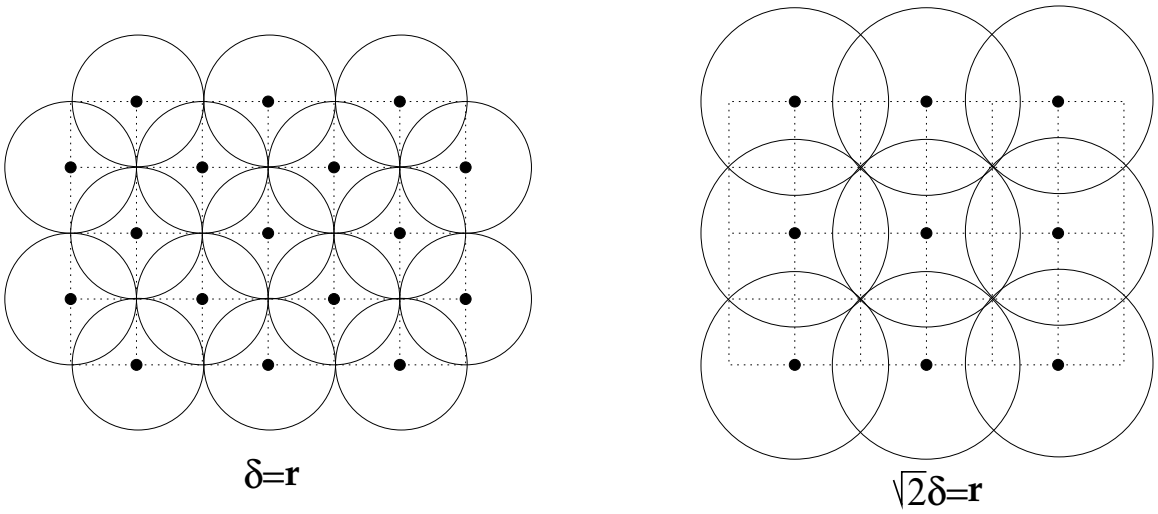


Figure 2.7: **Theorem 2.9, Case 1.** Two tilings of the plane by discs centered on a grid that do not cover each other's centers.

**Proof of Theorem 2.9.**

**Case 1.** We can restrict our attention to $\frac{R}{r} = 1$. That is because if a grid covering algorithm does not form an unbounded connected component when $\frac{R}{r} = 1$, then it does not form such a component when $\frac{R}{r} < 1$ either.

Note that, for $\frac{R}{r} = 1$, two disc centers are considered connected if and only if the corresponding discs of radius $r$ cover each other's centers. Moreover, in order to be able to cover all points on the plane by using only grid discs of radius $r$, the grid spacing $\delta$ must be at most $\sqrt{2}r$. We now consider all values of the grid spacing $\delta \leq \sqrt{2}r$, subdivided into intervals.

For $r < \delta \leq \sqrt{2}r$, any grid covering algorithm places discs on the plane that do not touch each other's centers.

For $\frac{r}{\sqrt{2}} < \delta \leq r$, consider the tiling of the plane depicted in the left part of Figure 2.7. Discs of this tiling do not cover each other's centers, therefore, any grid covering algorithm that covers all the points of $X$ using only the grid discs depicted in the left part of Figure 2.7 does not form an unbounded connected component, a.s., for any value of $\lambda$.

For $r/2 < \delta \leq \frac{r}{\sqrt{2}}$, consider the tiling depicted in the right part of Figure 2.7. Discs of this tiling do not cover each other's centers, therefore, any grid covering

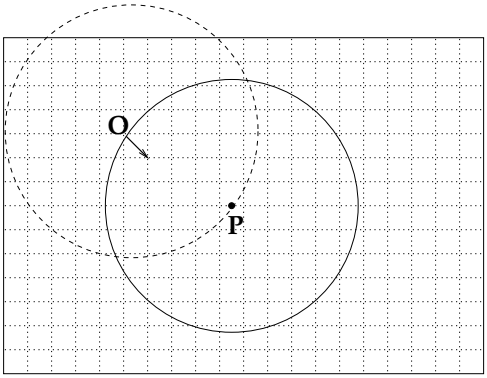


Figure 2.8: **Theorem 2.9, Case 2.** A Poisson point $P$ is covered by a disc centered at point $O$, that is within $r$ from $P$. The covering disc can be moved to a nearby grid vertex, that is inside the solid disc and is within $\sqrt{2}\delta$ from $O$, and still covers point $P$.

algorithm that covers all the points of $X$ using only the grid discs depicted in the right part of Figure 2.7 does not form an unbounded connected component, a.s., for any value of $\lambda$.

For the remaining values of $\delta$, we can use the same tiling of the two cases depicted in Figure 2.7, scaled by the appropriate factor.

**Case 2.** In this case, two disc centers are considered connected if and only if the corresponding discs of radius $r$ overlap by a region of measure at least $\epsilon > 0$, where the value of $\epsilon$ depends on the ratio $\frac{R}{r}$.

We follow a similar construction as that used to prove Proposition 2.4. Draw circles of radii $\{3kr, k \in \mathbb{N}\}$ around the origin, and notice that a.s. no Poisson point falls on any of these circles. Then cover the Poisson points, each with a disc of radius $r$, without intersecting these circles. Notice that the circles divide the plane into finite annuli, whose boundaries are not covered by discs. We now approximate this covering using a grid covering. Consider a square grid $G$ and move each disc of the above covering to the nearest vertex of $G$ that still allows to cover its corresponding Poisson point. Note that each disc needs to be translated by at most $\sqrt{2}\delta$. That is because a Poisson point is covered by a disc centered within $r$ from it, and there is always a grid vertex, within radius $r$ from the Poisson point, that is also within $\sqrt{2}\delta$ from this center (see Figure 2.8). By this translation, some discs may intersect

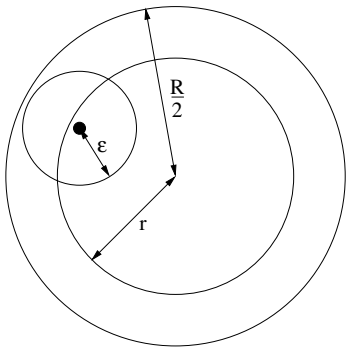


Figure 2.9: **Theorem 2.9, Case 4.** A small discs of radius $\epsilon = R/2 - r$ around a point of $X$ must lie inside the disc of radius R/2 around the center of the covering disc.

the boundaries of the annuli, that were previously untouched. We then take the grid size $\delta$ so small, that any two discs that intersect these boundaries do not overlap by an area of measure greater than or equal to $\epsilon$, and are therefore not connected. It immediately follows that, for any given value of the density $\lambda$, a.s. there is not any unbounded connected component for this covering.

**Case 3.** This case is proven by Theorem 2.4.

**Case 4.** In this case, two discs centers are considered connected if and only they are at a distance of at most $R$ (see right-hand side of Figure 2.6). In other words, we are interested in the percolation of large discs of radius $R/2$ around the disc centers. A small disc of radius $\epsilon = R/2 - r > 0$ centered at a point of the Poisson process must be contained in the large disc of radius $R/2$ around the center of the disc covering that point. See Figure 2.9. Therefore if these small discs percolate, as they will when $\lambda > \lambda(\epsilon)$, the large discs must also percolate. □

## 2.5 Optimal algorithms

In this section we explore the notion of optimal algorithms, i.e., those which uses as few discs as possible, and show that $n$-square algorithms are asymptotically optimal. The work in this section is philosophically close to that in Yukich (1998).

Fix the density of points, $\lambda$, and $r$, and extend the definition of the density of a

covering, $\mathcal{A}$, to be

$$\delta_{\mathcal{A}} = \lim_{n\to\infty} \frac{\text{number of discs centered in } B_n}{n^2}$$

if this exists and is a constant a.s., and $\infty$ otherwise. We then define the *optimal density* to be

$$\delta^{opt} = \inf_{\mathcal{A}} \delta_{\mathcal{A}},$$

where the infimum runs over all covering algorithms. An *optimal algorithm*, $\mathcal{A}^{opt}$, is one for which, a.s., $\delta^{opt} = \delta_{\mathcal{A}^{opt}}$. We would not expect in general such an algorithm to have a finite horizon.

First we show that $n$-square algorithms can get as close as we like to the optimal density. Define $\delta_n$ to be the density of discs under an $n$-square algorithm. By ergodicity $\delta_n < \infty$ exists. Notice that $\delta_n$ does not depend upon the particular $n$-square algorithm we choose.

**Theorem 2.10** *Given $\epsilon > 0$, there exists $n_\epsilon$ such that $\delta_{n_\epsilon} < \delta^{opt} + \epsilon$, and hence $\delta^{opt} = \inf_n \delta_n$.*

**Proof of Theorem 2.10** We prove this theorem by contradiction, so suppose that we can find an $\epsilon$ such that there is no $n$-square covering with density between $\delta^{opt}$ and $\delta^{opt} + \epsilon$. We can find another covering, $\hat{\mathcal{A}}$ say, with density $\delta_{\hat{\mathcal{A}}} \in [\delta^{opt}, \delta^{opt} + \epsilon/4]$, by the definition of $\delta^{opt}$.

Choose $\gamma > 0$ such that $(1-\gamma)(\delta^{opt} + \epsilon/2) + \gamma(1+\epsilon/2)/r^2 < \delta^{opt} + \epsilon$. Note that the number of discs necessary to cover an $n$-square is at most $\lceil n/r \rceil^2$.

As $\delta_{\hat{\mathcal{A}}} = \lim_{n\to\infty} \frac{\text{number of discs centered in } B_n}{n^2}$, a.s., we can choose $n_\epsilon > 1$ sufficiently large that a) the number of discs centered in $B_{n_\epsilon}$ is less than $n_\epsilon^2(\delta^{opt} + \epsilon/2)$ with probability larger than $1-\gamma$, and b) $\lceil n/r \rceil^2 (1/n)^2 \le (1+\epsilon/2)/r^2$.

Given a finite set of points there are a finite number of distinct possible coverings of those points, where we call two coverings *distinct* if there exist a set of points covered by one disc in one of the coverings but covered by two or more in the other. Coverings that are not distinct are *equivalent*. We will occasionally work with the

equivalence classes of theses coverings.

We now define a covering of the box $B_{n_\epsilon}$ which is based upon $\hat{\mathcal{A}}$ but is independent of the points outside $B_{n_\epsilon}$. Given a point configuration, $\pi$, in $B_{n_\epsilon}$ there is a finite set of equivalent classes of coverings of these points. Let $S_\pi$ be the subset of equivalence classes which occur with positive probability if we use $\hat{\mathcal{A}}$ to cover $\pi \cup X|'_{B^c_{n_\epsilon}}$, where $X|'_{B^c_{n_\epsilon}}$ is a Poisson process on $B^c_{n_\epsilon}$ independent of $\pi$ and $X$. In each equivalence class all coverings use the same number of discs so we can choose an equivalence class from $S_\pi$ in which the number of discs used is minimal, according to some deterministic rule. Choose a covering from this class, according to some other deterministic rule. This is the covering we use to cover $B_{n_\epsilon}$. Note that this is independent of the actual point process outside $B_{n_\epsilon}$. The expected number of discs required to cover the points in $B_{n_\epsilon}$ under this algorithm can be at most that under $\hat{\mathcal{A}}$.

We now divide up the plane into squares of size $n_\epsilon$, and cover each square independently using the same algorithm in each as we use on $B_{n_\epsilon}$. For those squares for which this requires at most $n_\epsilon^2(\delta^{opt} + \epsilon/2)$ discs, we use this covering. In the other squares we cover optimally, which means that we have a density of at most $(1 + \epsilon/2)/r^2$ on these squares.

We have created an algorithm that covers each square of size $n_\epsilon$ independently, and which therefore cannot have a density less than $\delta_{n_\epsilon}$. However, the density of the covering is at most $(1 - \gamma)(\delta^{opt} + \epsilon/2) + \gamma(1 + \epsilon/2)/r^2 < \delta^{opt} + \epsilon$, and we have a contradiction. □

Next, we strengthen the previous proposition.

**Theorem 2.11** *Let $\delta_n$ be the density of discs under an $n$-square algorithm. Then* $\lim_{n\to\infty} \delta_n = \delta^{opt}$ .

**Proof of Theorem 2.11** We know that $\delta^{opt} = \inf_n \delta_n$, and that $\delta_n n^2$ is the expected number of discs needed to cover an $n$-square. For the sake of contradiction suppose that there exist $\epsilon > 0$ and a sequence $\{t_1, t_2, \ldots\}, \lim_i t_i = \infty$ such that $\delta_{t_i} > \delta^{opt} + \epsilon$ for all $i$. However, we can choose $\alpha$ so that $\delta_\alpha < \delta^{opt} + \epsilon/3$. We can also choose $i$ so large that $\left(1 - \left\lfloor \frac{t_i}{\alpha} \right\rfloor^2 \left(\frac{\alpha}{t_i}\right)^2\right) \lambda < \epsilon/3$. The reason we need this will become clear

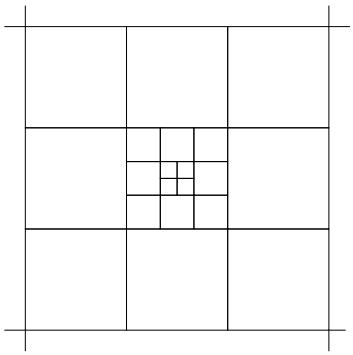

Figure 2.10: **Division of the plane into squares of increasing size.**

shortly.

We cover the square $B_{t_i}$ as follows. We first divide as much of the square as possible into squares of size $\alpha$. Each of these we cover optimally. We have an area of $(t_i^2 - \alpha^2 \left\lfloor \frac{t_i}{\alpha} \right\rfloor^2)$ left, and each of the points in this area we cover with one disc. This gives us a covering with expected density,

$$\left\lfloor \frac{t_i}{\alpha} \right\rfloor^2 \left(\frac{\alpha}{t_i}\right)^2 \delta_\alpha + \left(1 - \left\lfloor \frac{t_i}{\alpha} \right\rfloor^2 \left(\frac{\alpha}{t_i}\right)^2\right) \lambda \leq \delta^{opt} + \epsilon/3 + \epsilon/3.$$

However, the minimal expected density for any algorithm covering the box $B_{t_i}$, $\delta_{t_i} > \delta^{opt} + \epsilon$, so we have a contradiction. □

Note that it is still not clear a priori that an optimal algorithm should exist. The existence of an optimal density, defined as the infimum over all attainable densities, does not have to be attainable itself. However, we have the following proposition:

**Proposition 2.12** *There exists an optimal algorithm.*

**Proof of Proposition 2.12** Divide the plane into squares of increasing size, as in Figure 2.10. Cover the points in each of the squares in some optimal way. This gives a covering of the plane and we claim that it is optimal. To see this choose some $\epsilon > 0$ and notice that by Theorem 2.11 we can find $n = 2^m$ so large that $\delta_n < \delta^{opt} + \epsilon$. The fraction of the plane covered by squares of side length smaller than $n$ is 0, so our algorithm has density at most $\delta^{opt} + \epsilon$. However, $\epsilon$ was arbitrary, and therefore our

algorithm must be optimal. □

## 2.6 Open problems

We would like to mention a number of open problems:

- For which classes of algorithms does there exist a critical density? By this we mean a critical value $\lambda_c$, such that percolation occurs for $\lambda > \lambda_c$ and does not occur for $\lambda < \lambda_c$.

- For which classes of algorithms is the infinite cluster unique? In other words, when do we have either 0 or 1 infinite cluster, a.s.?

- We have shown in Theorem 2.6 that if we have an algorithm with a finite horizon, which is shift invariant under two linearly independent shifts and has a bounded density of discs, then we must have percolation for $\lambda$ high enough. We have also shown in Theorem 2.8 that we can have a completely shift invariant covering algorithm with an unbounded density of discs and no finite horizon that does not percolate, even for high values of $\lambda$. Do we have percolation for $\lambda$ high enough for a finite horizon algorithm invariant under a pair of shifts, with an unbounded density of discs? Do we necessarily have percolation for $\lambda$ high enough if we have a bounded density of discs and shift invariance but no finite horizon?

- We have described an optimal algorithm that is not shift invariant. It is rather simple to design a shift invariant algorithm that works for $\lambda$ less than the critical density $\lambda_c$ of standard continuum percolation. Does there exist a shift invariant algorithm that is optimal for all $\lambda$?

## 2.7 A long counterexample

In this last section of the chapter, we give a formal proof of Theorem 2.8, showing an example of shift invariant algorithm that never percolates. The proof is constructive

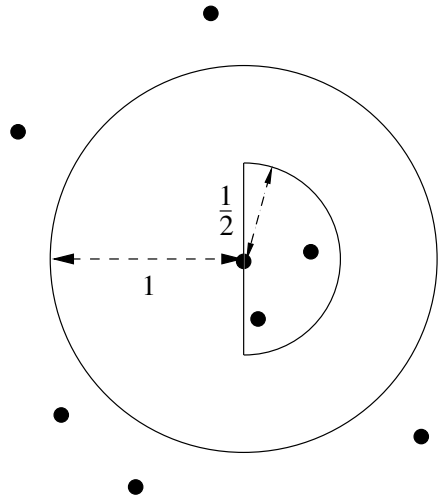


Figure 2.11: **A potential point** A potential point is a Poisson point with at least one other point in the half-disc of radius $\frac{1}{2}$ to the right of it, and no points in the disc of radius 1 centered at it, except in that half-disc.

and rather technical. The covering we describe will have density $\lambda$.

Without loss of generality, consider covering discs of radius $r = 1$. The main idea is the following: given a realization of the Poisson point process, we first build a large structure of circles similar to those obtained in continuum fractal percolation models. We do this by placing circles of radii $18^m$, with $m \in \mathbb{N}$, where we see certain configurations of points in the plane. The resulting structure is composed of clusters that are finite, but contain every bounded region of the plane. We then derive a shift invariant covering of all the points of $X$ by discs of radius $r = 1$, leaving an empty space near to the boundaries of these clusters.

We illustrate the proof taking the density $\lambda$ to be 1. The proof for the covering of a Poisson process of another density follows in the same way (in the proofs to follow, only the values of the $\epsilon$'s change).

We define a *potential-point* to be a Poisson point with at least one other point in the half-disc of radius $\frac{1}{2}$ to the right of it, and no points in the disc of radius 1 centered at it, except in the aforementioned half-disc (see Figure 2.11). Notice that the potential points cannot come within distance 1 of each other.

Given a decreasing sequence of positive numbers, $b_1 = \frac{1}{2}, b_2, b_3 \ldots$, an *m-point*, for

$m \in \mathbb{N}$, is a potential-point which has its nearest neighboring point between $b_m$ and $b_{m+1}$ away.

We start by proving a few lemmas.

**Lemma 2.13** *For $\epsilon > 0$ sufficiently small, there exists a sequence $b_1 = \frac{1}{2}, b_2, b_3, \ldots$, such that the density of $m$-points is exactly $\epsilon 18^{-2m}$, for each $m \in \mathbb{N}$.*

**Proof of Lemma 2.13.** The density of potential points, $\lambda_p$, is calculable. Choose $\epsilon > 0$ so that

$$\sum_{m=1}^{\infty} \epsilon 18^{-2m} = \epsilon \frac{1}{18^2 - 1} \leq \lambda_p.$$

We can now define $b_i$ inductively, i.e., given $b_m$ we choose $b_{m+1}$ so that the density of $m$-points is exactly $\epsilon 18^{-2m}$. □

We consider a circle of radius $18^m$ around every $m$-point. Call such a circle an *$m$-circle*.

**Lemma 2.14** *Every bounded region of the plane is a.s. wholly contained in some $m$-circle, for some $m$.*

We will use Proposition 7.3 of Meester and Roy (1994). This states:

**Proposition 2.15 (Meester and Roy, 1994)** *Let $S$ be a stationary point process in $\mathbb{R}^d$, and let $\rho$ be a non-negative random variable. If $E(\rho^d) = \infty$, then in the Boolean model $(S, \rho)$ the occupied component is a.s. $\mathbb{R}^d$.*

Furthermore the proof of the theorem can be adapted to show that, under the conditions of the theorem, every bounded region of the plane is a.s. wholly contained in some circle.

**Proof of Lemma 2.14.** Let $S$ be the random collection of $m$-points, for all $m$. $S$ is stationary. Note that the radii associated with points in $S$ are independent, as the points of $S$ do not come within distance 1 of each other. Let $\rho$ be the radius distribution of the circles. Then $(S, \rho)$ is a Boolean model, and the occupied component

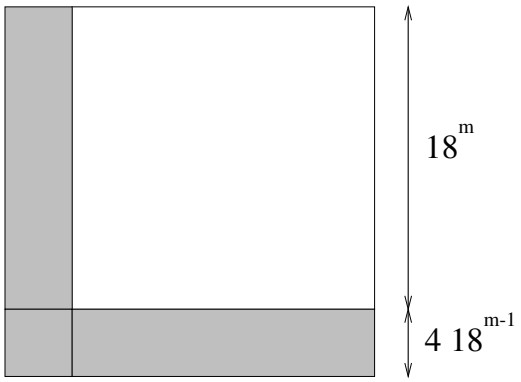


Figure 2.12: **Sets of possible dependence.**

corresponds to all areas contained in some circle. In addition

$$E(\rho^2) = \sum_{m=1}^{\infty} (18^m)^2 \epsilon 18^{-2m} = \infty,$$

so we can apply the proof of Proposition 2.15 and conclude that every bounded region is contained in some circle.

□

Now that we have shown that our circles a.s. contain any bounded region, we want to show that any cluster of intersecting circles is a.s. finite. To do this, we give a slight variation of a proof for fractal percolation that is in the book by Meester and Roy (1996) (Theorem 8.1). Again, we proceed by proving a series of lemmas but first we need a couple of definitions.

We define the *sets of possible dependence* to the square $[0, 18^m]^2$ as the rectangles $(I_1 \times I_2 : I_i \in \{[-4 \times 18^{m-1}, 0], [0, 18^m]\}) \backslash [0, 18^m]^2$ (see Figure 2.12). Sets of possible dependence to other squares of the same size are the natural translations of this. Call a union of sets of possible dependence to a certain square, a *known region*. Define $A_m$ to be the number of $m$-points in the square $[0, 18^m]^2$, and $A_{>m}$ to be the number of $k$-points, with $m < k \in \mathbb{N}$, within distance 4 of the square. Let $C_m^J$ be the number of $m$-points in the known region $J$ to the square.

**Lemma 2.16** *For any $\delta > 0$, we can find $m'$ and, uniformly in $m > m'$, $\epsilon > 0$,*

*sufficiently small that*

$$P(A_m > 0 | A_{>m} = 0 \cap C_m^J = 0) \leq \delta,$$

*for any known region, $J$, to the square $[0, 18^m]^2$.*

**Proof of Lemma 2.16.** We are interested in

$$\begin{aligned} P(A_m > 0 | A_{>m} = 0 \cap C_m^J = 0) &= \frac{P(A_m > 0 \cap A_{>m} = 0 \cap C_m^J = 0)}{P(A_{>m} = 0 \cap C_m^J = 0)} \\ &\leq \frac{P(A_m > 0)}{P(A_{>m} = 0 \cap C_m^J = 0)} \\ &\leq \frac{P(A_m > 0)}{1 - P(A_{>m} > 0) - P(C_m^J > 0)}, \end{aligned}$$

if $P(A_{>m} > 0) + P(C_m^J > 0) < 1$. We recall that, for a non-negative integer-valued random variable $N$, $P(N > 0) \leq E(N)$, obtaining

$$\begin{aligned} P(A_m > 0 | A_{>m} = 0 \cap C_m^J = 0) &\leq \frac{P(A_m > 0)}{1 - E(A_{>m}) - E(C_m^J)} \\ &\leq \frac{E(A_m)}{1 - E(A_{>m}) - E(C_m^J)}. \end{aligned}$$

if $E(A_{>m}) + E(C_m^J) < 1$.

Now, $E(A_{>m}) = (18^{2m} + 4(18^m + 1))18^{-2m}\frac{\epsilon}{18^2-1}$, which is the area of the region within distance 4 of the square multiplied by the total density of $k$-points, for all $k > m, k \in \mathbb{N}$. Noting that the maximum area of the known region is $(18^m(1 + 4/18))^2 - (18^m)^2$, we see that

$$E(C_m^J) \leq ((18^m(1 + 4/18))^2 - (18^m)^2)\epsilon 18^{-2m}.$$

The bound becomes

$P(A_m > 0 | A_{>m} = 0 \cap C_m^J = 0) \leq$

$$\frac{\epsilon}{1 - (18^{2m} + 4(18^m + 1))18^{-2m}\frac{\epsilon}{18^2-1} - ((18^m(1 + 4/18))^2 - (18^m)^2)\epsilon 18^{-2m}},$$

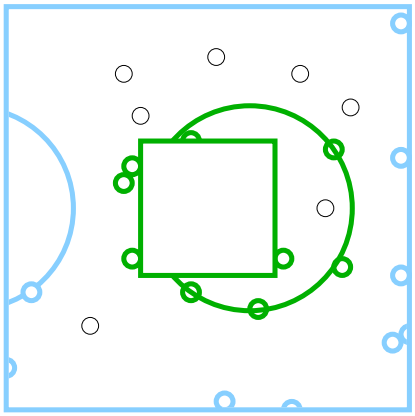

Figure 2.13: **The sets $I_{H(18^n)}$ and $O_{H(18^n)}$.** $I_{H(18^n)}$ is shown in dark gray and $O_{H(18^n)}$ in light gray.

which we can make uniformly less than $\delta$ by choosing $\epsilon$ small enough. □

Let $H(18^n) = [-\frac{3}{2} \times 18^n, \frac{3}{2} \times 18^n]^2 \backslash (-\frac{1}{2}18^n, \frac{1}{2}18^n)^2$. Define $I_{H(18^n)}$ to be the maximal connected cluster of (possibly partial) circles and the boundary of the box $[-\frac{1}{2}18^n, \frac{1}{2}18^n]^2$, fully contained in $H(18^n)$, and define $O_{H(18^n)}$ to be the maximal connected cluster of circles and the boundary of $[-\frac{3}{2} \times 18^n, \frac{3}{2} \times 18^n]^2$, fully contained in $H(18^n)$. See Figure 2.13.

Let $G(18^n)$ be the event that there is a *gap* in $H(18^n)$, i.e., the minimal distance between $I_{H(18^n)}$ and $O_{H(18^n)}$ is at least 18.

**Lemma 2.17** *For $\epsilon > 0$ sufficiently small,*

$$\lim_{n \to \infty} P(G(18^n)) \geq \frac{1}{2}.$$

We prove Lemma 2.17 in two parts. Let $G_1(18^n)$ be the event that there is a gap between $I_{H(18^n)}$ and $O_{H(18^n)}$ in $H(18^n)$, when we consider circles only of radius $18^{n-1}$ or less. The size $18^{n-1}$ is chosen because it is a convenient size comparable to the size of $H(18^n)$. Let $G_2(18^n)$ be the event that no circles of radius $18^n$ or greater intersects $H(18^n)$ at all. Clearly, if $G_1(18^n)$ and $G_2(18^n)$ both occur, then $G(18^n)$ does also. Thus, Lemma 2.17 follows from the following two lemmas.

**Lemma 2.18** *For $\epsilon > 0$ sufficiently small,*

$$\lim_{n\to\infty} P(G_1(18^n)) \geq \frac{3}{4}.$$

**Lemma 2.19** *For $\epsilon > 0$ sufficiently small,*

$$\lim_{n\to\infty} P(G_2(18^n)) \geq \frac{3}{4}.$$

**Proof of Lemma 2.18.** This proof closely follows that of Theorem 8.1 of Meester and Roy (1996) for fractal percolation, except for a number of extra technicalities. We are going to show that we dominate a version of the process which has more independence.

We first divide $H(18^n)$ into $8 \times 18^2$ sub-squares of size $18^{n-1}$ in the obvious way. We call two squares of the same size neighbors if they share an edge or corner.

Suppose for a moment that the probability that a square of size $18^m$ contains an $m$-point, is uniformly $\delta$, for all $m$, independently of the occurrence of $k$-points anywhere, with $k \neq m, k \in \mathbb{N}$, and independently of the occurrence of $m$-points outside the square. We give our proof initially under this assumption, and then compare our original process with this.

We consider the $8 \times 18^2$sub-squares of $H(18^n)$, and in an order such that for any two squares, $B$ and $B^{'}$ say, $B$ is considered before $B^{'}$ if $B$ is neither to the right of nor above $B^{'}$. We examine, in this order, these sub-squares of size $18^{n-1}$, looking for $(n-1)$-points, in the following inductive fashion:

- to begin, all squares are declared to be neither corrupt nor bad.
- if a sub-square is not corrupt, then we examine the whole of it, looking for $(n-1)$-points. If it contains any, then we call it *bad*, and its neighboring squares of the same level *corrupt*.

- if a sub-square is corrupt then we do not examine it.

Squares are bad if they contain centers of circles of comparable size to themselves, which then may extend into the corrupt squares. Corrupt squares may or may not contain $(n-1)$-points. We are careful not to find out this information, as it might tell us something about the distribution of points in the squares we have not yet considered.

We can then divide up each of the *good* squares (those that are neither bad nor corrupt) into $18^2$ pieces, obtaining at most $8 \times 18^{2\times 2}$ squares of size $18^{n-2}$, and we examine those, in an order such those squares nearer the bottom left-hand corner are considered first, looking for $(n-2)$-points, in the same inductive fashion as above. We end up declaring each of the squares of size $18^{n-2}$ that are sub-squares of good squares in $H(18^n)$ to be good, bad or corrupt.

We divide up each of the good squares of size $18^{n-2}$ into $18^2$ squares of size $18^{n-3}$, and use the same procedure to declare each good, bad or corrupt. We can then divide up each of the good squares, and repeat this procedure, while we still have good squares, and to a minimum square size of 18.

We then work backwards through the squares, starting with the smallest, to declare each either *dreadful* or not. A square of size 18 is dreadful if it is bad. In an inductive fashion, a square of size $18^m$ is dreadful if it is either (a) bad or (b) good but contains 2 or more dreadful squares of size $18^{m-1}$. We call $H(18^n)$ dreadful if it contains any dreadful squares of size $18^{n-1}$.

Under our temporary independence assumption, a square of size 18 is dreadful with probability $\delta$, conditioned on the fact that it has not been declared corrupt before being checked. Thus, the probability that it is dreadful is at most $\delta$. Then the probability $p_m$ that a square of size $18^m$ is dreadful, is the probability it is a) bad or b) good but contains 2 or more dreadful squares of size $18^{m-1}$. The probability that it is bad, is, as for a square of size 18, at most $\delta$. The probability that it is good is at most $1-\delta$. It may be that some of the sub-squares of size $18^{m-1}$ of this square are corrupt, due to being neighbors of bad squares of the same size outside this square. Let $N$ be the number of such squares. As the probability of a square being dreadful

is maximal when $N = 0$, it follows that

$$p_m \leq \delta + (1-\delta)((1-p_{m-1})^{18^2} - 18^2 p_{m-1}(1-p_{m-1})^{18^2-1}) .$$

Letting

$$f(p,\delta) = \delta + (1-\delta)(1-(1-p)^{18^2} - 18^2 p(1-p)^{18^2-1}),$$

this becomes $p_m \leq f(p_{m-1}, \delta)$. Note that $p_1 = \delta$. If we can now show, for all $\delta$, that

$$0 \leq p \leq b(\delta) \text{ implies } 0 \leq f(p,\delta) \leq b(\delta),$$

for some $b(\delta) \geq \delta$, it will follow that $p_m \leq b(\delta)$ for all $m$. We need $b(\delta)$ to be a bound that tends to 0 with $\delta$.

Note that $f(p,\delta)$ is continuous in $p$ and $\delta$, that $f(0,\delta) = \delta$ and that $\frac{\partial f}{\partial p}(0,\delta) = 0$. It follows that $f(p,\delta) = p$ has a solution in $[0,1]$ for $\delta$ sufficiently small. The smallest such solution we call $b(\delta)$. Notice that $b(\delta) \geq \delta$, as $f(0,\delta) = \delta$ and $\frac{\partial f}{\partial p}(p,\delta) \geq 0$ on $[0,1]$. $\frac{\partial f}{\partial p}(p,\delta) \geq 0$ on $[0,1]$ also tells us that $0 \leq p \leq b(\delta)$ implies $0 \leq f(p,\delta) \leq b(\delta)$. Since $f(0,0) = 0$, $\frac{\partial f}{\partial p}(0,\delta) = 0$ and $f$ is continuous, $\lim_{\delta \downarrow 0} b(\delta) = 0$.

We have shown that the probability that a square of size $18^m$ is dreadful is bounded from above, uniformly in $m$, by a function of $\delta$ that we can make arbitrarily small by choosing $\delta$ small enough. It then follows that the probability that $H(18^n)$ is dreadful (i.e., contains any dreadful squares of size $18^{n-1}$) can be made as small as we like by choosing $\delta$ sufficiently small. We choose $\delta$ so that this probability is less than $\frac{1}{4}$.

We can now come back to our original process, and give up the independence assumption. We make the following comments:

- The probability that a square of size $18^m$ contains an $m$-point, when we come to check it, given any of the information we already have found, is at most $\delta$, by Lemma 2.16, and because we never consider a corrupt square.

- By choosing $\epsilon$ sufficiently small we can make the bound $\delta$ as small as we need.

Let us consider what it means for $H(18^n)$ not to be dreadful. We argue that, in this

case, we cannot have a connection by circles, of the appropriate sizes, from the inside to the outside of the box.

We first note that any $m$-point in $H(18^n)$ is either in a bad or a corrupt box of size $18^m$. An $m$-circle may thus only intersect a box of size $18^m$, if that box is either bad, corrupt, or neighbors a corrupt square of the same size, unless it neighbors the boundary of $H(18^n)$.

We now give a series of definitions. Call a box of size $18^m$ *dodgy* if it is either bad, corrupt, neighbors a corrupt square of the same size, is dreadful, neighbors a dreadful square, or neighbors the border of $H(18^n)$. Call it *clean* if it is not dodgy. Call two boxes of size $18^m$ adjacent if they share an edge. Define an *$m$-circuit* to be a series of boxes of size $18^m$, $(B_1, B_2, B_3, \ldots, B_k)$ where $B_i$ is adjacent to $B_{i+1}$ for $i = 1, 2, \ldots, k-1$ and $B_k$ is adjacent to $B_1$. We also require that the circuit cuts off the origin from infinity.

A sub-circuit of boxes of size $18^j$,$(B_1^j, B_2^j, B_3^j, \ldots, B_{k_j}^j)$, of a circuit of boxes of size $18^m$ (with $j < m$),$(B_1^m, B_2^m, B_3^m, \ldots, B_{k_m}^m)$, is a circuit of boxes of size $18^j$ inside the circuit of boxes of size $18^m$, such that there exists $0 = i_1, i_2, i_3, \ldots, i_{k_m-1}, i_{k_m} = k_j$, such that $B_{i_l+1}^j, B_{i_l+2}^j, B_{i_l+3}^j, \ldots, B_{i_{l+1}}^j$ are contained in $B_l^m$. This means that the first few boxes of size $18^j$ are contained in $B_1^m$, the next few are in $B_2^m$, and so on.

We say that the property $E_m$ holds if any $m$-circuit consisting of clean boxes of size $18^m$ contains a sub-circuit of boxes of size 18 that are not intersected by $k$-circles, for all $k \leq m$. Our objective is to show that $E_m$ holds for $m = 1, 2, \ldots, n-1$, by induction on $m$.

If $m = 1$, we have a 1-circuit of clean boxes. Therefore there can be no 1-circle intersecting any of these boxes, and $E_1$ holds.

The inductive hypothesis is that $E_{m-1}$ holds. In order to perform the induction step and prove that $E_m$ also holds, consider an $m$-circuit of clean boxes of size $18^m$, as depicted by in Figure 2.14. In this figure, the smallest squares are of size $18^{m-1}$. If we show the existence of a sub-circuit of clean boxes of size $18^{m-1}$ inside the $m$-circuit, then, by the inductive hypothesis, the occurrence of $E_m$ will follow.

By construction, all the boxes of size $18^m$ in our circuit are clean. This tells us

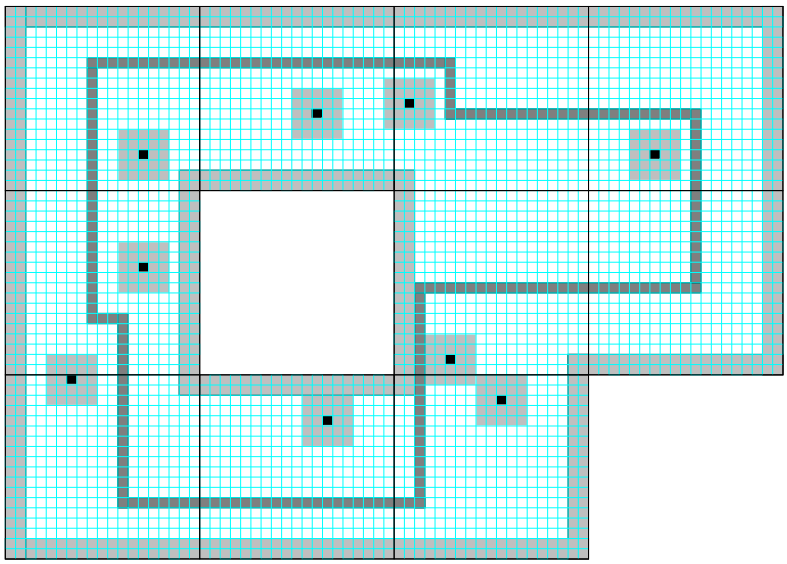

Figure 2.14: **Avoiding dodgy squares.** A circuit of squares of size $18^m$ contains a circuit of squares of size $18^{m-1}$, avoiding dodgy squares.

that none of them intersects an $m$-circle. It also means that there is at most one dreadful square inside each box of size $18^m$ in the circuit. These are depicted in Figure 2.14 as black squares. A dreadful square may cause a $5 \times 5$ block of squares of size $18^{m-1}$ to be dodgy (gray $5 \times 5$ blocks in Figure 2.14). This can happen because the dreadful square can neighbor a corrupt square, which also has neighbors. Finally, any of the squares of size $18^{m-1}$ neighboring the edge of the circuit, or the neighbors of these squares, may be dodgy, due to the proximity of dreadful squares just outside the circuit. This latter case is depicted in Figure 2.14 by the two gray circuits of width $2 \times 18^{m-1}$, along the edges of the $m$-circuit. These are all the possibilities for dodgy squares of size $18^{m-1}$ in our circuit.

By considering all possible arrangements of the dodgy squares we see that there must be a circuit of squares of size $18^{m-1}$ inside our circuit that avoids those dodgy squares (see Figure 2.14). Then, by the inductive hypothesis, there must also be a sub-circuit of squares of size 18, so $E_m$ holds.

$H_{18^n}$ is a circuit of boxes of size $18^n$, and if all are clean, by the argument above, it follows that we must have a sub-circuit of boxes of size 18 that are not intersected by any $m$-circles, for $m = 1, 2, \ldots, n$, which is what we wanted to prove. □

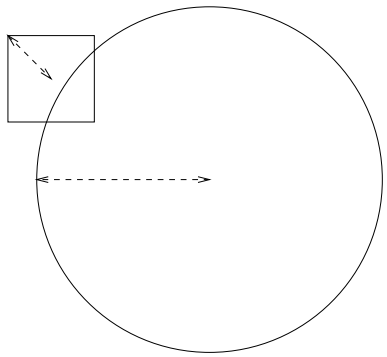

Figure 2.15: **Intersection between circle and box.** A circle of radius at least $18^n$ can touch the boundary of the box $[-\frac{3}{2} \times 18^n, \frac{3}{2} \times 18^n]^2$ only if the distance between the center of the circle and the center of the box is within $3 \times 18^n \times \frac{1}{\sqrt{2}}$ of the circle's radius.

**Proof of Lemma 2.19.** Let $X$ be the number of circles of radius at least $18^n$ that intersect $[-\frac{3}{2} \times 18^n, \frac{3}{2} \times 18^n]^2$. A circle can only intersect the boundary of the box if the distance between the center of the circle and the center of the box is within $3 \times 18^n \times \frac{1}{\sqrt{2}}$ of the circle's radius (see Figure 2.15). Now write

$$\begin{aligned} P(X > 0) &\leq E(X) \\ &\leq \sum_{b=n}^{\infty} \epsilon 18^{-2b} \pi((18^b + \frac{3 \times 18^n}{\sqrt{2}})^2 - (18^b - \frac{3 \times 18^n}{\sqrt{2}})^2). \end{aligned}$$

We can make this less than $1/4$ for all $n$ by our choice of $\epsilon$, implying that the probability of a large circle intersecting the box is less than $1/4$. □

We can now prove the finiteness of our clusters. We define a *thickened cluster* as a maximal connected component of points strictly within distance 9 of any circle.

**Lemma 2.20** *All thickened clusters are finite, for $\epsilon > 0$ sufficiently small.*

**Proof of Lemma 2.20.**

By Lemma 2.17 there is a gap between $[-\frac{18^m}{2}, \frac{18^m}{2}]^2$ and $[-\frac{3 \times 18^m}{2}, \frac{3 \times 18^m}{2}]^2$, with probability at least $1/2$, by our choice of $\epsilon$, for every $m$.

We now need to show that such a gap exists around the origin a.s., for some $m$. If we can do this then we can conclude, by the stationarity of the circle configuration, that every point will be surrounded by some gap. We need to be careful in showing

this, so that the negative information gained by the knowledge that there is no such gap, for a certain $m$, does not prejudice our attempts to find one in a later $m$. We proceed as follows.

We begin by looking whether there is a gap between the boundaries of $[-\frac{18}{2}, \frac{18}{2}]^2$ and $[-\frac{3\times 18}{2}, \frac{3\times 18}{2}]^2$. In order to do this we search for the centers of the circles that might intersect this area, in order of increasing size. Either there is no gap, in which case a (random) $K_1 < \infty$ exists, so that these boundaries are connected by circles of radius up to $18^{K_1}$, or there is a gap (with probability of at least 1/2). In the latter case we would be satisfied. In the first case, we can find an $M_1$ so large that $[-\frac{18^{M_1}}{2}, \frac{18^{M_1}}{2}]^2$ and $[-\frac{3\times 18^{M_1}}{2}, \frac{3\times 18^{M_1}}{2}]^2$, cannot be overlapped by any circle of radius up to $18^{K_1}$ that could also have overlapped $[-\frac{3\times 18}{2}, \frac{3\times 18}{2}]^2$. We know nothing about larger circles.

We have no information about the circles that may connect $[-\frac{18^{M_1}}{2}, \frac{18^{M_1}}{2}]^2$ and $[-\frac{3\times 18^{M_1}}{2}, \frac{3\times 18^{M_1}}{2}]^2$; hence, the probability that there is a gap between them is again at least 1/2. We search for a connection between the boundaries of $[-\frac{18^{M_1}}{2}, \frac{18^{M_1}}{2}]^2$ and $[-\frac{3\times 18^{M_1}}{2}, \frac{3\times 18^{M_1}}{2}]^2$, again starting by looking at the smallest circles. Either there is a gap, or there exists $K_2 < \infty$ such that there is a connection from one of these boundaries to the other using circles of size up to $18^{K_2}$. In this latter case, we can find an $M_2 > M_1$ so large that $[-\frac{18^{M_2}}{2}, \frac{18^{M_2}}{2}]^2$ and $[-\frac{3\times 18^{M_2}}{2}, \frac{3\times 18^{M_2}}{2}]^2$, cannot be overlapped by any circle of radius up to $18^{K_2}$ that could also have overlapped $[-\frac{3\times 18^{M_2}}{2}, \frac{3\times 18^{M_2}}{2}]^2$.

We now search again for a gap, this time between $[-\frac{18^{M_2}}{2}, \frac{18^{M_2}}{2}]^2$ and $[-\frac{3\times 18^{M_2}}{2}, \frac{3\times 18^{M_2}}{2}]^2$, and repeat. At every stage we have a probability of at least 1/2 of there being a gap, independently of the previous times. If there is no gap (which happens with a probability of at most 1/2), then we find this out at some time and search in a larger annulus. It follows that there is almost surely a gap.

□

Finally, we can now give a proof of Theorem 2.8, by describing a shift invariant covering algorithm that a.s. never forms an unbounded component of covering discs, for all $\lambda$.

**Proof of Theorem 2.8.** We nearly have a covering algorithm, but everything we have done up to now depends upon $\lambda$, the density of points. As the covering should be a deterministic function of the points, we must first calculate $\lambda$ in the realization of the point configuration. We do this by setting

$$\lambda = \lim_{n\to\infty} \frac{\text{number of points in } B_n(0)}{n^2}$$

if this limit exists and is constant, which happens with probability 1, and otherwise we take $\lambda = 1$. Note that this definition is translation invariant.

Fix $\epsilon$ at half the supremum of all values of $\epsilon$ that allow all our proofs to work at this particular value of $\lambda$.

We construct *smooth* curves based upon the finite circle clusters. Consider some maximal set of circles such that, if we take the locus of points at a maximal distance of 4 from the points in the circles, then this forms a connected set, and run a disc of radius two around the outside of this set (see Figure 2.5). The disc traces out a kind of sausage shape around the clusters. We note that all such sausages must be finite by Lemma 2.20. In formulas we take a maximal set of circles, $C$, such that $\bigcup_{c\in C}\{x : |x-y| \le 4, y \in c\}$ is connected, and then define the sausage to be the set on the exterior of $C$,

$$\{x : \exists y : |x-y| \le 2, \exists p \in \bigcup_{c\in C} c : |y-p| = 2, \{w : |w-y| < 2\} \cap \bigcup_{c\in C} c = \emptyset\}.$$

We take the inside edge of this sausage as our curve, and note that a covering disc (of radius 1) can get arbitrarily close to any point of it without touching it.

We construct these smooth curves for each set of sufficiently close clusters, noting that they surround every region, are always finite, and never come within distance 18 of each other.

We finally cover our Poisson points as follows:

- if a point is at a distance more than 2 from every smooth curve, then we center a covering disc at the point.

- if a point is within distance 2 of a smooth curve, then we place a disc so that its perimeter covers the point, and so that the center of the disc is at the maximum distance away from the smooth curve. If there are a number of such possible positions, we choose the leftmost.

It immediately follows that, for any given value of $\lambda$, a.s. there is no percolation. $\square$

# Chapter 3 The magic numbers in network design

In this chapter we give a proof of the following geometric theorem, that has applications in wireless network design.

**Theorem 3.1** *Consider a square lattice where the distance between two neighboring lattice vertices is $L$. Call a closed disc of fixed radius $r$, centered at a lattice vertex, a grid disc. The number $\mathcal{N}$ of grid discs that are necessary and sufficient to cover any disc of radius $r$ placed on the plane, is given by:*

- *CASE 1. For $r/L < \frac{\sqrt{2}}{2}$, $\mathcal{N}$ does not exist.*
- *CASE 2. For $\frac{\sqrt{2}}{2} \leq r/L < \frac{\sqrt{10}}{4}$, $\mathcal{N} = 6$.*
- *CASE 3. For $\frac{\sqrt{10}}{4} \leq r/L < 1$, $\mathcal{N} = 5$.*
- *CASE 4. For $1 \leq r/L < \frac{5\sqrt{2}}{4}$, $\mathcal{N} = 4$.*
- *CASE 5. For $r/L \geq \frac{5\sqrt{2}}{4}$, $\mathcal{N} = 3$.*

The proof makes use of simple geometric arguments, but is by no means trivial. It involves finding a disc that requires the prescribed number of grid discs to be fully covered, and then finding different configurations of grid discs that are sufficient to cover any disc on the plane. The number of these configurations that we need to find increases with $r/L$. The rest of the chapter contains nothing but proofs.

## 3.1 Proof of Case 1

To simplify the notation, in the following we fix $L = 1$. For $r < \frac{\sqrt{2}}{2}$ the grid discs do not cover the plane compactly, since they do not cover the centers of the lattice squares. It follows that any number of grid discs is not sufficient to cover any disc that covers the center of a lattice square. □

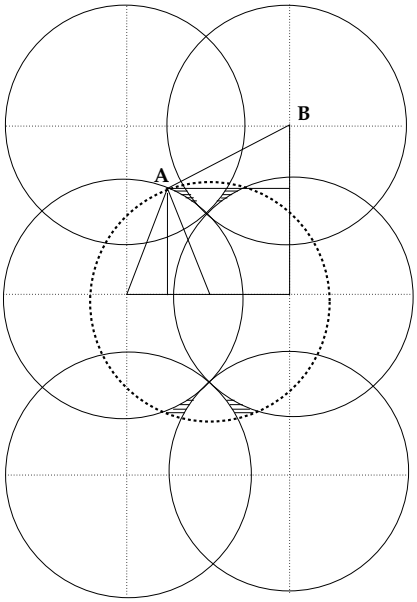


Figure 3.1: **Case 2, necessary condition.** *The four shaded areas exist when* $\overline{AB} > r$.

## 3.2 Proof of Case 2

The necessary condition is proven by showing that there exists a disc that requires six grid discs to be covered. The sufficient condition is proven using a tiling argument: we first show that there exists a triangle $ABC$, such that any disc centered inside triangle $ABC$ is covered by six grid discs, and then we show that, by symmetry, we can tile the entire plane using triangles that have this property.

### 3.2.1 Necessary condition

Consider $r \geq \frac{\sqrt{2}}{2}$ and a disc centered halfway between two neighboring lattice vertices. Such a disc is the dashed disc depicted in Figure 3.1. We have that the six (solid) grid discs depicted in Figure 3.1 are necessary to completely cover the dashed disc if $\overline{AB} > r$, i.e., when the four shaded areas in Figure 3.1 exist. By repeatedly applying Pythagoras' theorem, we have

$$\overline{AB} = \sqrt{\left(1 - \sqrt{r^2 - \frac{1}{16}}\right)^2 + \frac{9}{16}}\,; \tag{3.1}$$

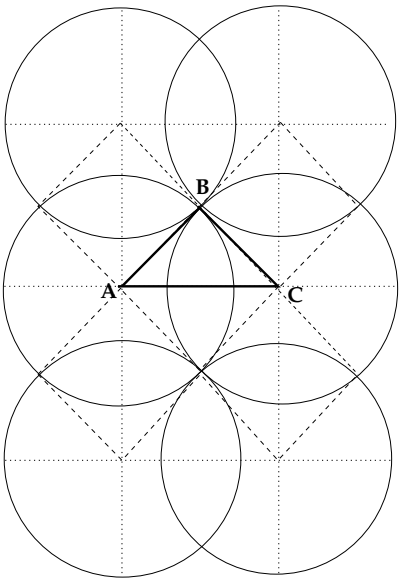


Figure 3.2: **Case 2, sufficient condition.** *Any disc centered inside triangle $ABC$ is covered by the six grid discs.*

imposing $\overline{AB} > r$, we obtain $r < \frac{\sqrt{10}}{4}$.

### 3.2.2 Sufficient condition

Call $\mathcal{A}$ the area covered by the six grid discs in Figure 3.2. Any point inside triangle $ABC$ has distance greater than $r$ from the border of area $\mathcal{A}$. Therefore, a disc can be centered inside triangle $ABC$ and be covered by the six grid discs depicted in Figure 3.2. By symmetry, we can tile the plane with triangles inside which discs can be centered and covered by six grid discs. □

## 3.3 Proof of Case 3

### 3.3.1 Necessary condition

Consider $r \geq \frac{\sqrt{10}}{4}$ and a disc centered at a distance $\epsilon$ to the left from halfway between two neighboring lattice vertices (dashed disc in figure 3.3). By the same reasoning as for in Case 2, we have that the five (solid) grid discs depicted in Figure 3.3 are necessary to completely cover the dashed disc, if $\overline{AB} > r$. By repeatedly applying

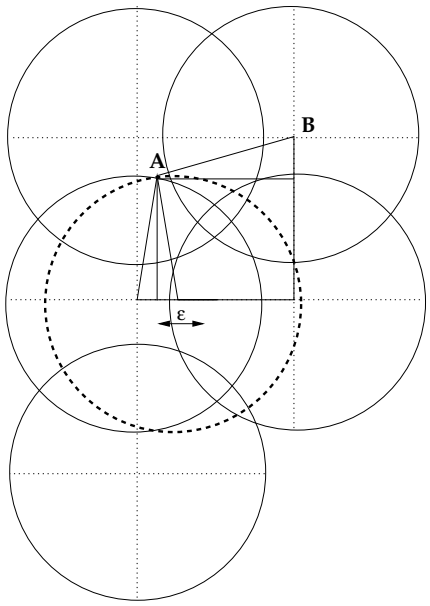


Figure 3.3: **Case 3, necessary condition.** *The dashed disc is shifted by $\epsilon$ to the left from halfway between two lattice vertices.*

Pythagoras' theorem, we have in this case:

$$\overline{AB} = \sqrt{\left[1 - \sqrt{r^2 - \left(\frac{1}{4} - \frac{\epsilon}{2}\right)^2}\right]^2 + \left(\frac{3}{4} + \frac{\epsilon}{2}\right)^2}\,; \tag{3.2}$$

imposing $\overline{AB} > r$ we obtain

$$\sqrt{\frac{\epsilon^2 + \epsilon}{2} + \frac{5}{8}} > r\,. \tag{3.3}$$

We can restrict the $\epsilon$ range to: $0 < \epsilon < \frac{1}{2}$, and for any $r < 1$ inequality (3.3) is verified.

### 3.3.2 Sufficient condition

Call $\mathcal{A}$ the area covered by the five grid discs in Figure 3.4. Any point inside triangle $AOB$ has distance greater than $r$ from the border of area $\mathcal{A}$. Therefore, a disc can be centered inside triangle $AOB$ and be covered by the five grid discs depicted in Figure 3.4. By symmetry, we can tile the plane with triangles inside which discs can

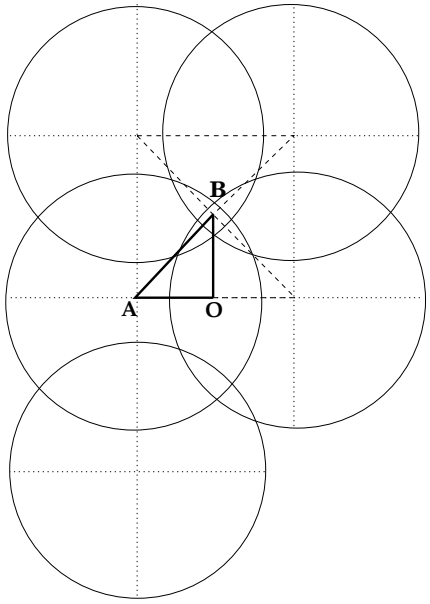


Figure 3.4: **Case 3, sufficient condition.** *Point O is halfway between two lattice vertices. Any disc centered inside triangle AOB is covered by the five grid discs.*

be centered and covered by five grid discs. □

## 3.4 Proof of Case 4

### 3.4.1 Necessary condition

Consider $r \geq 1$ and a disc placed at the center of a lattice square. If we place the grid discs as depicted in the left section of Figure 3.5, four grid discs are always necessary to cover the dashed disc placed at the center of a lattice square, because

$$\overline{EF} = \overline{DF} > \overline{OF} = r\,; \tag{3.4}$$

the same holds whenever two grid discs are centered at neighboring lattice vertices or at lattice vertices on the same diagonal of a lattice square. If we examine the only remaining possible placement of grid discs, depicted on the right-hand side of Figure 3.5, we have that four grid discs are necessary only if $\overline{BC} = \overline{CD} > r$. By

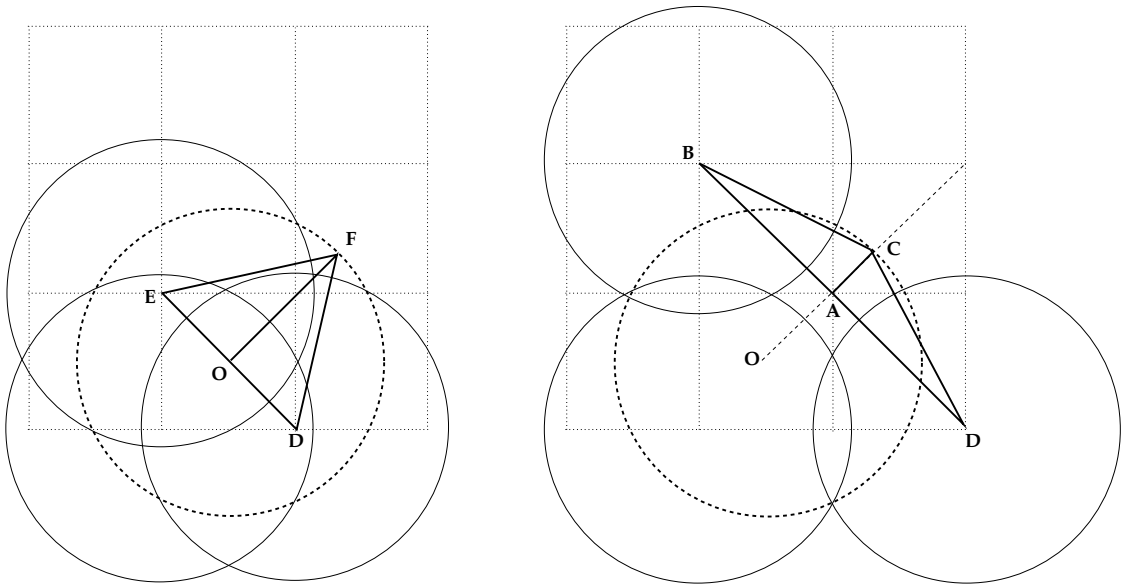


Figure 3.5: **Case 4, necessary condition.** *Point O is at the center of a lattice square. On the left-hand side of the figure, the dashed disc centered at point O always requires one more grid disc to be covered. On the right-hand side of the figure, the dashed disc centered at point O requires one more grid discs to be covered, if* $\overline{BC} > r$.

Pythagoras' theorem, we have in this case:

$$\overline{BC} = \sqrt{\left(r - \frac{\sqrt{2}}{2}\right)^2 + 2} \tag{3.5}$$

imposing $\overline{BC} > r$ we obtain $r < 5\frac{\sqrt{2}}{4}$.

### 3.4.2 Sufficient condition

Consider the left-hand side of Figure 3.6. The four grid discs cover any disc centered inside the shaded area $ABCE$. This area is defined by the triangle $ABC$ and by the circle centered at point $P$. This circle is the locus of the centers of the discs to be covered that touch point $P$. Any disc centered inside the remaining area $ACE$ is not covered by the four grid discs. Consider now the right-hand side of Figure 3.6, the four (solid) grid discs cover, in this case, any disc centered inside the shaded area $CDEF$. This area is defined by triangle $BCD$ and by the circle centered at point $Q$. This circle is the locus of the centers of the discs to be covered that touch point $Q$.

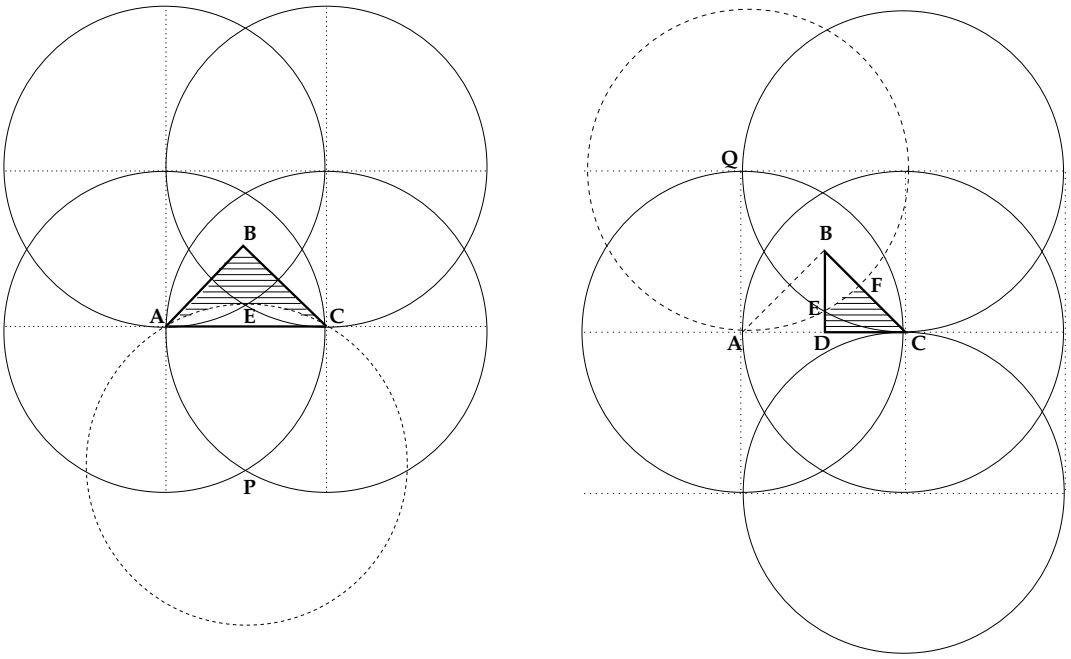


Figure 3.6: **Case 4, sufficient condition.** *Four grid discs cover any disc centered inside the shaded areas. Intersecting the two shaded areas, we obtain triangle $BCD$.*

Such circle passes by point $E$, therefore, adjoining the two shaded areas $ABCE$ and $CDEF$, we fully cover the area of triangle $BCD$. Any disc centered inside triangle $BCD$ is covered by four grid discs: the four depicted on the left-hand side or the four depicted on the right-hand side of Figure 3.6. By symmetry, the same holds for triangle $ABD$ and we can tile the plane with triangles inside which discs can be centered and covered by four grid discs. □

## 3.5 Proof of Case 5

### 3.5.1 Necessary condition

By symmetry, any two discs with the same radius, centered at an arbitrary distance $\epsilon > 0$ apart, cover less than half of each other's perimeter, therefore, any grid disc must cover less than half of the perimeter of any other disc not centered at a lattice point. It follows that any two grid discs must cover less than the entire perimeter of any other disc not centered at a lattice point. Hence, any disc not centered at a

lattice point requires at least three grid discs to be covered.

### 3.5.2 Sufficient condition

It is enough to prove this condition when $r$ is minimal, therefore we carry out calculations fixing $r = \frac{5\sqrt{2}}{4}$. We consider three different placements of three grid discs on the lattice and show that they are enough to cover any disc arbitrarily placed on the plane. Consider the upper left-hand side of Figure 3.7. Taking point $O$ as the origin of the coordinate system, the three grid discs are placed at points: $(-1,0),(-1,2),(1,0)$. The coordinates of point $P$, given by the intersection of the two lower grid discs in the upper left-hand side of Fig. 3.7, are calculated by applying Pythagoras' theorem to triangle $AOP$ obtaining: $P = \left(0, -\frac{\sqrt{34}}{4}\right)$. Therefore, the locus of the centers of the discs to be covered that touch point $P$, given by the circle centered at point $P$, is defined by the equation:

$$x^2 + \left(y + \frac{\sqrt{34}}{4}\right)^2 = r^2\,; \tag{3.6}$$

this circle passes by point $A$ and intersects segment $\overline{BH}$ at point $C = \left(-\frac{1}{2}, \frac{\sqrt{46}-\sqrt{34}}{4}\right)$. Note that any disc centered inside the shaded area $ABC$ is covered by the three grid discs centered at points: $(-1,0),(-1,2),(1,0)$.

We now consider the three grid discs depicted on the upper right-hand side of Figure 3.7, centered at points: $(-1,0),(0,1),(0,-1)$. First, let us focus on point $Q$. Its coordinates are calculated by applying Pythagoras' theorem to triangle $OQR$, obtaining: $Q = \left(\frac{\sqrt{34}}{4}, 0\right)$. Since $\overline{HQ} = \overline{HO} + \overline{OQ} = \frac{1}{2} + \frac{\sqrt{34}}{4} > r$, the locus of the centers of the discs to be covered that touch point $Q$, given by the circle centered at point $Q$, does not intersect triangle $ABH$. Now, let us focus on point $P'$. The coordinates of point $P'$ are calculated by intersecting the two grid circles:

$$\begin{cases} (x+1)^2 + y^2 &= r^2 \\ x^2 + (y-1)^2 &= r^2\,, \end{cases} \tag{3.7}$$

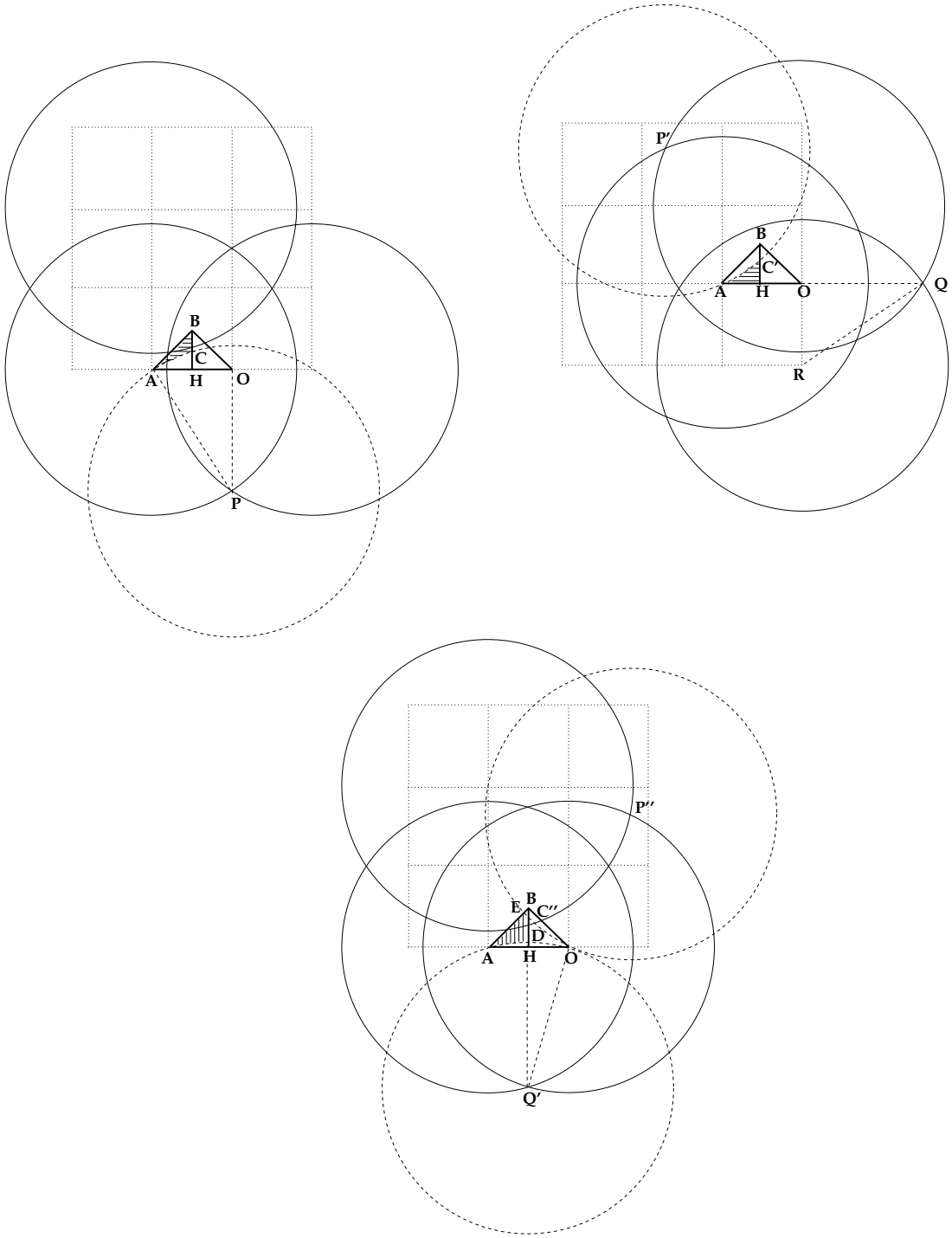


Figure 3.7: **Case 5, sufficient condition.** *Three grid discs cover any disc centered inside the shaded areas. Intersecting the three shaded areas, we obtain triangle $ABH$.*

obtaining: $P' = (\frac{-2-\sqrt{21}}{4}, \frac{2+\sqrt{21}}{4})$. Therefore, the locus of the centers of the discs to be covered that touch point $P'$, given by the circle centered at point $P'$, is defined by the equation:

$$\left(x + \frac{2+\sqrt{21}}{4}\right)^2 + \left(y - \frac{2+\sqrt{21}}{4}\right)^2 = r^2\,; \tag{3.8}$$

this circle passes by point $A$ and intersects segment $\overline{BH}$ at point $C' = \left(-\frac{1}{2}, \frac{2+\sqrt{21}-\sqrt{29}}{4}\right)$. Note that any disc centered in the shaded area $AC'H$ is covered by the three grid discs centered at points: $(-1,0), (0,1), (0,-1)$.

Intersecting the two circles centered at points $P$ and $P'$, defined by equations (3.6) and (3.8), respectively, we obtain two points:

$$\begin{aligned}(x_0, y_0) &= (-1, 0)\\ (x_1, y_1) &= \left(\frac{2-\sqrt{21}}{4}, \frac{2+\sqrt{21}-\sqrt{34}}{4}\right)\end{aligned}$$

depicted on the left-hand side of Figure 3.8. By the coordinates of these points, $(x_1, y_1)$ is placed inside triangle $ABH$. Hence, any disc centered inside the shaded area given by the intersection of the two discs depicted on the left-hand side of Figure 3.8 is covered by neither the three grid discs depicted on the upper left-hand side, nor by the three grid discs depicted on the upper right-hand side of Figure 3.7.

In order to cover such a disc, we consider the three grid discs depicted in the lower section of Figure 3.7, placed at points: $(-1,0), (-1,2), (0,0)$. In this case, the coordinates of point $Q'$ are calculated by applying Pythagoras' theorem to triangle $Q'OH$, obtaining $Q' = \left(-\frac{1}{2}, -\sqrt{\frac{23}{8}}\right)$. Therefore, the locus of the centers of the discs to be covered that touch point $Q'$, given by the circle centered at $Q'$, is defined by the equation:

$$\left(x + \frac{1}{2}\right)^2 + \left(y + \sqrt{\frac{23}{8}}\right)^2 = r^2\,; \tag{3.9}$$

this circle passes by points $A$ and $O$ and intersects segment $\overline{BH}$ at point $D = \left(-\frac{1}{2}, \frac{5\sqrt{2}-\sqrt{46}}{4}\right)$. The coordinates of point $P''$ are calculated by intersecting the two

grid circles:

$$\begin{cases} (x+1)^2 + (y-2)^2 &= r^2 \\ x^2 + y^2 = r^2 \,, \end{cases} \tag{3.10}$$

obtaining $P'' = \left(\frac{\sqrt{6}-1}{2}, \frac{\sqrt{6}+4}{4}\right)$. Therefore, the locus of the centers of the discs to be covered that touch point $P''$, given by the circle centered in $P''$, is defined by the equation:

$$\left(x - \frac{\sqrt{6}-1}{2}\right)^2 + \left(y - \frac{\sqrt{6}+4}{4}\right)^2 = r^2 \,; \tag{3.11}$$

this circle passes by point $O$ and intersects segment $\overline{BH}$ at point $C'' = \left(-\frac{1}{2}, \frac{4+\sqrt{6}-\sqrt{26}}{4}\right)$. Note that any disc centered inside the shaded area $AEC''D$ is covered by the three grid discs centered at points: $(-1,0), (-1,2), (0,0)$. In order to check that this placement of grid discs covers any disc centered inside the shaded area given by the intersection of the two discs depicted on the left-hand side of Figure 3.8, we intersect the two circles centered at points $P'$ and $Q'$ in Figure 3.7, defined by equations (3.8) and (3.9) respectively, obtaining two points:

$$\begin{aligned} (x_0, y_0) &= (-1, 0) \\ (x_2, y_2) &= \left(-\frac{\sqrt{21}}{4}, \frac{2+\sqrt{21}-\sqrt{46}}{4}\right) \end{aligned}$$

depicted on the right-hand side of Figure 3.8. Given the coordinates of these points, since $(x_2, y_2)$ is placed outside the area of triangle $ABH$, we conclude that the three grid discs placed at points: $(-1,0), (-1,2), (0,0)$, cover any disc centered inside the shaded area given by the intersection of the two discs depicted on the left-hand side of Figure 3.8. It follows that intersecting the three shaded areas of Figure 3.7: $ABC$,$AC'H$,$AEC''D$, we cover triangle $ABH$ completely. Hence, any disc centered inside triangle $ABH$ is covered by three grid discs, placed in one of the three configurations depicted in Figure 3.7. By symmetry, the same holds for triangle $OBH$ and we can tile the plane with triangles inside which discs can be centered and covered by three grid discs. □

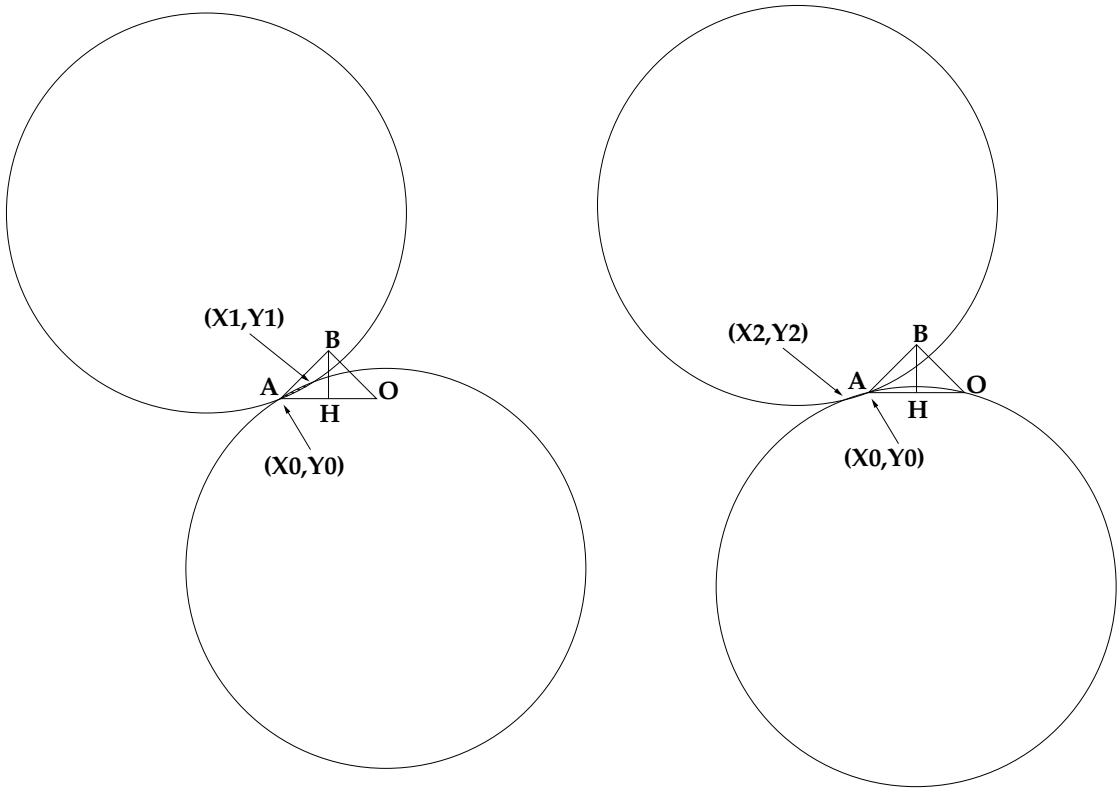


Figure 3.8: **Case 5, sufficient condition.** *Point $(x_1, y_1)$ is inside triangle $ABH$, point $(x_2, y_2)$ is outside triangle $ABH$.*

# Chapter 4 Wave propagation and random walks

In this chapter we present a model of wave propagation in microcellular urban environments, based on random walks.

We model the trajectory of each photon radiating from an isotropic narrow-band source as a piecewise linear random walk with absorbing probabilities (see Fig. 1.4). The average step length of the random walk is $1/\eta$, and we assume that each time the photon is about to turn in a random direction, it can be absorbed, with probability $\gamma$, by the reflecting obstacle and hence stop its random walk. Our procedure consists of finding an expression for the p.d.f. of the site where the random walk stops and then obtaining an expression for the radiated power flux and power density at a given distance from the transmitter. The former equals the number of photons entering a sphere of radius $\Delta r$ placed at distance $r$, normalized to the sphere surface, in the limit for $\Delta r \to 0$; the latter is defined as the number of photons leaving a sphere centered at the transmitter and of radius $r$, normalized to the sphere surface. At the end of the chapter, a comparison with the classical theory of wave propagation in random environments is given, and an experimental validation of the model is provided.

## 4.1 One dimension

We start by looking at the one-dimensional case. In one dimension, the trajectory of a photon occurs along a single straight line. We imagine each photon to behave as a sleepy drunk person walking on the line. The drunk starts walking in a random direction, proceeds at a constant pace, but at random, Poisson distributed intervals, he trips, at which point with probability $\gamma$ he falls asleep, and with probability $(1-\gamma)/2$ he continues in each direction. Accordingly, let $x$ be the coordinate on the line

and define $H$ and $\overline{H}$ to be the p.d.f. s:

$$H(x) = \eta e^{-\eta x} \quad (x \geq 0), \qquad \overline{H}(x) = \eta e^{\eta x} \quad (x \leq 0).$$

The overall p.d.f. of tripping at $x$, in the first step of the random walk, is given by

$$Q(x) = \frac{H + \overline{H}}{2} = \frac{\eta}{2} e^{-\eta |x|},$$

where $1/\eta$ is the photon's average step length.

We are now interested in the p.d.f. $G(x)$ of the site where the drunk falls asleep. With $*$ indicating convolution, this density can be found by solving the equation:

$$G(x) = \gamma Q(x) + (1 - \gamma) Q * G(x). \tag{4.1}$$

Use of Eq. (4.1) can be justified as follows. Let us iteratively substitute the expression for $G(x)$ in the convolution integral. We have $G(x) = G_0(x) + G_1(x) + G_2(x) + \ldots$, with $G_0(x) = \gamma Q(x)$, $G_1(x) = (1-\gamma)Q(x) * G_0(x)$, $G_2(x) = (1-\gamma)Q(x) * (1-\gamma)Q(x) * G_0(x), \ldots$ $G_0(x)$ describes the event that the drunk falls asleep at the first step of the random walk, hitting a single obstacle. $G_1(x)$ describes the event that the drunk falls asleep at the second step, hitting two obstacles and so on. Since all these events are disjoint, we sum all the $G_i$'s to obtain the overall p.d.f. $G(x)$ of the site where the drunk falls asleep.

The convolution in Eq. (4.1) suggests examining the Fourier transforms (characteristic functions in the terminology of probability theory) of the probability densities.

Let $g(\omega), h(\omega), \overline{h}(\omega), q(\omega)$ be the Fourier transforms (FT) of $G(x), H(x), \overline{H}(x), Q(x)$ respectively, and $h^*(\omega)$ be the complex conjugate of $h(\omega)$. We have

$$h(\omega) = \eta \int_0^\infty e^{-\eta x} e^{-i\omega x} dx = \frac{\eta}{\eta + i\omega} \quad (\eta > 0),$$

$$\overline{h}(\omega) = h^*(\omega) \quad (\eta > 0),$$

$$q(\omega) = \frac{h(\omega) + \overline{h}(\omega)}{2} = \frac{\eta^2}{\eta^2 + \omega^2}.$$

Noting that $H * \overline{H} = \frac{H+\overline{H}}{2} = Q$, we can write the analogue of Eq. (4.1) in the Fourier domain as

$$g(\omega) = \gamma h(\omega)h^*(\omega) + (1-\gamma)h(\omega)h^*(\omega)g(\omega). \tag{4.2}$$

Solving for $g(\omega)$ we have

$$g(\omega) = \frac{\gamma\eta^2}{\omega^2 + \gamma\eta^2}$$

and by inverse FT we find

$$G(x) = \frac{\sqrt{\gamma}\eta}{2} e^{-\eta\sqrt{\gamma}|x|}. \tag{4.3}$$

Discussion of Eq. (4.3) is now in order. Note that there is only one independent parameter, $\eta\sqrt{\gamma}$, for this family of distributions; the absorption probability $\gamma$ and the obstacle average density $\eta$ can be traded off against each other without affecting the distribution. As a check on this equation note that, for $\gamma = 1$ (perfectly opaque obstacles), the drunk falls asleep at the first step, and we have $G(x) = Q(x)$. Moreover, as the probability $\gamma$ of the drunk falling asleep at each given obstacle tends to zero, the density spreads more widely over the real line ($\eta\sqrt{\gamma} \to 0$).

Quantitatively, Eq. (4.3) provides an elegant prediction: at any fixed level of clutter in the environment, the effective radius of the signal scales as the square root of $1/\gamma$, the expected number of steps taken by the random walk. This phenomenon is closely related to the square-root-of-time scaling of the distance traveled by a symmetric random walk; however, the actual distributions in the two processes are quite different, being in this case a two-sided exponential rather than a normal distribution.

We can now obtain the average transmitted power flux at a distance $x_0 > 0$ from the origin, when radiating a narrow-band signal of unitary amplitude:

$$F(x_0) = \int_{x_0}^{\infty} G(x)dx = \frac{e^{-\eta\sqrt{\gamma}x_0}}{2}.$$

Note that when there are no obstacles ($\eta \to 0$), or when there is no absorption ($\gamma = 0$), $F(x_0) = 1/2$ as the power splits evenly along the two directions of the

lossless, obstacle free line.

## 4.2 Two dimensions

We now turn our attention to the two-dimensional case. The immediate generalization of Eq. (4.2) to two dimensions is

$$G(r) = \gamma Q(r) + (1-\gamma) Q * G(r), \tag{4.4}$$

where $G(r)$ is the probability of the drunk falling asleep at a given radial distance $r$ from the origin, and the probability density $Q(r)$ of the drunk finding the first obstacle at a radial distance $r$ from the origin is given by

$$Q(r) = \frac{\eta e^{-\eta r}}{2\pi r}.$$

For subsequent analysis, the FT of $Q(r)$ is needed:

$$q(u,v) = \int_{-\infty}^{+\infty} \int_{-\infty}^{+\infty} \frac{\eta e^{-\eta\sqrt{x^2+y^2}}}{2\pi\sqrt{x^2+y^2}} e^{-iux} e^{-ivy} dx dy.$$

By letting $x = r\cos\phi$, $y = r\sin\phi$, $u = \omega\cos\psi$, $v = \omega\sin\psi$, we have, for $\omega$ = distance from the origin:

$$q(\omega) = \frac{\eta}{2\pi} \int_0^{\infty} e^{-\eta r} dr \int_0^{2\pi} e^{-i\omega r\cos(\phi-\psi)} d\phi =$$

$$= \frac{\eta}{2\pi} \int_0^{\infty} e^{-\eta r} dr \int_0^{2\pi} \sum_{k=-\infty}^{+\infty} (-i)^k J_k(\omega r) e^{-ik(\phi-\psi)} d\phi =$$

$$= \eta \int_0^{\infty} e^{-\eta r} J_0(\omega r) dr,$$

where we use the Bessel functions $J_k(\cdot)$, and exploited the Bessel expansion 8.511.4 in Gradshteyn and Ryzhik (1994). Then, by means of identity 6.611.1 of Gradshteyn

and Ryzhik (1994), we obtain

$$q(\omega) = \frac{\eta}{\sqrt{\eta^2 + \omega^2}}.$$

Substituting $q(\omega)$ into the FT of Eq.(4.4), and solving for $g(\omega)$, we obtain

$$g(\omega) = \frac{\gamma\eta}{\sqrt{\eta^2 + \omega^2} - (1-\gamma)\eta},$$

and by inverse FT we obtain

$$G(r) = \frac{\gamma\eta}{(2\pi)^2} \int_0^\infty \frac{\omega}{\sqrt{\eta^2 + \omega^2} - (1-\gamma)\eta} d\omega \int_0^{2\pi} e^{i\omega r \cos(\psi - \phi)} d\psi =$$

$$= \frac{\gamma\eta}{(2\pi)^2} \int_0^\infty \frac{\omega}{\sqrt{\eta^2 + \omega^2} - (1-\gamma)\eta} d\omega \int_0^{2\pi} \sum_{k=-\infty}^{+\infty} i^k J_k(\omega r) e^{ik(\psi - \phi)} d\psi =$$

$$= \frac{\gamma\eta}{2\pi} \int_0^\infty \frac{\omega J_0(\omega r)}{\sqrt{\omega^2 + \eta^2} - (1-\gamma)\eta} d\omega. \tag{4.5}$$

Note that, for $\gamma = 1$ (perfectly opaque obstacles), the drunk falls asleep at the first step, and the integral reduces to

$$G(r) = \frac{\eta}{2\pi} \int_0^\infty \frac{\omega J_0(\omega r)}{\sqrt{\omega^2 + \eta^2}} d\omega = \frac{\eta e^{-\eta r}}{2\pi r} = Q(r),$$

as expected, see identity 6.554.1 in Gradshteyn and Ryzhik (1994).

In the general case of $\gamma \neq 1$ the integral in (4.5) is hard to compute. An exact solution, expressed in terms of an infinite series of Bessel polynomials is the following:

$$G(r) = \frac{\gamma\eta}{2\pi} \left[ \frac{e^{-\eta r}}{r} \left( 1 + \eta r \sum_{n=0}^{\infty} c_n \theta_n(\eta r) \right) + \alpha K_0(\sqrt{\eta^2 - \alpha^2} r) \right], \tag{4.6}$$

where

$$c_n = \frac{(1-\gamma)^{2(n+1)}}{(2n+1)!!},$$

$\alpha = \eta(1-\gamma)$, $\theta_n(\cdot)$ are the Bessel polynomials, see Grosswald (1980), and $K_0(\cdot)$ is the

modified Bessel function, see Gradshteyn and Ryzhik (1994). Derivation of Eq. (4.6) is reported in Section 4.10. In the following, we show a closed-form approximation.

We look at the Taylor expansion, with respect to $\eta$, of the function:

$$\frac{e^{-(\eta-\frac{\alpha^2}{\eta})r}}{r} = \sum_{n=0}^{\infty} \frac{1}{n!} \left(-\frac{\alpha^2}{\eta}\right)^n \frac{\partial^n}{(\partial\eta)^n} \left(\frac{e^{-\eta r}}{r}\right), \tag{4.7}$$

and note that the first two terms of this expansion are the same as the first two terms of $\frac{e^{-\eta r}}{r}\left(1+\eta r\sum_{n=0}^{\infty} c_n\theta_n(\eta r)\right)$. Therefore, neglecting higher-order terms, we obtain the following:

$$G(r) \approx \frac{\gamma\eta}{2\pi}\left[\frac{e^{-\frac{\eta^2-\alpha^2}{\eta}r}}{r} + \alpha K_0(\sqrt{\eta^2-\alpha^2}r)\right]. \tag{4.8}$$

We discuss the validity of the above approximation, numerically estimating the series of Bessel polynomials, in Section 4.11. Here we note that, in spite of being an approximation, Eq. (4.8) integrates to one as expected by a probability density:

$$\int_0^{2\pi} d\phi \int_0^{\infty} r\frac{\gamma\eta}{2\pi}\left[\frac{e^{-\frac{\eta^2-\alpha^2}{\eta}r}}{r} + \alpha K_0(\sqrt{\eta^2-\alpha^2}r)\right] dr =$$

$$= \gamma\eta\left(\frac{\eta}{\eta^2-\alpha^2} + \frac{\alpha}{\eta^2-\alpha^2}\right) = \frac{\gamma\eta}{\eta-\alpha} = 1.$$

Moreover, when $\gamma = 1$, $G(r) = Q(r)$ as expected.

Finally, exploiting Eq. (4.8), we calculate the average power flux at a distance $r_0 > 0$ from the origin, when radiating a narrow-band signal of unitary amplitude:

$$F(r_0) = \frac{1}{2\pi r_0}\int_0^{2\pi} d\phi \int_{r_0}^{\infty} rG(r)dr =$$

$$= \frac{1}{2\pi r_0}\left[\frac{1}{2-\gamma}e^{-\frac{\eta^2-\alpha^2}{\eta}r_0} + \frac{\sqrt{\gamma}\eta(1-\gamma)}{\sqrt{2-\gamma}}r_0 K_1(\sqrt{\eta^2-\alpha^2}r_0)\right], \tag{4.9}$$

see identity 5.52.1 in Gradshteyn and Ryzhik (1994).

It is interesting to check two limiting cases. When there are no obstacles ($\eta = 0$)

we have

$$F(r_0) = \frac{1}{2\pi r_0}\left[\frac{1}{2-\gamma} + \frac{\sqrt{\gamma}\eta(1-\gamma)}{\sqrt{2-\gamma}} r_0 K_1(z \to 0)\right] =$$

$$= \frac{1}{2\pi r_0}\left(\frac{1}{2-\gamma} + \frac{1-\gamma}{2-\gamma}\right) = \frac{1}{2\pi r_0},$$

having used the series expansion 8.446, of Gradshteyn and Ryzhik (1994), for $K_1(z)$. Similarly, when we have no absorption ($\gamma = 0$), we have

$$F(r_0) = \frac{1}{2\pi r_0}\left(\frac{1}{2} + \frac{1}{2}\right) = \frac{1}{2\pi r_0},$$

as in the case of propagation of a cylindrical wave over a free plane.

## 4.3 Three dimensions

In the three-dimensional case $Q(r)$ becomes

$$Q(r) = \eta \frac{e^{-\eta r}}{4\pi r^2},$$

and its FT, $q(\omega)$, is given by

$$q(\omega) = \int_0^{2\pi} d\phi \int_0^{\pi} \sin\theta d\theta \int_0^{\infty} r^2 e^{-i\omega\cos\theta r} Q(r) dr =$$

$$= \frac{\eta}{2}\int_0^{\pi} \sin\theta d\theta \int_0^{\infty} e^{-(\eta + i\omega\cos\theta)r} dr = \frac{\eta}{2}\int_0^{\pi} \frac{\sin\theta}{\eta + i\omega\cos\theta} d\theta =$$

$$= \frac{\eta}{\omega}\arctan\frac{\omega}{\eta}.$$

By substituting $q(\omega)$ into the Fourier transform of the equation:

$$G(r) = \gamma Q(r) + (1-\gamma) Q * G(r) \tag{4.10}$$

and solving for $g(\omega)$ we obtain

$$g(\omega) = \frac{\gamma \frac{\eta}{\omega} \arctan \frac{\omega}{\eta}}{1 - (1-\gamma)\frac{\eta}{\omega} \arctan \frac{\omega}{\eta}}; \tag{4.11}$$

by inverse FT we have,

$$G(r) = \frac{1}{(2\pi)^3} \int_0^{2\pi} d\phi \int_0^{\pi} \sin\theta d\theta \int_0^{\infty} \omega^2 g(\omega) e^{i\omega r \cos\theta} d\omega =$$

$$= \frac{1}{(2\pi)^2} \int_0^{\infty} \omega^2 g(\omega) d\omega \int_0^{\pi} \sin\theta \; e^{i\omega r \cos\theta} d\theta = \frac{2}{(2\pi)^2} \int_0^{\infty} \omega^2 g(\omega) \mathrm{sinc}(\omega r) d\omega, \tag{4.12}$$

where we have defined $\mathrm{sinc}\, x = (\sin x)/x$.

We note that the integrand in Eq. (4.12) oscillates as $\sin(\omega r)$, for $\omega \to \infty$. We regularize the integrand behavior, making the integral well defined, and compute it in Section 4.12, thus obtaining the following expression:

$$G(r) \approx \frac{\gamma\eta}{4\pi r^2} \left\{ \eta r (1-\gamma) e^{-\sqrt{1-(1-\gamma)^2}\eta r} + \frac{2}{\pi}[1-(1-\gamma)^2]\eta r \; K_1[(1-(1-\gamma)^2)\eta r] \right\}. \tag{4.13}$$

As a check, note that, in spite of being an approximation, the expression in Eq. (4.13) integrates to one, and so it is a probability density:

$$\int\int\int G(r) d\underline{\mathbf{v}} = \int_0^{2\pi} d\phi \int_0^{\pi} \sin\theta d\theta \int_0^{\infty} r^2 G(r) dr =$$

$$= \gamma\eta^2 \left\{ (1-\gamma) \int_0^{\infty} r e^{-\sqrt{1-(1-\gamma)^2}\eta r} dr + \frac{2}{\pi}[1-(1-\gamma^2)] \int_0^{\infty} r K_1[(1-(1-\gamma)^2)\eta r] \right\} =$$

$$= \gamma\eta^2 \left\{ \frac{1-\gamma}{[1-(1-\gamma)^2]\eta^2} + \frac{2}{\pi} \frac{1-(1-\gamma)^2}{[1-(1-\gamma)^2]^2\eta^2} \, \Gamma(3/2) \, \Gamma(1/2) \right\} =$$

$$= \frac{\gamma(2-\gamma)}{1-(1-\gamma)^2} = 1,$$

having used identity 6.561.16 in Gradshteyn and Ryzhik (1994).

Finally, exploiting Eq. (4.13), we calculate the average power flux at a distance

$r_0 > 0$ from the origin, when radiating a narrow-band signal of unitary amplitude:

$$F(r_0) = \frac{1}{4\pi r_0^2} \int_0^{2\pi} d\phi \int_0^{\pi} \sin\theta d\theta \int_{r_0}^{\infty} r^2 G(r) dr =$$

$$= \frac{\gamma\eta^2(1-\gamma)}{4\pi r_0^2} \int_{r_0}^{\infty} r e^{-\sqrt{1-(1-\gamma)^2}\eta r} dr - \frac{1}{4\pi r_0^2} \frac{2\gamma\eta}{\pi} \int_{r_0}^{\infty} r \frac{\partial}{\partial r} K_0[(1-(1-\gamma)^2)\eta r] dr =$$

$$= \frac{1}{4\pi r_0^2} \frac{\gamma(1-\gamma)}{1-(1-\gamma)^2} \left(\sqrt{1-(1-\gamma)^2}\eta r_0 + 1\right) e^{-\sqrt{1-(1-\gamma)^2}\eta r_0} + \frac{\gamma\eta}{2\pi^2 r_0^2} \left\{ r_0 K_0[(1-(1-\gamma)^2)\eta r_0] + \right.$$

$$\left. + \int_{r_0}^{\infty} K_0[(1-(1-\gamma)^2)\eta r] dr \right\}. \tag{4.14}$$

Letting $[1-(1-\gamma)^2]\eta = \beta$, we use the asymptotic approximation 8.451.6 for $K_0(\cdot)$ in Gradshteyn and Ryzhik (1994) to calculate the last integral in Eq. (4.14):

$$\int_{r_0}^{\infty} K_0(\beta r) dr = \frac{1}{\beta} \int_{\beta r_0}^{\infty} K_0(x) dx \approx \frac{1}{\beta} \sqrt{\frac{\pi}{2}} \int_{\beta r_0}^{\infty} \frac{1}{\sqrt{x}} e^{-x} dx =$$

$$= \frac{1}{\beta} \sqrt{2\pi} \int_{\sqrt{\beta r_0}}^{\infty} e^{-u^2} du = \frac{\pi}{\sqrt{2}\beta} \operatorname{Erfc}(\sqrt{\beta r_0}) \tag{4.15}$$

having defined $u = \sqrt{x}$, and $\operatorname{Erfc}(u) = 1 - \operatorname{Erf}(u) = \frac{2}{\sqrt{\pi}} \int_u^{\infty} e^{-t^2} dt$.

The asymptotic approximation that we have used for $K_0(\cdot)$ is accurate only for large values of the argument. Hence, accuracy of the integral in (4.15) depends on the value of $\beta r_0$. If we let $\beta r_0 \to 0$ we discover that while

$$\lim_{\beta r_0 \to 0} \int_{\beta r_0}^{\infty} K_0(x) dx = \frac{\pi}{2},$$

$$\lim_{\beta r_0 \to 0} \frac{\pi}{\sqrt{2}} \operatorname{Erfc}(\sqrt{\beta r_0}) = \frac{\pi}{\sqrt{2}}.$$

To improve the approximation in Eq. (4.15) for small values of $\beta r_0$, we introduce an additional factor as follows:

$$\int_{\beta r_0}^{\infty} K_0(x) dx \approx \frac{\pi}{2} \operatorname{Erfc}(\sqrt{\beta r_0}) \frac{1/\sqrt{2} + 10\beta r_0}{1 + 10\beta r_0}. \tag{4.16}$$

Defining

$$Err_1 = \left| \int_{\beta r_0}^{\infty} K_0(x)dx - \frac{\pi}{2}\mathrm{Erfc}(\sqrt{\beta r_0}) \right|,$$

$$Err_2 = \left| \int_{\beta r_0}^{\infty} K_0(x)dx - \frac{\pi}{2}\mathrm{Erfc}(\sqrt{\beta r_0})\frac{1/\sqrt{2}+10\beta r_0}{1+10\beta r_0} \right|,$$

numerical estimation shows that the additional factor improves the error of the approximation from $Err_1 < \pi/2 - \pi/\sqrt{2} = 0.65$ to $Err_2 < 0.067$.

Substituting Eq. (4.16) into Eq. (4.14), we finally have

$$F(r_0) = \frac{1}{4\pi r_0^2}\left\{ \frac{\gamma(1-\gamma)}{1-(1-\gamma)^2}(\sqrt{\beta\eta}r_0+1)e^{-\sqrt{\beta\eta}r_0} + \right.$$

$$\left. + \frac{2\gamma\eta r_0}{\pi}K_0(\beta r_0) + \frac{\sqrt{2}\gamma\eta}{\beta}\mathrm{Erfc}(\sqrt{\beta r_0})\frac{1/\sqrt{2}+10\beta r_0}{1+10\beta r_0} \right\}. \qquad (4.17)$$

It is interesting to check two limiting cases. When there are no obstacles ($\eta = 0$), we have

$$F(r_0) = \frac{1}{4\pi r_0^2}\left[ \frac{\gamma(1-\gamma)}{1-(1-\gamma)^2} + \frac{\gamma}{1-(1-\gamma)^2} \right] = \frac{1}{4\pi r_0^2}$$

When there is no absorption ($\gamma = 0$), we have

$$F(r_0) = \frac{1}{4\pi r_0^2}\left(\frac{1}{2}+\frac{1}{2}\right) = \frac{1}{4\pi r_0^2},$$

as in the case of propagation of a spherical wave in free space.

## 4.4 Modeling the power density

In the previous sections we derived the expression of the average power flux at a given distance from the transmitter. In this section we are interested in computing the corresponding power density. In our probabilistic model this is defined as the number of photons $P(r)$ per unit area that hit the external surface of a sphere of radius $\Delta r$ centered at distance $r$ from the source. The power flux has been related to $G(r)$; similarly, we want now to find the connection between $P(r)$ and $G(r)$.

We start by considering the number of photons absorbed inside the sphere of radius $\Delta r$, which is given by $G(r)(4\pi/3)\Delta r^3$. Letting $l$ be the average path length of a photon inside the sphere, this quantity also equals (in the limit for $\Delta r \to 0$) the number of photons $P(r)4\pi\Delta r^2$ that enter the sphere times the absorption coefficient $\gamma$ and the average number of reflections $\eta\, l$ experienced by a single photon inside the sphere. Clearly, $L = P(r)4\pi\Delta r^2\ l$ is the total path length of the photons inside the sphere, and we have the equation:

$$\frac{4}{3}\pi\Delta r^3 G(r) = L\gamma\eta. \tag{4.18}$$

Similarly, in 2-D we have $L = P(r)2\pi\Delta r\ l$, where $P(r)$ is the number of photons per unit length that enter a circle of radius $\Delta r$ centered at distance $r$ from the source, and Eq. (4.18) becomes

$$\pi\Delta r^2 G(r) = L\gamma\eta. \tag{4.19}$$

A simple trigonometric exercise leads to the expression:

$$L = P(r)\frac{4}{3}\pi\Delta r^3$$

in 3-D, and similarly in 2-D:

$$L = P(r)\pi\Delta r^2.$$

Substituting the total path length $L$ into Eqs. (4.18) and (4.19), we find the expression for the power density:

$$P(r) = \frac{G(r)}{\gamma\eta}. \tag{4.20}$$

## 4.5 Results of the theoretical model

The power density and power flux predicted by our three-dimensional model are compared with free space propagation in Fig. 1.11, for values of the parameters corresponding to having on average one reflection every ten meters and an absorption coefficient of the obstacles of approximately 15%. These values are determined by

fitting the model using experimental data collected in a microcell located in the city of Rome, Italy. Details on the data collection method and on the fitting procedure are given in the subsequent sections. We point out that the point of transition from an inverse square law to an exponential attenuation depends on the values of the parameters that can be tuned to different environments. In particular, in the case of an empty environment without absorbing obstacles, this transition does not occur and the model correctly predicts an inverse square attenuation law, as appropriate to isotropic radiation. On the contrary, in the presence of absorbing obstacles, the flux model presents a smooth transition from the $1/r^2$ law to an exponential attenuation; the power density model, although providing a very similar fit to the experimental data, predicts slightly higher power near the source. This is due to having part of the power being reflected back by the obstacles toward the source. A more detailed explanation of this phenomenon is given in the next section.

## 4.6 Relationships with the classical theory

The obvious starting point to characterize propagation in a wireless channel would be to use Maxwell equations. In principle, these can provide a complete characterization of the propagation loss in any given media. However, in the case of a rich scattering environment such as an urban area, this approach does not lead to closed-form solutions. Hence, numerical solvers, empirical formulas, experimental measurements, and computer simulations are often used in practice.

An alternative approach is to treat the city as a random environment, and consists in studying propagation in a random medium. We acknowledge the existence of extensive literature on propagation in random media which dates back to the beginning of last century, with the study of radiation of light in foggy atmospheres. Historically, the problem has been investigated from two distinct points of view. One is "radiative transfer theory" or "transport theory," and the other is "multiple scattering theory" or "analytical theory."

Radiative transfer theory is heuristic and deals directly with the transport of en-

ergy through a medium containing particles, it is based on the equation of radiative transfer, which is a differential equation equivalent to the Maxwell-Boltzmann collision equation used in the kinetic theory of gases and in neutron transport theory.

Analytical theory is more rigorous and starts with the wave equation or with Maxwell equations, obtains a solution for the scattering by a single particle, introduces the interaction effects of many particles, and then considers statistical averages.

The two theories deal with the same phenomena, even though their starting points are different, therefore there are fundamental relationships between them. These are outlined in the classic book by Ishimaru (1978), which shows (see Chapter 14) that under certain approximations it is possible to derive the transport equation using analytical theory.

It is interesting that our proposed wandering photon model can also be related to transport theory, although it starts from different premises.

The (numerical) solution of the transport theory model in the case of a spherical wave radiating in a random medium of isotropic scatterers is outlined in Chapter 12 of Ishimaru (1978). The transport equation reduces to an integral equation for the specific intensity (Eq. (12.4) in Ishimaru(1978)) that is similar to our Eq. (4.10). However, the terms in the two equations have different meanings in the two models and are multiplied by different coefficients. Nevertheless, the functional form of the equation, and hence of the solution, is similar in the two cases. The similarity between Eq. (12.4) of Ishimaru and our Eq. (4.10) suggests that the p.d.f. of the location where the random walk stops must be related to the specific intensity in transport theory. In the following, we explore this relationship.

A graphical comparison of the power density and the power flux, analytically derived from the p.d.f. of the location where the random walk stops, with the corresponding transport theory quantities, numerically derived solving the equation of radiative transfer, is depicted in Fig. 4.1. Our 3-D formulas (4.17) and (4.20) are plotted on the right-hand side of the figure, while plots, derived numerically as in Ishimaru (1978), appear on the left-hand side. Note that to be coherent with Fig.12.3 of Ishimaru (1978), we have normalized both plots by an $r^2$ factor.

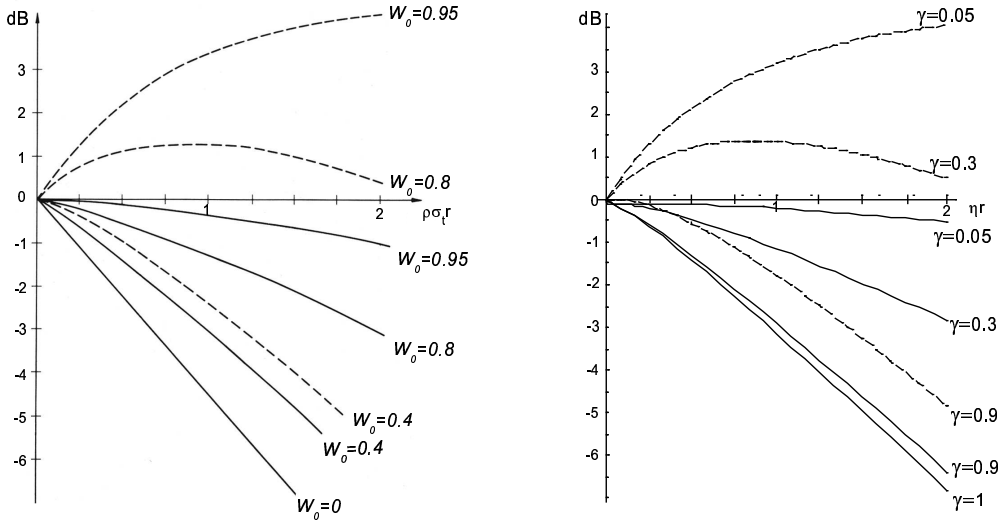


Figure 4.1: **Comparison with transport theory.** *The dashed curves represent the power density (normalized by an $r^2$ factor), and the solid line curves represent the power flux (normalized by an $r^2$ factor). Left-hand side: results from transport theory obtained numerically solving the equation of transfer. Right-hand side: analytical results according to the wandering photon model.*

There is no doubt that the graphical behavior of the two sets of curves is very similar. However, we limit ourselves only to a qualitative comparison of the two plots, for two reasons. First, the parameters of the two theories are different: we use the absorption coefficient ($\gamma$), and the average step length ($1/\eta$) of the random walk, whereas transport theory uses the particles number per unit volume ($\rho$) and the absorption ($\sigma_a$), scattering ($\sigma_s$), and total ($\sigma_t = \sigma_a + \sigma_s$) particle cross section. Second, the transport theory curves are parametrized by the albedo $W_0 = \sigma_s/\sigma_t$, which is not independent from the abscissa coordinate $\rho\sigma_t r$; whereas the wandering photon curves are parametrized by the absorption coefficient $\gamma$, that is totally independent from the abscissa coordinate $\eta r$. Another difficulty is in the absence of an analytical solution for the transport theory approach, so that no direct comparison between equations is possible.

We now look at some limiting cases. We note that on both plots, when we move toward a lossless medium ($\gamma \to 0, W_0 \to 1$), the flux (solid line) curves tend to the $1/r^2$ abscissa line; while the density (dashed line) curves tend to diverge, as they tend

| *PARAMETERS* | *OBSTACLES* | *Power Density, 2-D* | *Power Density, 3-D* |
|---|---|---|---|
| $\gamma \to 1$, $\eta > 0$ | mostly absorbing | exponential attenuation | exponential attenuation |
| $\gamma \to 0$, $\eta r < \infty$ | mostly scattering | $\infty$ | $\sim 1/r$ |
| $\eta = 0$ | no obstacles | $\sim 1/r$ | $\sim 1/r^2$ |
| | | *Power Flux, 2-D* | *Power Flux, 3-D* |
| $\gamma \to 1$, $\eta > 0$ | mostly absorbing | exponential attenuation | exponential attenuation |
| $\gamma \to 0$, $\eta r < \infty$ | mostly scattering | $\sim 1/r$ | $\sim 1/r^2$ |
| $\eta = 0$ | no obstacles | $\sim 1/r$ | $\sim 1/r^2$ |

Table 4.1: **Power at large distance as predicted by our model.**

to $1/r$. This phenomenon of $1/r$ slow decay of the power density is known in transport theory and is due to part of the energy being reflected back toward the source. It can also be interpreted, in our model, in terms of recurrent properties of random walks. Let us look at the decay laws predicted by our model and depicted in Table 4.1, and let us focus on the power density. According to our formulas, when obstacles are mostly scattering, the power density attenuates as $1/r$ in 3-D and diverges, with a log singularity, in 2-D. The explanation is that random walks in 2-D are recurrent, hence, when there is no absorption, the same photon visits infinitely many times the same disc of arbitrary radius $\epsilon$. On the contrary, in 3-D the probability of the random walk to re-visit the same sphere of arbitrary radius $\epsilon$ is less than one, hence, perfectly reflecting scatterers lead only to a decrease of the rate of decay of the power density from $1/r^2$ to $1/r$, due to a finite number of recurrent visits and eventual diffusion of photons in space. Note that random walks recurrence properties do not effect the power flux decay law, because, according to its definition, the power flux simply measures the number of photons that escape beyond a given radial distance, hence does not count recurrent photons multiple times. Accordingly, the power density plots reported in Figure 4.1 can become greater than unity, due to recurrent visits, but the total power flow in the radial direction, given by the power flux, can never be greater than one (total source of power).

## 4.7 Experiments

We now apply our theoretical model of propagation to predict the path loss of a wireless channel. By using a non-linear regression algorithm we fit Eq. (4.17) and Eq. (4.20) to experimental data collected in a microcell located in an urban area and we measure the accuracy of the prediction by evaluating the root mean square error $\sigma_{std}$ of the model on the measured data. The two equations that we use to fit experimental data correspond to two different ideal measurements: the power flux equation measures the flux of photons passing through an antenna of given area oriented toward the source; the power density equation measures the total number of photons passing through the antenna, coming from any direction. Hence, Eq. (4.17) is more suited to model directional receiving antennas, while Eq. (4.20) is more suited to model isotropic receiving antennas. However, we note that Eq. (4.20) counts photons multiple times, if they are reflected back toward the receiver. Our experimental analysis shows that in practice both formulas lead to a similar result of a propagation loss that, due to absorption, presents a smooth transition from free space propagation to exponential attenuation (see Fig. 1.11).

We summarize our experimental findings as follows:

- The propagation law predicted by our model is in good agreement with experimental data. To have an idea of the quality of the matching we perform monotonic regression, see Berlow et al. (1972), to find the best, in mean square, non-decreasing function fitting the data. This function provides a lower bound on the minimum value of $\sigma_{std}$ that can be achieved by any theoretical model of propagation. Comparing the $\sigma_{std}$ obtained by fitting our model with the one achieved by monotonic regression, we find a less than 2 $dB$ increase.

- The values found for the parameters $\eta$ and $\gamma$ when fitting our model to the experimental data are reasonable when physically interpreted as density and absorption coefficient of the obstacles in the considered urban area, thus suggesting a possible direct use of our formulas without experimental tuning of the

parameters. The parameters are are also very stable under random perturbation of the data.

- We introduce a simplified, exponential path loss formula that proves to be as powerful for prediction as the complete formulas derived in our model. The parameters of this simple formula, however, do not have any physical meaning and must be determined by fitting experimental data.

- We find that our model provides a superior fit to the data than the simple power law model (Hata (1980) formula). In addition, it provides good theoretical ground to empirical models that use a transition from low to high order power laws to fit experimental data.

## 4.8 Data collection method

Experimental measurements, collected in Rome, Italy, are courtesy of Ericsson Telecomunicazioni SpA. The transmitting antenna was a vertical dipole located at a height of 6m and transmitting a continuous wave (CW) at a frequency of 900 MHz, with a radiated power $P_t = 6.3\ W$, transmitting gain $G_t = 2\ dB$, and $EIRP = P_t G_t = 40\ dBm$. The antenna was located in "Piazza dei Quiríti," in the "Prati" district of Rome, near the Vatican city, at 12.46591E latitude, 41.91017N longitude (see map in Fig. 4.2). The receiving antenna, a dipole of $G_r = 2\ dB$, was mounted on top of a moving vehicle at a height of approximately 1.5m. The vehicle was equipped with a GPS, to record the position of each sampled data point, and drove around the transmitting site (see right-hand side of Fig. 4.2). Each data point consisted of the received power averaged over 50 measurements along a path of 40 wavelengths (Lee method) .

Fig. 4.3 depicts the collected data: the received power is represented by a vertical line drawn at each data point. Fig. 4.4 depicts a view of the location where some of the measurements were taken and shows the presence of different scatterers in the environment. For subsequent analysis, a reduction in the size of the data was performed as follows. The receiving equipment rounded the smallest value of received

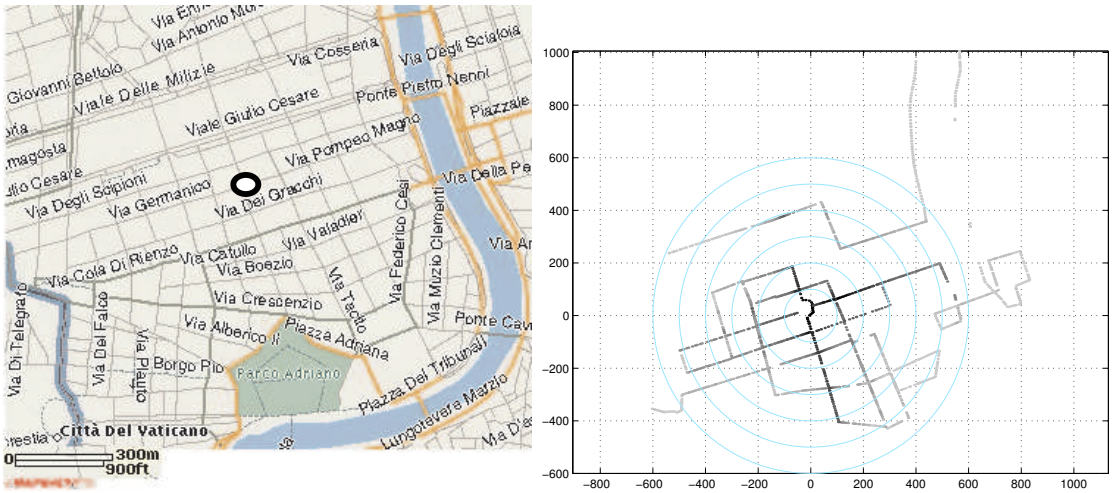


Figure 4.2: **Measurements location.** *Measurements were taken in the "Prati" district of Rome, near the Vatican city. The transmitting antenna was placed in "Piazza dei Quiríti," which is highlighted by the black circle in the map on the left-hand side of the figure. The right-hand side of the figure shows the path taken by the van as it drove around the transmitting site. Each data point is shown with a gray level proportional to the power of the received signal. Circles centered at the transmitting site are drawn with increasing radii of* 100 *m steps. The map on the left-hand side of the figure is taken from* `http://www.mapquest.com`*. Power level measurements are courtesy of Ericsson Telecomunicazioni SpA.*

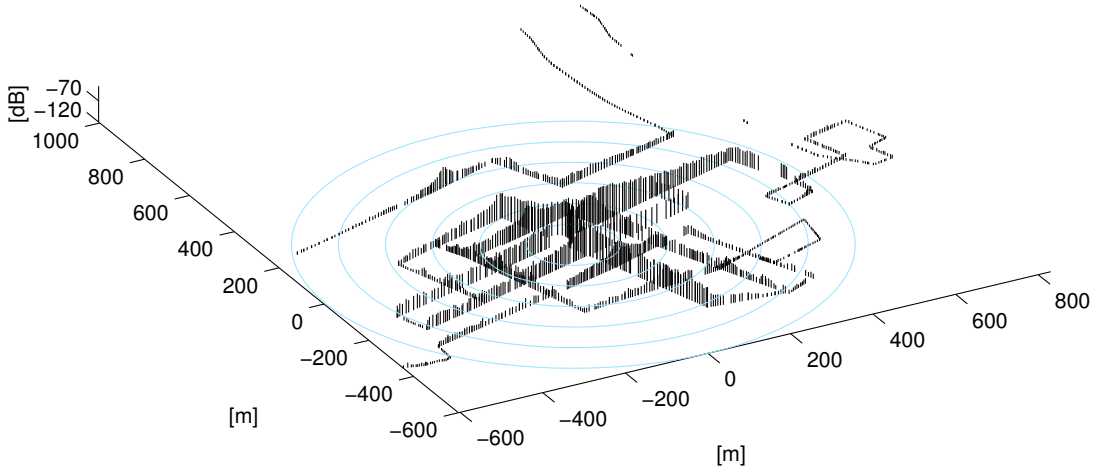


Figure 4.3: **Plot of the received power.** *A vertical line is drawn at each data point. The height of the line corresponds to the value of the received power expressed in dB. Circles centered at the transmitting site are drawn with increasing radii of* 100 *m steps.*

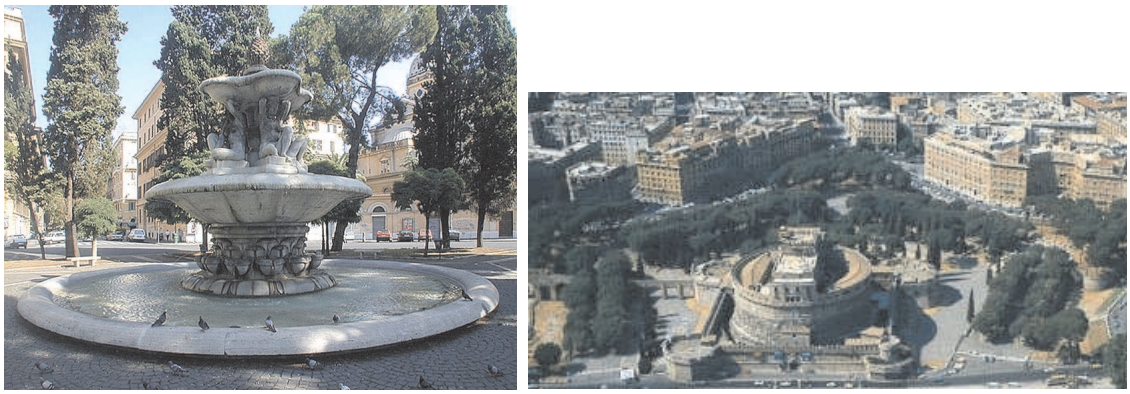

Figure 4.4: **View of the location.** *The left-hand side of the figure depicts "piazza dei Quiríti," where the transmitting antenna was located. The right-hand side of the picture depicts a view of "Parco Adriano" and of the surrounding streets where some of the measurements were taken.*

power to -114 dB; therefore, in order to have an unbiased set of data, we considered only points located at a radial distance from the transmitter less than 317m, for which the received power was always higher than -114 dB. Moreover, the vehicle moving around the transmitting site collected a larger amount of data points as the radial distance from the transmitter increased. For example, a larger number of data points were collected on an ideal circle of radius 200m centered at the transmitting site, compared to the number of data points collected on an ideal circle of radius 50m. Hence, in order to remove this unwanted bias toward farther points, we averaged all data points inside annuli of 5m intervals, generating a uniform set of measurements along the radial direction. This corresponds to performing a local spatial average similar to the standard Lee method, but performed on a small annular area.

Finally, we point out that all measurements were taken along the streets of a fairly regular neighborhood. We expect our model to even better fit data collected in a more open environment, filled with random scatterers, such as, for example, a park.

## 4.9 Model fitting

In order to fit the propagation loss formulas to the measured data we need to convert the flux and density in our 3-D model expressed by Eqs. (4.17) and (4.20) to the actual received power of the antenna in our system. We do so by adding a multiplicative factor $C$ to the formulas that takes into account for the transmitted power, gain of the transmitting antenna, effective area of the receiving antenna, and additional hardware losses in the system. Then we perform a non-linear least squares procedure to determine values of $C$, $\eta$ and $\gamma$ that minimize the $rms$ error $\sigma_{std}$ from the sampled data.

By including the multiplicative factor $C$ to Eqs. (4.17) and (4.20) we obtain an expression for the power received by an antenna located at a distance $r_0$ from the transmitter of the type:

$$P_{recv}(r_0) = \frac{C}{r_0^2}\, f(\eta r_0, \gamma), \tag{4.21}$$

where $f(\cdot)$, which is $r_0^2$ times either Eq. (4.17) or (4.20), is a function of the two dimensionless parameters $\eta r_0$ and $\gamma$, and $C$ is expressed in $[Wm^2]$ units. We use Eq. (4.21) to define the measured Path Loss for the considered experiments as the expression in dB:

$$PL(r_0) = -[P_{recv}(r_0)]_{dB}, \tag{4.22}$$

and the $rms$ error of the predicted path loss from the sampled data as

$$\sigma_{std} = \sqrt{\frac{\sum_{j=1}^{n}[PL_m(r_j) - PL(r_j)]^2}{n}},$$

where $n$ is the number of measured data points, $PL_m(r_j)$ is the measured path loss at the jth point located at a radial distance $r_j$ from the transmitter, and $PL(r_j)$ is the corresponding predicted path loss derived from Eq. (4.22). To minimize the $rms$ error we use the standard MATLAB procedure `lsqnonlin()` that is a fairly sophisticated non-linear least squares routine based on the Gauss-Newton algorithm. Accordingly (see Fig. 1.11), we find the values $\eta = 0.09$, $\gamma = 0.17$, $C = 0.065$, and a corresponding

$\sigma_{std} = 3.72\ dB$, for the flux model; and the values $\eta = 0.12$, $\gamma = 0.12$, $C = 0.02$, $\sigma_{std} = 3.6\ dB$, for the power density model. These values correspond to having on average one obstacle every ten meters, with an absorption coefficient of $12\% \sim 17\%$. These values are reasonable for the considered urban area. In addition, with reference to the flux model for which the Friis formula is appropriate, see Rappaport(1996), we can compute the value of $C$ analytically: the Friis formula becomes

$$P_{recv}(r_0) = (EIRP)\ \ A\ \ F(r_0),$$

$A$ being the effective area of the receiving antenna, because $F(r_0) \to 1/(4\pi r_0^2)$ in the uncluttered environment. Accordingly, $C = (EIRP)A = 0.069$ for the experimental equipment and radiated power, where we have included the extra factor 0.5 accounting for the random incident polarization on the receiving dipole.

All of this suggests that, in principle, values of the parameters that match the characteristics of the environment and of the used equipment can be chosen without performing experiments, but by estimating directly the amount of clutter in the environment (i.e., the density of the scatterers), the absorption coefficient of the scatterers, and the gains and losses in the equipment. This method can be considerably less expensive than performing experiments, and can be used to obtain rough, initial guidelines on the path loss of a given environment.

### 4.9.1 Sensitivity of the model to noise

As indication of robustness of our theoretical model, we check if the physical parameters, absorption coefficient ($\gamma$) and average number of reflections per meter ($\eta$), are stable under random perturbation of the data. We do so by adding log-normal random noise of zero mean and standard deviation $\sigma_{noise}$ to the data and determining, via non-linear regression, the parameters $\eta$ and $\gamma$ for different values of $\sigma_{noise}$. Results are presented in Fig. 4.5. We note that the parameters are very stable under perturbations up to 7 dB. This suggests that they capture real physical properties of the environment that are invariant to random noise. Moreover, we note that the values of

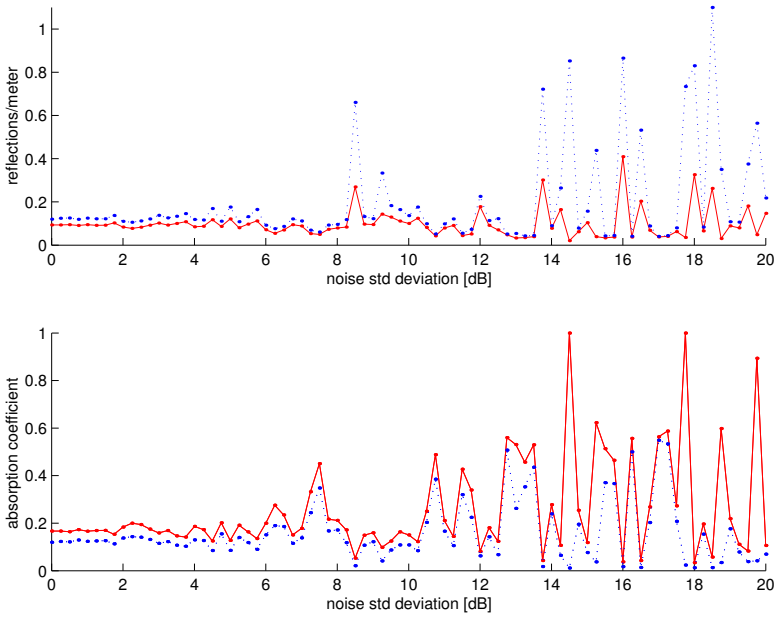


Figure 4.5: **Sensitivity analysis.** *Predictions of the flux model are indicated with continuous lines, predictions of the density model are indicated with dotted lines.*

the parameters predicted by the power flux model (continuous line) are very close to the values predicted by the power density model (dotted line), up to perturbations of 13 dB; which implies that either of the two models can be used to fit the parameters. For higher values of the perturbation noise, the flux model is more stable in predicting the average number of reflections per meter $\eta$, while the density model is more stable in predicting the absorption coefficient $\gamma$.

### 4.9.2 A simplified exponential formula

For quick, practical calculation purposes, engineers may prefer to express the path loss using a simple formula, rather than the more elaborate formulas that we have derived in our model. The plots of our elaborate formulas, depicted in Fig. 1.11, suggest a behavior that follows an inverse square law, with a smooth transition to an exponential law, as the distance between transmitter and receiver increases. Accordingly, we are led to the following simplified formula for path loss prediction:

$$PL^{-1}(r) = B\frac{e^{-br}}{r^2}. \tag{4.23}$$

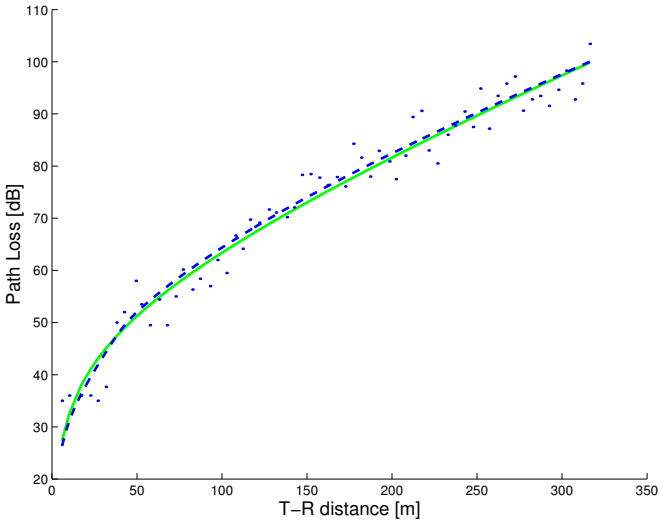


Figure 4.6: **Complete vs. simplified formula.** *The scattered points represent measured data. The dashed line represents the fit of the data using our flux model. The continuous line represents the fit of the data using our simplified formula (4.23). The rms error of the flux model, is* $\sigma_{std} = 3.72\ dB$*; the rms error of the simplified formula is* $\sigma_{std} = 3.75\ dB$*.*

The above formula proves to be as powerful in fitting the experimental data as the complete formulas derived directly from the theoretical model. In Fig. 4.6 we compare results of the simplified formula with the complete formula using the flux model. Values of the $rms$ errors are practically indistinguishable at $\sigma_{std} = 3.72\ dB$ for the complete formula and $\sigma_{std} = 3.75\ dB$ for the simplified one. The physical meaning of the parameters is, however, lost in the simplified formula.

### 4.9.3 Comparison with Hata formula and best fit

Finally, we compare our results with the simple power law model (Hata (1980) formula) and with the result of monotonic regression performed on the measured data. The monotonic regression of a function is the best, in mean square, nondecreasing function fitting the data, see Barlow et al. (1972). It provides a lower bound on the minimum value of $\sigma_{std}$ that can be achieved by any theoretical model of propagation: Any path loss prediction that does not depend on specific knowledge of an inhomogeneous environment, and in particular that is a function only of distance from the transmitter and general properties of the environment, must be a nondecreasing func-

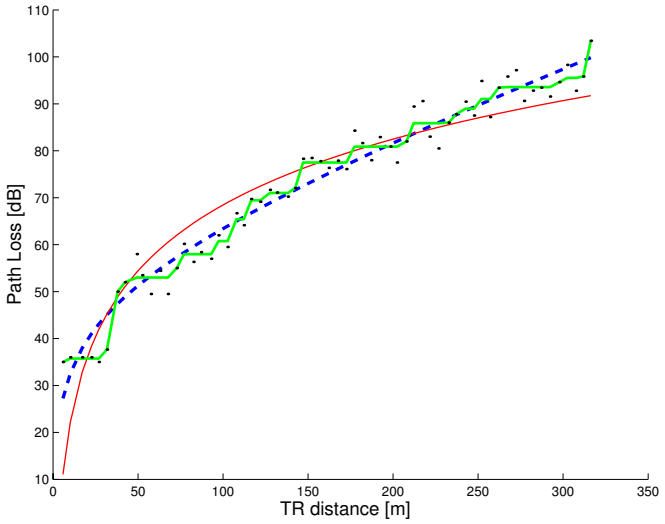


Figure 4.7: **Comparison.** *The dashed line represents the fit of the data using the simplified path loss formula. The thin continuous line represents the fit of the data using a power law. The "staircase" line is the result of the monotonic regression, representing the best nondecreasing function fitting the data. Values of the rms error are reported in Table 4.2*

.

tion of distance. The comparison is depicted in Fig. 4.7 and Table 4.2, and validates our model that closely follows the monotonic regression line depicted in Fig. 4.7.

In Fig. 4.7, it is also evident what is the typical problem of applying the simple Hata formula, popular in cellular systems design, to predict the path loss in micro-cellular systems: a power law with a fixed exponent (4.66 in this case) overestimates the real path loss in the close range, where the signal undergoes few reflections to reach the receiver and propagation is almost as in free space, and it underestimates the real path loss at larger distances, where there is an exponential attenuation, due to the absorption of many reflecting obstacles. Empirical formulas characterized by two different power laws, one with an exponent close to two, to be used close to the transmitter, and another with a high-order exponent, to be used after a breakpoint distance, are better suited for prediction in this kind of environments and can be theoretically justified by our model.

| *Model* | $\sigma_{std}$ | *Exponent* | *Multiplicative Factor* |
|---|---|---|---|
| $PL^{-1}(r) = A(\frac{1}{r})^a$ | 6.053 $dB$ | $a = 4.66$ | $A = .0034$ |
| $PL^{-1}(r) = B\frac{e^{-br}}{r^2}$ | 3.75 $dB$ | $b = 0.028$ | $B = .0765$ |
| Monotonic Regression | 2.04 $dB$ | | |

Table 4.2: **Regression Results.** *The first line of the Table is relative to the Hata formula. The second line is relative to the simplified formula of Eq. (4.23). The third line is relative to monotonic regression.*

## 4.10 Exact calculation of G(r), 2-D

In this section we show the exact derivation of $G(r)$ in 2-D, written as a series of Bessel polynomials. Let $\alpha = \eta(1-\gamma)$. We rewrite Eq. (4.5) as follows:

$$G(r) = \frac{\gamma\eta}{2\pi}\int_0^\infty \frac{\omega J_0(\omega r)}{\sqrt{\omega^2+\eta^2}-\alpha}d\omega =$$

$$= \frac{\gamma\eta}{2\pi}\int_0^\infty \frac{\omega J_0(\omega r)}{\omega^2+\eta^2-\alpha^2}\left(\sqrt{\omega^2+\eta^2}+\alpha\right)d\omega =$$

$$= \frac{\gamma\eta}{2\pi}\left[\alpha\int_0^\infty \frac{\omega J_0(\omega r)}{\omega^2+\eta^2-\alpha^2}d\omega + \int_0^\infty \frac{\omega J_0(\omega r)\sqrt{\omega^2+\eta^2}}{\omega^2+\eta^2-\alpha^2}d\omega\right] =$$

$$= \frac{\gamma\eta}{2\pi}\left(\widehat{\mathcal{I}}_1+\widehat{\mathcal{I}}_2\right) = \frac{\gamma\eta}{2\pi}\left[\alpha K_0(\sqrt{\eta^2-\alpha^2}r)+\widehat{\mathcal{I}}_2\right],$$

having used identity 6.532.4, in Gradshteyn and Ryzhik (1994), to calculate integral $\widehat{\mathcal{I}}_1$. We can then write integral $\widehat{\mathcal{I}}_2$ as a series of integrals,

$$\widehat{\mathcal{I}}_2 = \int_0^\infty \frac{\omega J_0(\omega r)}{\sqrt{\omega^2+\eta^2}\left(1-\frac{\alpha^2}{\omega^2+\eta^2}\right)}d\omega =$$

$$= \int_0^\infty \frac{\omega J_0(\omega r)}{\sqrt{\omega^2+\eta^2}}\sum_{n=0}^\infty \frac{\alpha^{2n}}{(\omega^2+\eta^2)^n}d\omega = \sum_{n=0}^\infty \alpha^{2n}\int_0^\infty \frac{\omega J_0(\omega r)}{(\omega^2+\eta^2)^{n+1/2}}d\omega = \sum_{n=0}^\infty \mathcal{I}_n.$$

We have the following recurrence relation:

$$\begin{cases} \mathcal{I}_0 = & \displaystyle\int_0^\infty \frac{\omega J_0(\omega r)}{\sqrt{\omega^2+\eta^2}} d\omega = \frac{e^{-\eta r}}{r} \\ \\ \mathcal{I}_{n+1} = & \displaystyle\frac{-\alpha^2}{(2n+1)} \frac{1}{\eta} \frac{\partial}{\partial \eta} \mathcal{I}_n. \end{cases} \tag{4.24}$$

We recall that Bessel polynomials are defined, see Grosswald (1980), as

$$\theta_n(z) = \sum_{j=0}^{n} a_j z^{n-j},$$

where all coefficients are integers given by

$$a_j = \frac{(n+j)!}{2^j \ (n-j)! \ j!}.$$

From the recurrence (4.24) and the definition of $\theta_n$, it follows that

$$\widehat{\mathcal{I}_2} = \sum_{n=0}^{\infty} \mathcal{I}_n = \frac{e^{-\eta r}}{r} \left[ 1 + \eta r \sum_{n=0}^{\infty} c_n \theta_n(\eta r) \right], \tag{4.25}$$

where

$$c_n = \frac{(1-\gamma)^{2(n+1)}}{(2n+1)!!},$$

which gives the exact formula for $G(r)$ reported in Eq. (4.6).

## 4.11 Estimate of the approximation error, 2-D

In this section we discuss the validity of the approximation in Eq. (4.8), numerically estimating the series of Bessel polynomials. Letting $\eta r = R$, we have

$$G(R) = \frac{\gamma \eta^2}{2\pi} \left[ \frac{e^{-R}}{R} \left( 1 + R \sum_{n=0}^{\infty} c_n \theta_n(R) \right) + (1-\gamma) K_0(\sqrt{1-(1-\gamma)^2} R) \right] =$$

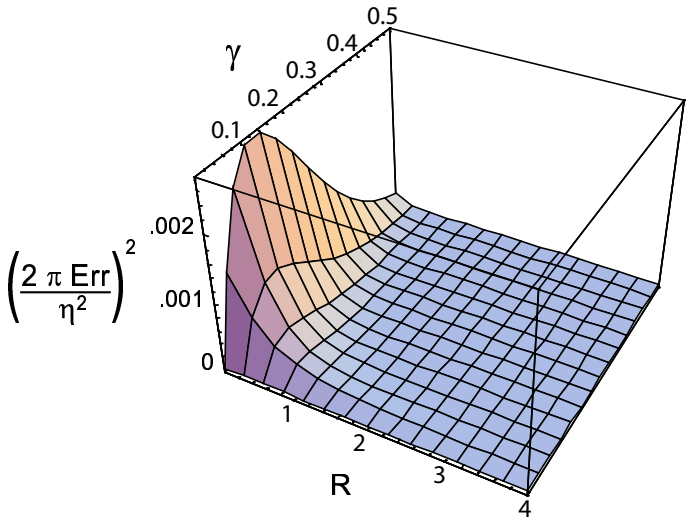


Figure 4.8: **Estimate of the error.** *The plot depicts an estimate of the squared error of the approximation.*

$$\approx Appr(R) = \frac{\gamma\eta^2}{2\pi}\left[\frac{e^{-R}}{R}\ e^{(1-\gamma)^2 R} + (1-\gamma)K_0(\sqrt{1-(1-\gamma)^2}R)\right].$$

Note that it would be misleading to refer to the relative error, because both $G(R)$ and $Appr(R)$ tend to zero, as $R \to \infty$. Accordingly, we evaluate the absolute error. Letting $Err = G - Appr$, we depict in Fig. 4.8 a plot of the function:

$$\left(\frac{2\pi Err}{\eta^2}\right)^2 = \left\{\gamma\frac{e^{-R}}{R}\left[1 + R\sum_{n=0}^{\infty} c_n\theta_n(R) - e^{(1-\gamma)^2 R}\right]\right\}^2;$$

numerical estimation suggests that the error is bounded by

$$|Err| < \frac{\sqrt{0.0027}}{2\pi}\eta^2.$$

## 4.12 Calculation of $G(r)$, 3-D

In order to compute $G(r)$, we use the following approximation (see Gradshteyn and Ryzhik (1994), identity 1.644.1) in Eq. (4.12):

$$\arctan\frac{\omega}{\eta} \approx \frac{\omega/\eta}{\sqrt{1+\left(\frac{\omega}{\eta}\right)^2}},$$

that does not change the observed oscillatory behavior of the integrand. Note that this approximation is accurate for small values of the argument and has a bounded error for large values of it. However we show that after regularizing the oscillatory integrand, the approximation does not introduce any inaccuracy in the evaluation of the integral even for $\omega >> \eta$ because, in this case, the integrand provides a negligible contribution to the integral.

Substituting Eq. (4.11) into Eq. (4.12) we obtain

$$G(r) \approx \frac{2}{(2\pi)^2}\int_0^\infty \omega^2 \frac{\gamma\eta}{\sqrt{\eta^2+\omega^2}-(1-\gamma)\eta}\,\mathrm{sinc}(\omega r)d\omega =$$

$$= \frac{\gamma\eta}{(2\pi)^2}\left[(1-\gamma)\eta\int_{-\infty}^{+\infty}\frac{\omega^2\mathrm{sinc}(\omega r)}{\omega^2+\eta^2-(1-\gamma)^2\eta^2}d\omega + \int_{-\infty}^{+\infty}\frac{\omega^2\sqrt{\eta^2+\omega^2}\mathrm{sinc}(\omega r)}{\omega^2+\eta^2-(1-\gamma)^2\eta^2}d\omega\right] =$$

$$= \frac{\gamma\eta}{(2\pi)^2}\left(\widehat{\mathcal{I}}_1+\widehat{\mathcal{I}}_2\right) = \frac{\gamma\eta}{(2\pi)^2}\left[(1-\gamma)\eta\frac{\pi}{r}\,e^{-\sqrt{1-(1-\gamma)^2}\eta r}+\widehat{\mathcal{I}}_2\right], \qquad (4.26)$$

having used identities 3.721.1, 3.725.1 in Gradshteyn and Ryzhik (1994) to calculate integral $\widehat{\mathcal{I}}_1$. Note that the oscillatory behavior of the integrand is limited to $\widehat{\mathcal{I}}_2$. In the following we first make $\widehat{\mathcal{I}}_2$ well defined, by integrating its integrand with respect to $r$, and then, by following a similar procedure as the one employed in Section 4.10 for the two-dimensional case, we calculate $\widehat{\mathcal{I}}_2$ by writing it as a series of integrals and exploiting a recurrence relation.

Letting $\alpha = \eta(1-\gamma)$, we have

$$\widehat{\mathcal{I}}_2 = \int_{-\infty}^{+\infty}\frac{\omega\sqrt{\eta^2+\omega^2}}{\omega^2+\eta^2-\alpha^2}\,\frac{e^{i\omega r}-e^{-i\omega r}}{2ir}\,d\omega =$$

$$= \frac{1}{ir}\int_{-\infty}^{+\infty} \frac{\omega\sqrt{\eta^2+\omega^2}}{\omega^2+\eta^2-\alpha^2}\, e^{i\omega r} d\omega = -\frac{1}{r}\frac{\partial}{\partial r}\int_{-\infty}^{+\infty} \frac{\sqrt{\eta^2+\omega^2}}{\omega^2+\eta^2-\alpha^2}\, e^{j\omega r} d\omega =$$

$$= -\frac{2}{r}\frac{\partial}{\partial r}\int_{0}^{+\infty} \frac{\cos\omega r}{\sqrt{\omega^2+\eta^2}} \sum_{n=0}^{\infty}\left(\frac{\alpha^2}{\omega^2+\eta^2}\right)^n d\omega =$$

$$= -\frac{2}{r}\frac{\partial}{\partial r}\sum_{n=0}^{\infty}\int_{0}^{+\infty} \frac{\alpha^{2n}\cos\omega r}{(\omega^2+\eta^2)^{n+1/2}} d\omega = -\frac{2}{r}\frac{\partial}{\partial r}\sum_{n=0}^{\infty}\mathcal{I}_n,$$

where we have defined $\mathcal{I}_n = \int_0^{+\infty} \frac{\alpha^{2n}\cos\omega r}{(\omega^2+\eta^2)^{n+1/2}} d\omega$. Note that the integration with respect to $r$ performed above introduces a decay of the integrand for large values of $\omega$, thus rendering $\widehat{\mathcal{I}_2}$ well defined. We now have a recurrence relation similar to the one obtained in the two-dimensional case, see equation (4.24):

$$\begin{cases} \mathcal{I}_0 = & \displaystyle\int_0^{\infty} \frac{\cos\omega r}{\sqrt{\omega^2+\eta^2}} d\omega = K_0(\eta r) \\ \\ \mathcal{I}_{n+1} = & \displaystyle\frac{-\alpha^2}{(2n+1)}\frac{1}{\eta}\frac{\partial}{\partial\eta}\mathcal{I}_n, \end{cases} \tag{4.27}$$

where the expression for $\mathcal{I}_0$ has been obtained by exploiting identity 3.754.2 in Gradshteyn and Ryzhik (1994). Following the same procedure as in Section 3, we now look at the first two terms of recurrence (4.27) and note that these correspond to the first two terms of the Taylor expansion, with respect to $\eta$, of the function:

$$K_0\left[\left(\eta - \frac{\alpha^2}{\eta}\right) r\right].$$

Hence, neglecting the higher-order terms of the expansion, we have the following:

$$\widehat{\mathcal{I}_2} = -\frac{2}{r}\frac{\partial}{\partial r}\sum_{n=0}^{\infty}\mathcal{I}_n \approx -\frac{2}{r}\frac{\partial}{\partial r}K_0\left[\left(\eta - \frac{\alpha^2}{\eta}\right) r\right] =$$

$$= 2\eta\frac{1-(1-\gamma)^2}{r}K_1[(1-(1-\gamma)^2)\eta r]. \tag{4.28}$$

Substituting Eq. (4.28) into Eq. (4.26), we finally obtain the expression for $G(r)$ given in Eq. (4.13).

# Chapter 5 Future Directions

In this chapter we discuss some of the possible extensions of the work in this thesis that we are currently considering.

One extension to the connectivity model presented in Chapter 2 is to consider more realistic communication channels. In percolation theory one assumes that two points are connected if they are at a given distance of each other. This corresponds to making two assumptions in the underlying wireless network model: reliable communication and rotational symmetric transmission range. A natural question to ask is what happens if we drop these assumptions.

We also discuss an extension to our work on propagation, considering the application of our random walk model to determine the impulse response of a wireless channel.

## 5.1 Ad hoc wireless networks with noisy links

First, we discuss unreliable wireless links. To do this, let us focus on flat ad hoc networks. Recall that in these kind of networks all nodes are considered equal, and can route data packets to destination, see Fig. 1.4.

We assume all nodes to be distributed on the plane according to a bi-dimensional Poisson point process $X$, and we model imperfect links by considering a random connection model where each pair of points $(x, y)$ of the point process is connected with probability $g(x - y)$, for some given function $g : \mathbb{R}^2 \to [0, 1]$.

We may, for example, pick a function $g(\cdot)$ such that the probability of existence of a link between a transmitter and a receiver decreases as the two points get farther away. For generality, however, we prefer to let $g$ be an arbitrary function. Accordingly, we do not require $g(\cdot)$ to have bounded support, be spherically symmetric, nor monotonic. The only requirement (in order to avoid a trivial model) is that its *effective area*

$e(g) = \int_{x \in \mathbb{R}^2} g(x)$ must be $0 < e(g) < \infty$. We call $H$ the class of functions that satisfy this requirement.

The effective area, when multiplied by the density of points, gives the expected number of points connected to a point of the Poisson process, hence the two cases $e(g) = 0,\ e(g) = \infty$ do not lead to any phase transition —see Meester and Roy (1996), Chapter 6, for details. However, any function $g(\cdot)$ such that $0 < e(g) < \infty$, has a phase transition. Namely, there exists a critical value $\lambda_c(g)$ for the density of the Poisson process, such that

$$0 < \lambda_c(g) = \inf\{\lambda : \exists \text{ infinite connected component}\} < \infty.$$

Note that the standard continuum percolation model, where Poisson points are connected with probability one, if discs of radius $r$ centered at each point overlap, is a random connection model with a connection function

$$g(x) = \begin{cases} 1 & \text{if } \|x\| \leq 2r \\ 0 & \text{if } \|x\| > 2r. \end{cases} \tag{5.1}$$

It is interesting to see how the percolation properties of the model change when we change the form of the connection function, while preserving its effective area. We start by "squishing and squashing" the connection function.

### 5.1.1 Squishing and squashing

Given a function $g \in H$ define $g_p^{squash}$ by $g_p^{squash}(x) = p * g(\sqrt{p}x)$. This function, as illustrated in Figure 5.1, is a version of $g$ in which probabilities are reduced by a factor of $p$ but the function is stretched to give the original effective area. Therefore, the average number of connections of each point remains the same, but these connections have a wider range of lengths.

Note that considering the squashed version of a rectangular connection function as the one in Eq. (5.1), corresponds to connect Poisson points with probability $p$ if

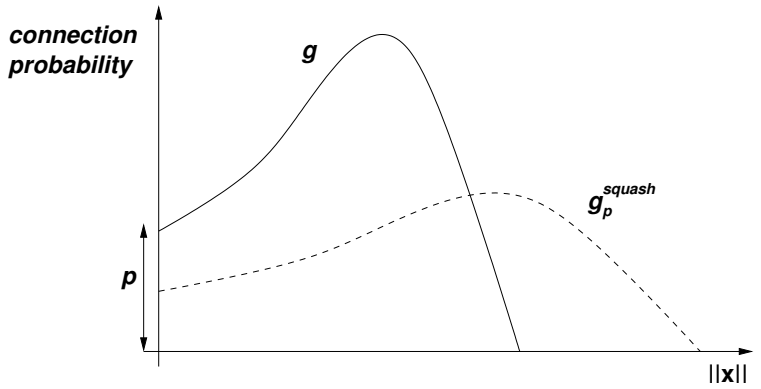


Figure 5.1: **Squishing and squashing.** *The function $g$ is squished and squashed to give the function $g_p^{squash}$.*

discs of radius $\sqrt{p}r$ around them overlap.

We can now state and prove the following theorem:

**Theorem 5.1** ***(The Squishing and Squashing Theorem)***
*For all $g \in H$,*

$$\lambda_c(g) \geq \lambda_c(g_p^{squash}).$$

**Proof of Theorem 5.1** Form the graph based upon the connection function $g(\sqrt{p}x)$ and call it $G$. Note that if we remove every edge from $G$ independently and with probability $1-p$ we make the graph based upon the connection function $g_p^{squash}(x) = p * g(\sqrt{p}x)$. Alternatively we can remove each Poisson point independently and with probability $1-p$, giving a density of points $\lambda p$. If we then scale by $\sqrt{p}$ in each direction we find again a density $\lambda$ of points and our connection function has become $g(x)$. Essentially we are performing site or bond percolation on $G$ with parameter $p$ and we wish to compare the two.

Based upon the above observations we see that it suffices to give a coupling in which we simultaneously remove edges in one realization of $G$ and points from a copy $G'$ of this, in which we will have an infinite cluster after removing points only if we have an infinite cluster after removing edges. It is vital that the coupling is "dynamic", i.e., it is propagated from edges originating only at vertices that have

already been determined to survive. We proceed as follows: starting at a root vertex $x_0$, we build survivor clusters in $G$ and $G'$. When the clusters at $x_0$ are complete, another vertex is selected as root and the process is iterated. First we examine all edges departing from $x_0$ in $G$ that connect to nodes that are not yet marked in $G'$. Each of these edges is marked dead in $G$, independently, with probability $1-p$, or it is declared a survivor otherwise. Each time an edge is declared dead, the node it connects $x_0$ to is also declared dead in $G'$, or survivor otherwise. When all edges departing from $x_0$ have been marked, we move to a surviving node and do the marking in the same way. Once all survivors have been examined, another, not yet marked vertex, is selected as root of a new cluster.

Finally, we can mark the remaining edges in $G$ and the remaining vertices (roots) in $G'$, independently, dead with probability $1-p$, or survivors, with probability $p$.

Now convince yourself that after all of this, if there is a path of survivor nodes in $G'$ then there is a (possibly longer) path of survivor edges in $G$. More details on the dynamic coupling procedure can be found in Grimmett and Stacey (1998). □

The theorem above has a certain depth. Essentially, it states that unreliable links are at least as good at providing connectivity as reliable links, if the average number of connections per node is the same. Another way of looking at this is that the longer links introduced by stretching the connection function are trading off for the unreliability of the connections introduced by reducing it.

In some related work Penrose (1993) has shown that (speaking roughly) as a connection function of effective area 1 gets more spread out, its critical density for percolation converges to 1. This can be seen as the limiting case of our Theorem 5.1. Meester, Penrose, and Sarkar (1997) proved a similar result as the dimension tends to infinity. Philosophically, the idea that some longer connections help to reach percolation at a lower density of points is also related to the small world networks described, for example, in the paper by Watts and Strogatz (1998).

The same kind of dynamic coupling used in the proof of the Theorem 5.1 is also used by Grimmett and Stacey (1998) to show the relationship between the critical

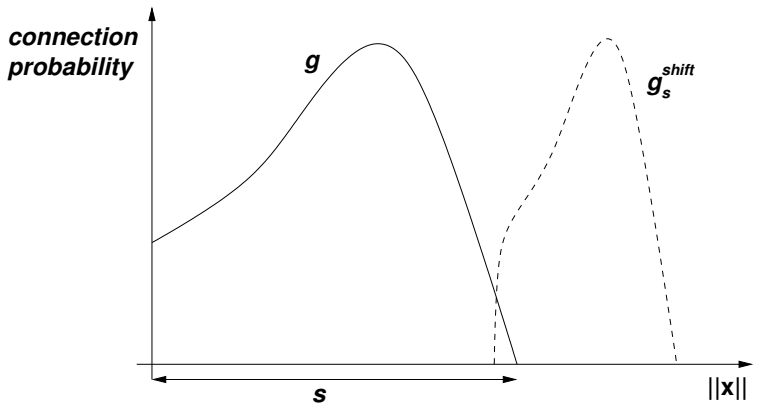


Figure 5.2: **Shifting and squeezing** The function $g$ is shifted and squeezed to give the function $g_s^{shift}$.

values of site and bond percolation on graphs. Sites of the discrete model are the analog of Poisson points in our continuum model. Grimmett and Stacey (1998) show that bond percolation is strictly easier to percolate than site percolation for quasi-transitive graphs. We conjecture that also our inequality can be made strict, following similar reasonings of Grimmett and Stacey (1998):

**Conjecture 5.2** ***(The Squishing and Squashing Conjecture)***
*For all* $g \in H$ *and* $p < 1$,

$$\lambda_c(g) > \lambda_c(g_p^{squash}).$$

### 5.1.2 Shifting and squeezing

Another transformation of $g$ that we consider is $g_s^{shift}(x)$. Here we shift the function $g$ outwards (so that a disc becomes an annulus, for example) by a distance $s$, but squeeze the function so that it has the same effective area. See Figure 5.2 for an example. Technically we define this through $g_s^{shift}(x) = g(h^{-1}(x))$ and

$$\int_s^{s+h(y)} r g_s^{shift}(r)dr = \int_0^y r g(r)dr.$$

Note that the shifting and squeezing transformation maintains on average the

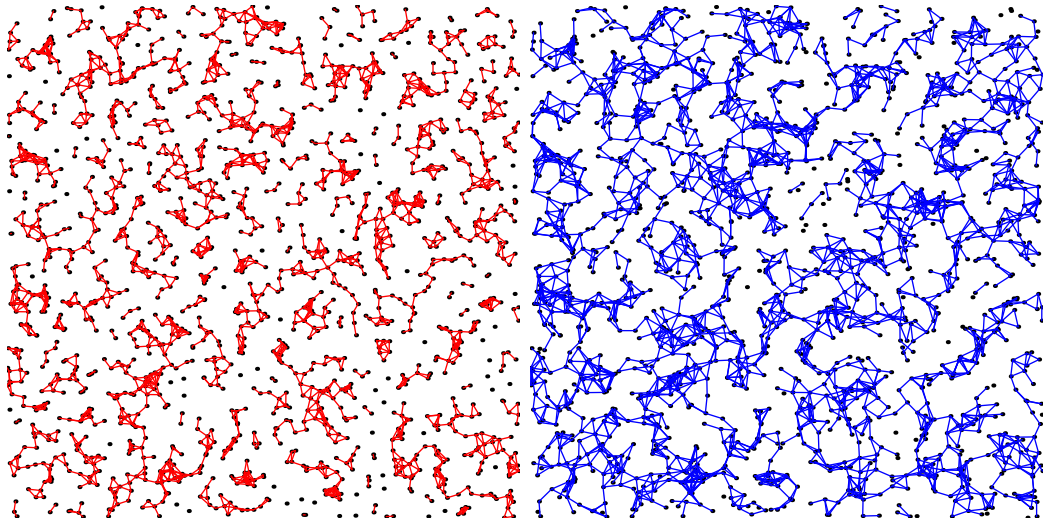

Figure 5.3: **Result of shifting and squeezing the connection function.** *Left-hand side: connections between random points at distance at most 1. Right-hand side: connections between random points at distance between 1 and* $\sqrt{2}$*. Note that it is possible to traverse the graph on the right-hand side from top to bottom and from left to right, but not the one on the left-hand side.*

same number of bonds per node, but makes them all longer. This contrasts with the squishing and squashing transformation which gives more of a mixture of short and long edges. Is the stretching of the edges enough to help the percolation process, or we need the mixture provided by squishing and squashing? We believe (supported by experimental evidence) that the longer edges introduced by the shifting and squeezing transformation are enough to help the percolation process. Accordingly, we make the following conjecture:

**Conjecture 5.3** ***(The Shifting and Squeezing Conjecture)***

*For all* $g \in H$ *and* $s > 0$,

$$\lambda_c(g) > \lambda_c(g_s^{shift}).$$

It is easy to check Conjecture 5.3 by simulation, using a rectangular connection function of the type described by Eq. (5.1). Results in Fig. 5.3 suggest that the shifting and squeezing conjecture is true (for this connection function), i.e., long bonds are more useful for percolation than short ones at a given density of points. However, it must be noted that a scaling of the whole picture will make the bonds longer

while changing the density of points. Naturally, this process does not change the connectivity, but is essentially different in that it changes the effective area.

At first sight, it may seem that Conjecture 5.3 does not have an immediate practical application to wireless networks, as the links unreliability/length trade-off expressed by Theoerem 5.1. However, we believe that proving it will provide some insight on how to compare the percolation properties of arbitrary connection functions of the same effective area, which will be of great practical interest.

## 5.2 Anisotropic radiation patterns

We now discuss another extension to the connectivity model: non-rotational symmetric transmission ranges. In practice, the communication range of a radio transmitter cannot be perfectly rotationally symmetric. The imperfection is due to the hardware characteristics of the transmitting antenna, and to the surrounding environment. It is therefore useful to understand how percolation properties are influenced by the shape of the transmitter footprint.

We consider centrally symmetric shapes that are not necessarily rotationally symmetric. Accordingly, we let $B \subset H$ be the set of all connection functions of the form $b_C(x) = 1$ if $x$ is inside some convex centrally symmetric shape $C$ of area 1 and 0 otherwise. Let $D$ be the disc of area 1 and let $S$ be the square of area 1.

Centrally symmetric shapes allow us to consider only bi-directional links: a particularly nice property of centrally symmetric shapes is that two nodes overlap each other's centers if and only if the shapes scaled by a factor of two in each direction overlap each other. This means that if a node falls in the shape of the another node for connection, also that the reverse is true. This property does not hold for non-centrally symmetric shapes, see Fig 5.4.

Jonasson (2001) has shown that if any convex shape of area 1 percolates at at certain density, then triangles (that are not centrally symmetric) of area 1 will also do so. Roy and Tanemura (2002) strengthened this result to show a strict inequality between the critical density of triangle and that of any other given convex shape

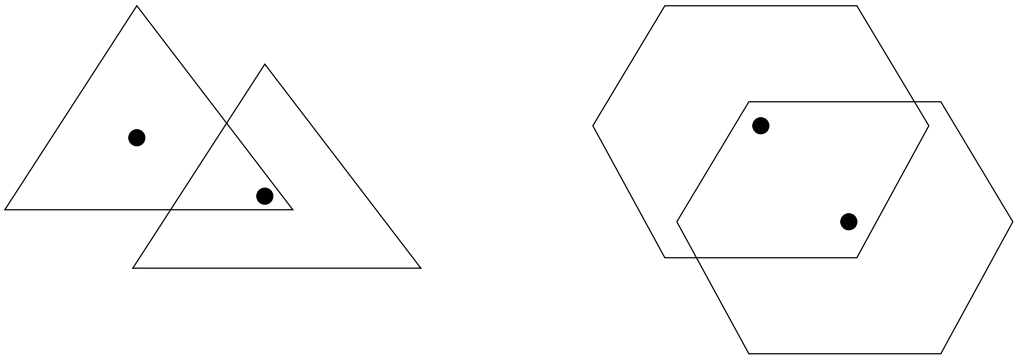

Figure 5.4: **Central symmetry and asymmetry of shapes.** Left-hand side, centrally asymmetric shapes: the lower point is contained in the triangle around the higher point but not vice versa. Right-hand side, centrally symmetric shapes. The lower point is contained in the hexagon around the higher point and vice versa.

of the same area. Jonasson (2001) has also shown that the convex shape with the highest critical density will be centrally symmetric. It is natural to ask which of the centrally symmetric shapes percolate most and least easily. We believe the answers are the square and the disc.

**Conjecture 5.4** ***(The Transubstantiated Shape Conjecture)***

*For all $b_C \in B$ we have*

$$\lambda_c(b_S) \leq \lambda_c(b_C) \leq \lambda_c(b_D).$$

There is an important practical consequence that follows if Conjecture 5.4 is true. If the disc is the centrally symmetric shape that percolates at the highest density, it follows from Jonasson (2001) that this is also the highest percolating density shape over all the convex shapes. This means that percolation theory results on the existence of an unbounded connected cluster, derived in the standard model where overlapping discs are connected with probability one, are robust. If an ideal model, where transmission footprints are perfect discs, allows long-distance multi-hop communication, then long-distance multi-hop communication is also possible, under the same density conditions, in a less idealistic model where transmission footprints can have any convex shape.

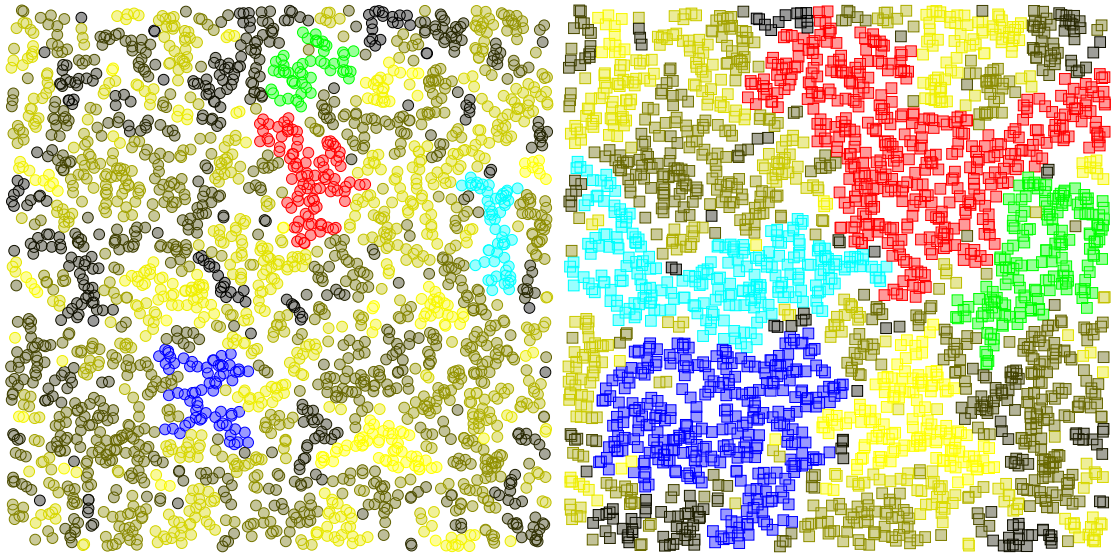

Figure 5.5: **Discs vs. squares**. In this simulation squares and discs have the same area and the same density on the left-hand side and on the right-hand side.

We now investigate the validity of Conjecture 5.4 with computer simulations. Fig. 5.5 depicts simulations of discs and squares shapes of area one at density one. We have also performed extensive computer simulations with different densities. We report the size of the largest and second largest clusters found in these simulations in Fig. 5.6.

We ran overnight on a desktop computer a total of 7000 experiments for discs (squares) of unit area, using 10000 randomly placed discs (squares) for each experiment. The density of the discs (squares) in the experiments varied from a minimum of 0.25 to a maximum of 0.32, with a 0.00001 incremental step. Each data point reported in Fig. 5.6 corresponds to an average of a sliding window of 100 consecutive experiments, giving a total of 7000 data points for each curve reported.

Results show that the size of the largest cluster of discs tends to diverge at a smaller value of the density than for squares. If we shift the plot obtained for squares by 3% (see Fig. 5.7), we find a striking matching of the curves. Accordingly, we conclude that squares seem to percolate at a value of the density 3% smaller than discs.

We plan to perform more simulations to determine if other centrally symmetric

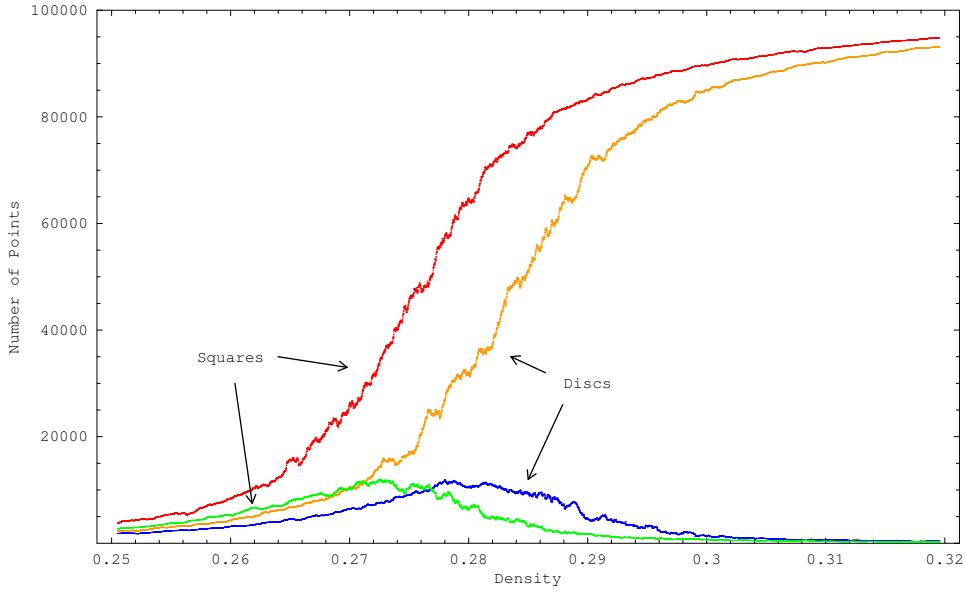


Figure 5.6: **Size of larger clusters.** We report the size of the largest and second largest clusters of discs and squares of area one. The size of the largest cluster of discs tends to diverge at a smaller value of the density than for squares.

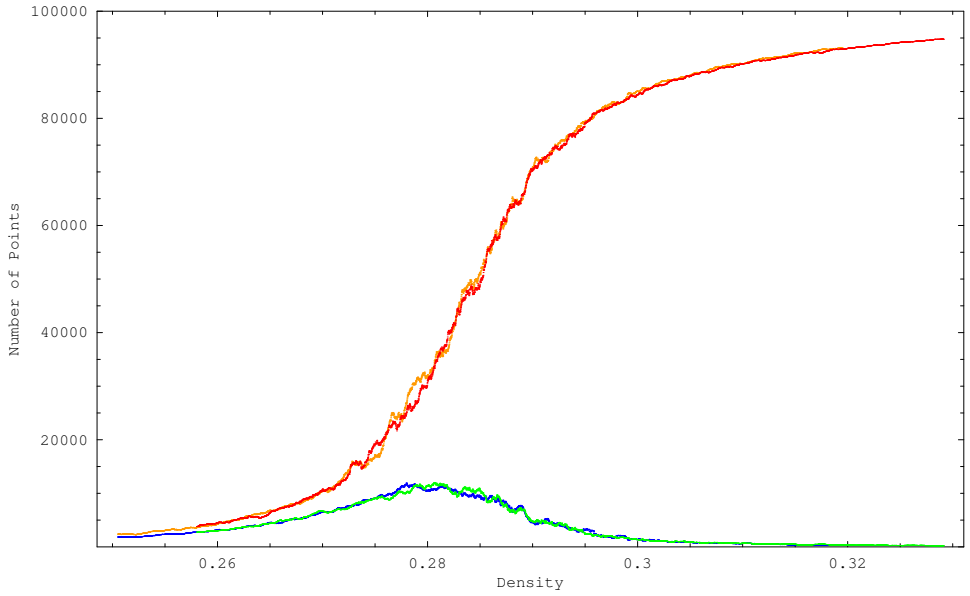


Figure 5.7: **Shifting by 3%.** After shifting the curves of the size of the largest and second largest clusters of squares by 3% , we find a striking matching with the corresponding curves plotted for discs. This indicates that squares percolate at a value of the density 3% smaller than discs.

shapes also percolate at a density smaller than the critical density for discs percolation, thus confirming the validity of our conjecture.

## 5.3 Impulse response of Mario's drunken walk

We now discuss a possible extension of our work on propagation. In Chapter 4 we have studied power loss in a wireless channel, that is essential to perform link budget calculations to determine the data rate allowed by the channel. This is not the only quantity of interest. In general a wireless channel is not only power limited, but also bandwidth limited. The delay spread of the signal, caused by the limited bandwidth of the channel, can cause intersymbol interference.

Our idea is to use Mario's drunken walk model to determine the impulse response, and hence the bandwidth, of an urban wireless channel. This involves the introduction of timing constraints into the model.

The main objective is to derive analytical solutions for Mario's drunken walk model, when one sends an impulse of a certain width $T$ and receives a (deformed) version of it, at a certain distance $r$ from the transmitter. In the following, we briefly outline the procedure to do this.

### 5.3.1 Path length after n reflections

The first step is to determine the p.d.f. of the path length $P(R_n)$ of the random walk after $n$ reflections. This is essentially a one-dimensional problem, as it does not depend on the direction of the turn taken at each step.

We already know (see Chapter 4) that the p.d.f. of a step of length $r$ is given by

$$Q(r) = \eta e^{-\eta r}.$$

The probability of having walked for a length $R_n$ after $n$ steps is immediately obtained

by convolving $Q(r)$with itself $n$ times, yelding

$$P(R_n) = \frac{(\eta R_n)^{n-1}}{(n-1)!}\eta e^{-\eta R_n}. \tag{5.2}$$

### 5.3.2 Delayed echoes

We can now write the expected value of the delayed impulse after $n$ reflections. Consider transmitting an impulse of the form:

$$f(t) = \frac{1}{T}e^{-t/T}u(t),$$

where $u(t)$ denotes the unit step function. Letting $c$ be the speed of light, the expected value after $n$ reflections at distance $r_0 = ct_0$ from the origin, can be written as

$$\mathcal{F}(t) = \int_{ct_0}^{ct} f(t - R_n/c)\; p(R_n)dR_n. \tag{5.3}$$

Note that, for any given $n$, this gives the average echo received at $r_0$ after $n$ reflections, when transmitting the signal $f(t)$.

Letting $\tau = 1/(\eta c)$ the average time between two successive steps, substituting Eq. (5.2) into Eq. (5.3), after some calculation we find, for $T << \tau$, $T << t - t_0$,

$$\tau\mathcal{F}(t) = \frac{(t/\tau)^{n-1}}{(n-1)!}e^{-t/\tau}u(t - t_0). \tag{5.4}$$

Eq. (5.4) is plotted in Fig. 5.8 for different values of $n$; plots have a physical meaning for $t > t_0$. We note that as the number of reflections $n$ increases, the echoes are more delayed and more spread out in time.

Finally, to obtain the impulse response, all of these echoes must be summed over $n$, weighting each term of the sum by the probability of reaching $r_0$ in $n$ reflections, and by an attenuation factor accounting for the absorption of the reflectors and the geometric attenuation. We are currently investigating how to calculate this sum. The final objective would be to see how the delay spread at the receiver is influenced by

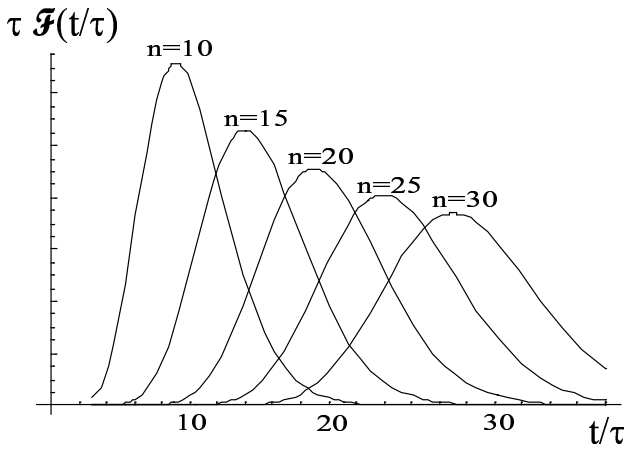


Figure 5.8: **Delayed echoes.** As the number of reflections increases, the echoes are more delayed and more spread out in time.

the transmitter-receiver distance, obstacles density, and absorption.

I think we are going to stop here, Mario is ready to go to sleep.

# Bibliography

[1] R. E. Barlow, D. J. Bartholomew, J. M. Bremner, and H. D. Brunk (1972). Statistical inference under order restrictions: theory and applications of isotonic regression. *John Wiley and Sons.*

[2] H. L. Bertoni, W. Honcharenko, L. Rocha Maciel, and H. H. Xia (1994). UHF propagation prediction for wireless personal communications. *Proceedings of the IEEE, 82(9), 1333-1359.*

[3] J. J. Binney, N. J. Dowrick, A. J. Fisher, and M. E. J. Newman (1992). The theory of critical phenomena. An introduction to the renormalization group. *Oxford University Press.*

[4] N. Blaunstein, R. Giladi, and M. Levin (1998). Characteristics' prediction in urban and suburban environments. *IEEE Transactions on Vehicular Technology, 47(1), 225-234.*

[5] N. Blaunstein, and M. Levin (1995). Prediction of UHF wave propagation in suburban and rural environments. *Proceedings of the URSI Symposium on Communication, 191-200.*

[6] N. Blaunstein, and M. Levin (1996). VHF/UHF wave attenuation in a city with regularly distributed buildings. *Radio Science, 31, 313-323.*

[7] B. Bolobás (1985). Random graphs. *Academic Press.*

[8] L. Booth, J. Bruck, M. Franceschetti, and R. Meester (2002). Power requirements for connectivity in clustered wireless networks. *Proceedings of the International Symposium on Information Theory (ISIT), 353.*

[9] L. Booth, J. Bruck, M. Franceschetti, and R. Meester (2002). Covering algorithms, continuum percolation, and the geometry of wireless networks. *Annals of Applied Probability, to appear.*

[10] S. R. Broadbent, and J. M. Hammersley (1957). Percolation processes I. Crystals and mazes. *Proceedings of the Cambridge Philosophical Society, 53, 629-641.*

[11] R. Durrett and D. Griffeath (1983). Supercritical contact processes on $\mathbb{Z}$. *Annals of Probability, 11(1), 1-15.*

[12] V. Erceg, L. Greenstein, S. Tjandra, S. R. Parkoff, A. Gupta, B. Kulic, A. Julius, and R. Bianchi (1999). An empirically based path loss model for wireless channels in suburban environments. *IEEE Journal on Selected Areas of Communications, 17(7), 1205-1211.*

[13] P. Erdős and A. Rényi (1959). On Random Graphs I. *Publicationes Mathematicae Universitatis Debreceniensis 6, 290-297.*

[14] P. Erdős and A. Rényi (1960). On the evolution of random graphs. *Publications of the Mathematical institute of the Hungarian Academy of Sciences 5,17-61.*

[15] P. Erdős and A. Rényi (1961). On the Evolution of Random Graphs. *Bulletin of the International Institute of Statistics of Tokio 38, 343-347.*

[16] P. Erdős and A. Rényi (1961). On the Strength of Connectedness of a Random Graph. *Acta Mathematica Acadamiae Scientiarum Hungaricae 12,261-267.*

[17] A. Fabrikant, E. Koutsoupias, and C. Papadimitriou (2002). Heuristically optimized trade-offs: a new paradigm for power laws in the internet. *Preprint, available on-line at:* `http://www.cs.berkeley.edu/~christos`

[18] M. J. Feurstein, K. L. Blackard, T. Rappaport, S. Y. Seidel, and H. H. Xia (1994). Path loss, delay spread, and outage models as functions of antenna height for microcellular systems design. *IEEE Transactions on Vehicular Technology, 43(3), 487-498.*

[19] P. J. Flory (1941). Molecular size distribution in three-dimensional gelation I-III. *Journal of the American Chemical Society, 63, 3083-3100.*

[20] G. Franceschetti, S. Marano, and F. Palmieri. Propagation without wave equation, toward an urban area model (1999). *IEEE Transactions on Antennas and Propagation, 47(9), 1393-1404.*

[21] M. Franceschetti, M. Cook, J. Bruck (2002). A geometric theorem for wireless network design optimization. *Technical report ETR044, preprint available on-line at:* `http://www.paradise.caltech.edu/ETR.html`

[22] M. Franceschetti, L. Schulman, J. Bruck (2002). Microcellular systems, random walks and wave propagation. *Proceedings of the International Symposium on Antennas and Propagation (AP-S).*

[23] M. Franceschetti, L. Schulman, J. Bruck (2002). Microcellular systems, random walks and wave propagation. Part I, theory. *Submitted to IEEE Transactions on Wireless Communications.*

[24] M. Franceschetti, L. Schulman, J. Bruck (2002). Microcellular systems, random walks and wave propagation. Part II, validation. *Submitted to IEEE Transactions on Wireless Communications.*

[25] E. N. Gilbert (1961). Random plane networks. *Journal of SIAM, 9, 533-543.*

[26] I. S. Gradshteyn and I. M. Ryzhik (1994). Table of integrals, series, and products. *Fifth edition, A. Jeffrey Editor, Academic Press.*

[27] E. Green (1989). Path loss and signal variability analysis for microcells. *Proceedings of the IEE fifth International Conference on Mobile and Personal Communications, 38-41.*

[28] L. Greenstein, N. Amitay, T. Chu, L. J. Cimini Jr., G. J. Foschini, M. J. Gans, A. J. Rustako Jr., R. A. Valenzuela, and G. Vannucci (1992). Microcells in personal communication systems. *IEEE Communications magazine, December, 76-88.*

[29] G. R. Grimmett (1999). Percolation. *Springer-Verlag, second edition.*

[30] G. R. Grimmett and A. M. Stacey (1998). Critical probabilities for site and bond percolation models. *Annals of Probability, 26(4), 1788-1812.*

[31] M. Grossglauser and D. Tse (2001). Mobility increases the capacity of ad hoc wireless networks. *Proceedings of IEEE Symposium on Information and Communication (INFOCOM).*

[32] E. Grosswald (1980). Bessel polynomials. *Lecture Notes in Mathematics 698. Springer Verlag.*

[33] P. Gupta and P. R. Kumar (1998). Critical power for asymptotic connectivity in wireless networks. *Stochastic Analysis, Control, Optimization and Applications: A Volume in Honor of W.H. Fleming, W. M. McEneaney, G. Yin, and Q. Zhang (Eds.), Birkäuser, Boston.*

[34] P. Gupta and P. R. Kumar (2000). The capacity of wireless networks. *IEEE Transactions on Information Theory, 46(2), 388-404.*

[35] M. Hata (1980). Empirical formula for propagation loss in land mobile radio services. *IEEE Transactions on Vehicular Technology, 29(3), 317-325.*

[36] A. Ishimaru (1978). Wave propagation and scattering in random media. Vol. 1, 2. *Academic Press.*

[37] ITU-T Focus Group on Traffic Engineering for Personal Communication (1999). E750-Series of recommendations on traffic engineering aspects of networks supporting mobile and UPT services. *Technical Reference of the International Telecommunication Union, Geneva.*

[38] J. Jonasson (2001). Optimization of shape in continuum percolation. *Annals of Probability, 29(2), 624-635.*

[39] L. P. Kadanoff (1966). Scaling laws for Ising model near $T_c$. *Physics, 2, 263-272.*

[40] H. Kesten (1980). Percolation theory for mathematicians. *Birkhäuser.*

[41] S. R. Kulkarni, and P. Viswanath (2001). A deterministic approach to throughput scaling in wireless networks. *Proceedings of the International Symposium on Information Theory (ISIT), 351.*

[42] L. Rocha Maciel, H. L. Bertoni, and H. H. Xia (1993). Unified approach to prediction of propagation over buildings for all ranges of base station antenna height. *IEEE Transactions on Vehicular Technology, 42(1), 41-45.*

[43] R. Meester and R. Roy (1994). Uniqueness of unbounded occupied and vacant components in boolean models. *The Annals of Applied Probability 4(3), 933-951.*

[44] R. Meester and R. Roy (1996). Continuum percolation. *Cambridge University Press.*

[45] R. Meester and M. D. Penrose and A. Sarkar (1997). The random connection model in high dimensions. *Statistics and Probability Letters, 35,145-153.*

[46] M. E. J. Newman (2002). Random graphs as models of networks. *Handbook of Graphs and Networks, S. Bornholdt and H. G. Schuster (Eds.), Wiley-VCH, Berlin.*

[47] Y. Okumura, E. Ohmori, T. Kawano, and K. Fukuda (1968). Field strength and its variability in VHF and UHF land-mobile radio service. *Review of the Electrical Communication Laboratory, 16(9-10), 825-873.*

[48] M. D. Penrose (1993). On the spread-out limit for bond and continuum percolation. *Annals of Applied Probability, 3(1), 253-276.*

[49] J. Quintanilla, S. Torquato, and R. M. Ziff (2000). Efficient measurement of the percolation threshold for fully penetrable discs. *Journal of Physics A: Mathematical and General, 33(42), L399-L407.*

[50] T. Rappaport (1996). Wireless communications, principles and practice. *Prentice Hall.*

[51] R. Roy and H. Tanemura (2002). Critical intensities of Boolean models with different underlying convex shapes. *Advances in Applied Probability, 34(1), 48-57.*

[52] J. Segers (2002). Personal communication.

[53] S. Smirnov, and W. Werner (2001). Critical exponents for two-dimensional percolation. *Mathematical Research Letters, 8(5-6), 729-744.*

[54] W. H. Stockmayer (1943). Theory of molecular size distribution and gel formation in branched-chain polymers. *Journal of Chemical Physics, 11, 45-55.*

[55] J. H. Tarng, and K. M. Ju (1999). A novel 3-D scattering model of 1.8-GHz radio propagation in microcellular urban environment. *IEEE Transactions on Electromagnetic Compatibility, 41(2), 100-106.*

[56] P. Tran-Gia, K. Leibnitz, and K. Tutschku (2000). Teletraffic issues in mobile communication network planning. *Telecommunication Systems, 15, 3-20.*

[57] K. Tutschku (1998). Demand based radio network planning of cellular communication systems. *Proceedings of the IEEE Symposium on Information and Communication (INFOCOM).*

[58] K. Tutschku, and P. Tran-Gia (1998). Spatial traffic estimation and characterization for mobile communication network design. *IEEE Journal on Selected Areas in Communications, 16(5), 804-811.*

[59] H. H. Xia, and H. L. Bertoni (1992). Diffraction of cylindrical and plane waves by an array of absorbing half-screens. *IEEE Transactions on Antennas and Propagation, 40(2), 170-177.*

[60] H. H. Xia, H. L. Bertoni, L. R. Maciel, A. Lindsay-Stewart, and R. Rowe (1993). Radio propagation characteristics for line of sight microcellular and personal communications. *IEEE Transactions on Antennas and Propagation, 41(10), 1439-1447*

[61] F. Xue, and P. R. Kumar (2002). The number of neighbors needed for connectivity of wireless networks. *Preprint, privately communicated by the authors.*

[62] J. E. Yukich (1998). Probability theory of classical euclidean optimization problems. *Lecture Notes in Mathematics 1675, Springer.*

[63] D. J. Watts, and S. H. Strogatz (1998). Collective dynamics of small world networks. *Nature, 393, 440-442.*

[64] K. G. Wilson (1971). Renormalization group and critical phenomena I. Renormalization group and the Kadanoff scaling picture. *Physical Review, B4, 3174-3183.*

[65] K. G. Wilson (1971). Renormalization group and critical phenomena II. Phase-space analysis and critical behavior. *Physical Review, B4, 3184-3205.*